STATUS OF THESIS

Title of thesis	PERFORMANCE ANALYSIS OF GROOVED HYDRODYNAMIC JOURNAL BEARING WITH TEXTURE AND SLIP SURFACE

I _____ KU MUHAMMAD FAEZ BIN KU ARIFFIN _____

hereby allow my thesis to be placed at the Information Resource Center (IRC) of Universiti Teknologi PETRONAS (UTP) with the following conditions:

1. The thesis becomes the property of UTP

2. The IRC of UTP may make copies of the thesis for academic purposes only.

3. This thesis is classified as

    ☐ Confidential

    ☑ Non-confidential

If this thesis is confidential, please state the reason:

_____

_____

The contents of the thesis will remain confidential for _____ years.

Remarks on disclosure:

_____

_____

                                                            Endorsed by

_____   _____

Signature of Author   Signature of Supervisor

Permanent address: Name of Supervisor

No. 172, _____   Assoc. Prof. Ir. Dr. Hamdan Hj Ya

Taman Raja Muda Musa, _____

32000 Sitiawan, Perak, Malaysia. ___

Date : _____   Date : _____

UNIVERSITI TEKNOLOGI PETRONAS

PERFORMANCE ANALYSIS OF GROOVED HYDRODYNAMIC JOURNAL

BEARING WITH TEXTURE AND SLIP SURFACE

By

KU MUHAMMAD FAEZ BIN KU ARIFFIN

The undersigned certify that they have read, and recommend to the Postgraduate Studies Programme for acceptance of this thesis for the fulfillment of the requirements for the degree stated.

Signature: _____

Main Supervisor: _____Assoc. Prof. Ir. Dr. Hamdan Haji Ya_____

Signature: _____

Co-Supervisor: _____Prof. Dr. Norani Muti Mohamed_____

Signature: _____

Head of Department: ___Assoc. Prof. Dr. Puteri Sri Melor binti Megat Yusof

Date: _____

PERFORMANCE ANALYSIS OF GROOVED HYDRODYNAMIC JOURNAL

BEARING WITH TEXTURE AND SLIP SURFACE

by

KU MUHAMMAD FAEZ BIN KU ARIFFIN

A Thesis

Submitted to the Postgraduate Studies Programme

as a Requirement for the Degree of

MASTER OF SCIENCE

MECHANICAL ENGINEERING

UNIVERSITI TEKNOLOGI PETRONAS

BANDAR SERI ISKANDAR,

PERAK

SEPTEMBER 2018

DECLARATION OF THESIS

Title of thesis	PERFORMANCE ANALYSIS OF GROOVED HYDRODYNAMIC JOURNAL BEARING WITH TEXTURE AND SLIP SURFACE

I _____ KU MUHAMMAD FAEZ BIN KU ARIFFIN _____

hereby declare that the thesis is based on my original work except for quotations and citations which have been duly acknowledged. I also declare that it has not been previously or concurrently submitted for any other degree at UTP or other institutions.

Witnessed by

_____   _____

Signature of Author   Signature of Supervisor

Permanent address: Name of Supervisor

No. 172,_____   Assoc. Prof. Ir. Dr. Hamdan Hj Ya

Taman Raja Muda Musa,_____

32000 Sitiawan, Perak, Malaysia.____

Date : _____   Date : _____

DEDICATION

I dedicate this research work to my parents, Ku Ariffin bin Ku Md Saad and Sarah binti Awang Ismail for their endless support and believing my future path. I am grateful for them to be with me through ups and downs during my research work.

ACKNOWLEDGEMENTS

ABSTRACT

Hydrodynamic journal bearings are one of the important components in hydrodynamic lubrication, ranging from small applications such as motors, up to large applications, such as engines and turbines. The problem is that the hydrodynamic journal bearing shows poor performance under low eccentricity ratio conditions. This study has been carried out to investigate the effect of partial texture with a slip surface towards the performance of hydrodynamic journal bearings; namely, pressure distribution, load carrying capacity, shear stress, and friction coefficient. The study has been carried out by formulating the partial texture with single and two-slip surfaces onto a bearing surface in a fluid film region, which was then solved by using long bearing and short bearing approximations, respectively. The approximations which were applied that, the long journal bearing was considered in the circumferential direction, whilst the axial direction was applied on short journal bearing. The applied partial texture with slip surface showed different performance outcomes on both the long and short journal bearings. The long journal bearing showed significant improvement on the pressure distribution and load capacity for both single-slip and two-slip configurations. The performance improvement at the 0.1 eccentricity ratio achieved for the single-slip was from 0.1% and up to 125%, whilst the partial two-slip textured surface managed to achieve the performance increase of up to 166% compared to the plain journal bearing. In addition, the partial texture, single-slip surface also reduced the friction coefficient up to 22% at the 0.1 eccentricity ratio. However, the results also showed that applying the proposed surface configuration, especially two-slip texture, greatly increased the shear stress and friction coefficient to some extent. On the other hand, applying the partial texture with both single and two slip configurations on the short journal bearing showed the decrease of performance of the short journal bearing compared to the plain journal bearing, reflected poor performance under numerical analysis of this research.

ABSTRAK

Galas jurnal hidrodinamik merupakan salah satu daripada komponen terpenting dalam pelinciran hidrodinamik, daripada aplikasi kecil seperti motor, sehingga aplikasi yang besar seperti enjin, turbin, dan lain-lain. Teknik mengaplikasi tekstur dan sempadan *slip* terhadap permukaan adalah sebahagian daripada pendekatan yang selalu diguna pakai, dan penyelidik mendakwa bahawa teknik ini mempunyai potensi dalam meningkatkan prestasi galas jurnal hidrodinamik pada kadar nisbah eksentrik yang rendah. Kajian ini dilakukan untuk mengenal pasti kesan pengaplikasian separa tekstur bersama *slip* keatas prestasi galas jurnal hidrodinamik; iaitu kadar pengedaran tekanan, kapasiti beban yang dibawa, tekanan ricih, dan juga pekali geseran. Kajian ini dilaksanakan dengan merumuskan formula permukaan separa tekstur dengan satu *slip* dan dua *slip* terhadap permukaan galas dalam pelinciran filem cecair, dan kemudiannya diselesaikan dengan menggunakan teknik penganggaran galas panjang dan pendek. Teknik penganggaran yang diguna pakai ialah galas panjang hanya terhad kepada arah keliling galas, manakala galas pendek hanya mempertimbangkan arah paksi. Pengaplikasian permukaan tekstur separa bersama sempadan *slip* telah menunjukkan prestasi yang berbeza daripada kedua-dua galas jurnal panjang dan pendek. Galas jurnal panjang menunjukkan peningkatan yang ketara terhadap kadar pengedaran tekanan dan kapasiti beban yang dibawa terhadap konfigurasi satu *slip* dan dua *slip*. Kadar peningkatan pada kadar 0.1 nisbah eksentrik yang diperoleh daripada konfigurasi satu *slip* ialah dari 0.1% ke 125%, manakala permukaan separa tekstur dengan dua *slip* mencatatkan peningkatan sehingga 166% berbanding galas jurnal yang kosong. Tambahan pula, permukaan separa tekstur dengan satu *slip* turut mencatatkan penurunan pekali geseran sehingga 22% pada kadar nisbah eksentrik 0.1. Walau bagaimanapun, keputusan yang diperoleh turut menunjukkan bahawa penggunaan konfigurasi yang dicadangkan, terutamanya permukaan tekstur dengan dua *slip* telah menunjukkan peningkatan yang ketara terhadap tekanan ricih dan pekali geseran pada suatu kadar yang tertentu. Selain itu, penggunaan konfigurasi separa tekstur dengan kedua-dua *slip* terhadap galas pendek telah menunjukkan prestasi yang menurun

berbanding galas jurnal yang kosong, menunjukkan bahawa keputusan yang tidak memberangsangkan di dalam analisis ini.

TABLE OF CONTENT

LIST OF FIGURES

LIST OF TABLES

LIST OF SYMBOLS

C   Radial clearance, m

h,H Lubricant film thickness, m; H=h/C

H_g Texture depth

L Bearing length, m

n   Journal bearing eccentricity ratio; n=ε/C

O_b Bearing center

O_p Pad center of curvature

O_j Journal center

P Pressure distribution in the fluid film, N/m^2 ; $P=pC^2/\mu\omega R^2$

P_0 Non-dimensional steady state pressure in the fluid film

P_j Non-dimensional pressure gradients in the fluid film; $j=x,y,\dot{x},\dot{y}$

P_g Non-dimensional pressure gradients in the end textured region

P_p Non-dimensional pressure gradients in the plain region

Q Flow volume rate

R Journal radius, m

u Velocity component along circumferential direction, m/s

w,W Load-carrying capacity, N; $W=wC^3/\mu\omega R^3 L$

W_ε,W_ϕ Radial and tangential load-carrying capacity, N

x,y,X,Y Horizontal and vertical coordinates with respect to bearing center,

          m; X=x/C, Y=y/C

ε Journal bearing eccentricity

ε_p	Eccentricity of the bearing pad
μ	Dynamic viscosity of fluid film, $N.s/m^2$
θ	Angular coordinate measured from the direction of maximum film thickness in journal bearing
θ_g	End texture width, deg.
θ_t	Textured length, deg.
Θ	Angular coordinate measured from the direction of load line in journal bearing
ω	Angular velocity of journal bearing, rad/s
ω_s	Non-dimensional threshold speed
$\Delta x, \Delta y$	Journal displacement in X and Y direction
U,V	Journal velocity in X and Y direction.
δ	Change of values or quantity with respect to different equations or expressions

CHAPTER 1

INTRODUCTION

1.1 Overview

Bearing is a mechanical component that limits the motion to the desired direction of motion and at the same time reduces motion friction to reduce the rate of wear and tear of the parts. It is precisely made and engineered to accommodate extreme speeds and load efficiently. One of the most commonly used of types of the bearing is a hydrodynamic journal bearing. Compared to other types of bearings, hydrodynamic journal bearing uses lubrication film to allow the movement between the parts involved in the journal bearing. The lubrication film is capable to tolerate forces exerted from the motion of the rotor as the lubrication condition maintains and separates the two-sliding surface of the journal and bearing surface from each other. The separation phenomenon is caused by the hydrodynamic pressure produced from the lubricant that
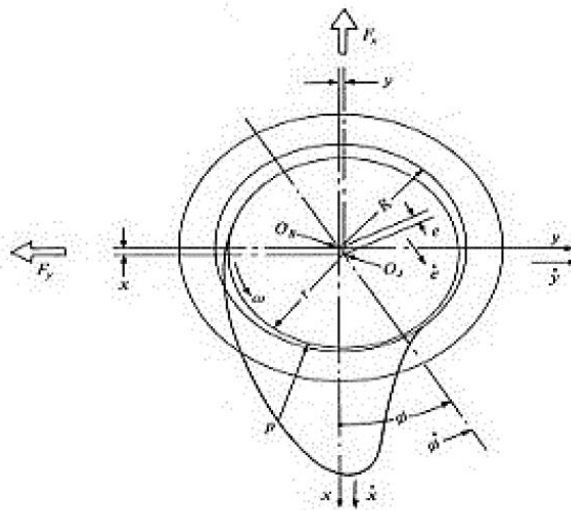
Figure 1.1: Coordinates and pressure profile of
hydrodynamic journal bearing [1, 2].

pumps into the converging region and leads to wedge action and shaft to rotates as shown in Figure 1.1.

The major concern on operating journal bearing is that to achieve high load carrying capacity and pressure distribution in low eccentricity ratio conditions. Surface texturing and boundary slip application are some of the techniques applied to overcome the problems, which improves the performance of the hydrodynamic journal bearing. The applied technique is used to manipulate the fluid film conditions due to the surface characteristics that are changed whether on the bearing surface or on the journal surface, which altered the internal conditions of fluid film lubrication during operation. Hydrodynamic journal bearing can be classified as a few, such as long journal bearing and short journal bearing as shown in Figure 1.2 and 1.3. The explanation of these classifications will be discussed later in the next chapter.
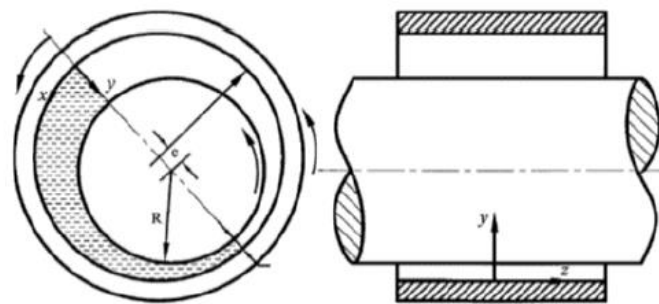
Figure 1.2: Illustration of long journal bearing [22].
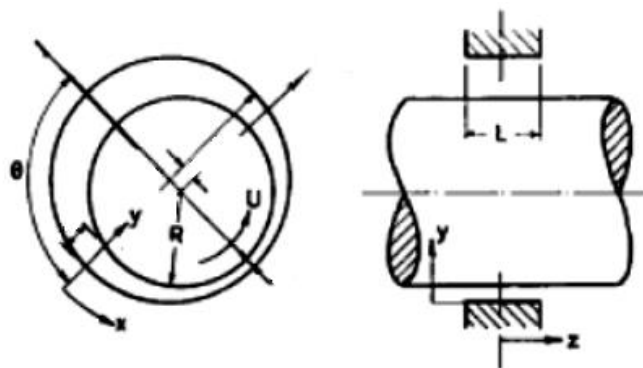
Figure 1.3: Illustration of short journal bearing [22].

1.2 Background of Study

The study of lubrication in bearings introduced by Osborne Reynolds [3] in 1886 in which introduced by Tower [4] back in 1883. During that time, Tower learned the capability of hydrodynamic journal bearings in carrying load based on the oil film pressure. Later, the first solution of Reynolds equation in hydrodynamic journal bearing is found by Sommerfeld [5] after Petroff [6], in his finding comes out with the bearings with the journals at the center. From these findings, bearings analysis has become an important topic to be discussed among researchers as it has an important role in the behavior of the whole system in terms of performance and efficiency.

Osborne Reynolds introduced the Reynolds equation of hydrodynamic lubrication in 1886. The theory comes from the experimental analysis of hydrodynamic journal bearing in pressure distribution profile done by Tower back in 1883 [7,8]. In the next few years ahead, Reynolds theory has been used for further analytical and experimental research in which the pressure gradient, lubricant viscosity, and the shape of the oil film derived from the partial differential technique.

Nowadays, the study of the hydrodynamic journal bearing has been widely spread in terms of improving its overall performance, either by using numerical simulation, mathematical modeling and also simulation. Well known researchers such as Tauviqirrahman [13], Brizmer [14], Tonder [12], Tala-Ighil [15, 51, 52], Rao [65, 70, 71, 72, 73] and many more has spreaded the potential of hydrodynamic journal bearing to keep improving by using various approaches and techniques which will be discussed later in the next chapter.

1.2.1 Surface Texture

Surface is defined as the outermost layer of the part in which can be describe in terms of texture or form. In early theory and previous studies of lubrication in tribology, the assumption made is that the bearing surface is perfectly smooth. In some other cases, asperities are also present at the covered surface, in which creates the possibilities of the rupture at the lubricant film to occur when the oil film is thin. Texture that presents at the surface can create a lubrication film, resulted the capability to handles load

capacity even with the no wedge condition. Texture surface can be in various shapes such as dimple, circle, ellipse, triangles, and many more as referred to Figure 1.2.
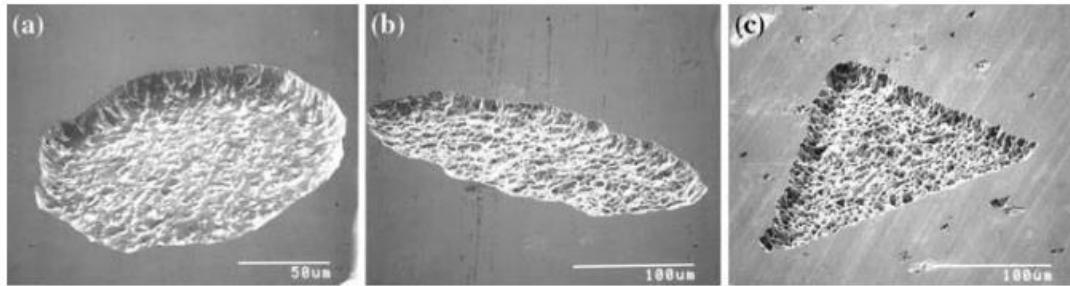
Figure 1.4: Surface texture with shape differences; (a) circular, (b) ellipse, and (c) triangular [9].

In hydrodynamic journal bearings, lubrication is important to provide smooth surface to reduce the friction motion and wear effects. Therefore, texture surface has become the interesting factor to improve the performance of hydrodynamic lubrication. Various studies have been done, analytically and experimentally for so many years with various types of texture surface to analyze the performance difference and improvements [10-12]. As for the examples, Figure 1.3 shows the parallel sliding surface performance is done with textured surface, meanwhile the textured surface on journal bearing sample can be seen at Figure 1.4. From rough observations, applying texture on the surface acts as an additional space for lubricants of to trap micro debris produced from the wear effect.
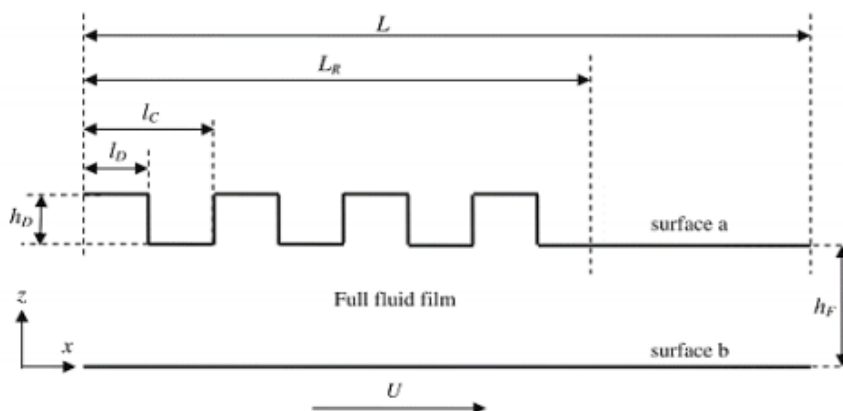
Figure 1.5: Surface texturing on stationary surface on lubricated parallel sliding contacts [13].

4
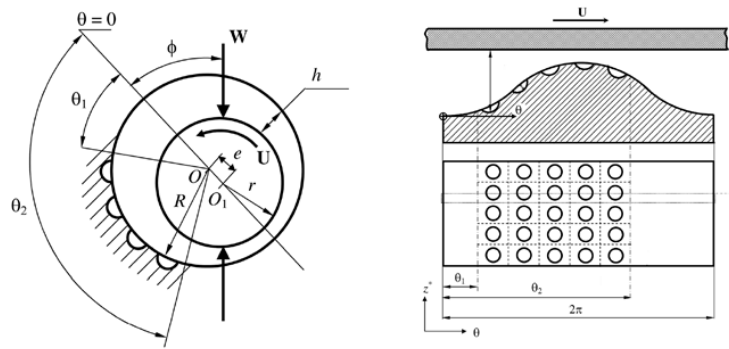
Figure 1.6: Surface texturing on journal bearing schematic diagram [14].

1.2.2 Boundary Slip

The history of boundary conditions has been discussed in the 19th century. The standard characterization of slip is introduced by Navier [16] and later proposed by Maxwell [17], which the component of the velocity tangent to the surface is directly proportional to the surface's shear rate. The research regarding the application of the slip boundary condition is greatly increased due to the development in microfluidic and microelectromechanical device field. The Maxwell-Navier slip interpretation is shown in Figure 1.5. The core concepts if the fluid mechanics is a no-slip condition, which the fluid has the same velocity as the surface contact. However, the boundary condition cannot be prove using hydrodynamic approach, but it can be demonstrated in the macroscopic analysis [19-21].
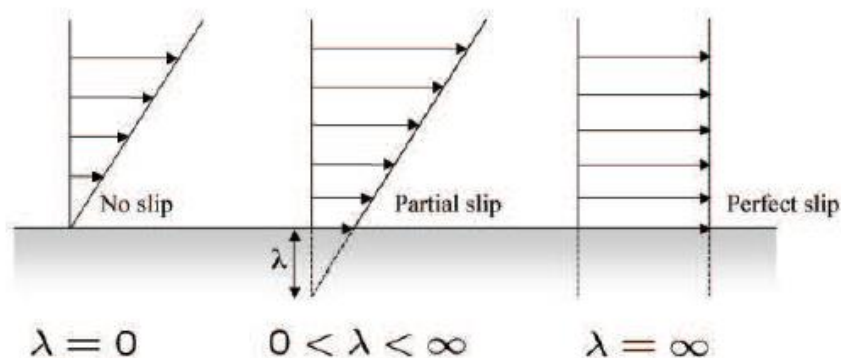
Figure 1.7: Maxwell-Navier slip length interpretation [18].

In hydrodynamic journal bearing and sliding contacts, the application of slip surface has been widely done. Most analytical analysis done has proven the capability of the slip surface to enhance journal and slider bearing's performance. The presence of slip surface controls the fluid film velocity between the contact surface, thus reduced the surface tension that occurs, which prolongs the component's durability.

1.3 Problem Statement

Increasing the performance of rotating machines required better performance of its components. The increasing demands for high-performance components lead to the engineers to upgrade the design to fulfill the requirements. Hydrodynamic performance of journal bearing is a great concern to increase its reliability, reduce energy loss and increase the efficiency to keep the rotation of the shaft to be smooth and withstand the forces for a long period of time. Recent studies in the science of tribology show that applying surface texture and slip surface configuration in a hydrodynamic journal bearing surface is a well known method to improve journal bearing's performance. However, the integration of surface texture and slip surface is not yet done thoroughly as it is not appropriately analyzed with fixed parameters such as the eccentricity ratio, texture depth and the ratio of slip/texture length. Therefore, this research is conducted to propose the new configuration that consists of surface texture and slip condition on the hydrodynamic journal bearing. This research also carried out to explore the potential improvements that can be done towards hydrodynamic journal bearings to replace plain journal bearing.

1.4 Research Objectives

From the problem stated above, the main target for this research is to analyze the textured surface and boundary slip effect on the performance of hydrodynamic journal bearing. To achieve this goal, the list of key objectives for this research are shown as below:

6

- To evaluate the performance of the new configuration of surface texture and boundary slip on the hydrodynamic journal bearing surface (partial single-slip texture and partial two-slip texture surface) by using modified Reynolds equation.
- To derive the solution of the Reynolds equation to accommodate sets of configurations proposed in long and short journal bearings.
- To determine the optimal slip and texture surface configuration for long and short bearing improvements compared to plain bearing performance based from the research conducted in this analysis.

1.5 Scope of Study

The scope of study for this research is limited with the following restrictions:

1. Hydrodynamic journal bearing is analyzed with load axes on the bearing surface.
2. The performance analysis for long and short bearing is carried out with eccentricity ratios ranging from 0.1 to 0.8 (low operating conditions).
3. The texture surface applied contains two different sections; varied textured region (θ_t) and fixed textured length (θ_g) which the texture depth (H_g) is varied according to different sets of configurations.
4. The dimensionless slip condition applied, A is defined according to proposed configurations on the textured surface.
5. The condition of the operation is steady state and the results calculated are presented in non-dimensional form.
6. The governing equation used is based on Reynolds equation, which Reynolds theory and Reynolds boundary conditions are applied in long journal bearing [22]. Meanwhile, Half-Sommerfeld (Gumbel) [21] boundary condition and DuBois and Ocvirk short bearing approximation [23] are applied in short journal bearing.

1.6 Thesis Structure

The research thesis requires a detailed numerical procedure in which includes the calculation of the static characteristics of hydrodynamic journal bearings with the combination of texture surface and boundary slip configuration.

- Chapter 2 covers wide range of literature review of work done by researchers. The literature review includes the utilization of surface texture and boundary slip in hydrodynamic lubrication of moving surfaces. Other than that, the chapter also shows the method used and the configuration proposed by previous researchers.

- Chapter 3 explains the research methodology. Reynolds equation will be used as the governing equation for the analysis. For long journal bearing, the Reynolds theory was applied [22]. Meanwhile for the short bearing, short bearing approximation [23] is applied.

- Chapter 4 presents the findings obtained for this research. The results obtained is recorded and evaluated together with the data obtained for the plain hydrodynamic journal bearing. The effect of surface texturing and boundary slip configuration is discussed and presented in terms of pressure distribution, load carrying capacity, shear stress, and friction coefficient.

- Lastly, Chapter 5 concludes the findings and remarks of the whole research. Recommendations and future work proposed is included as well as additional information.

CHAPTER 2

LITERATURE REVIEW

2.1 Overview

In this chapter, the static characteristics of the hydrodynamic journal bearing with surface texture and boundary slip is discussed. The introductory studies related to hydrodynamic lubrication discussed in Section 2.2. Next up, Section 2.3 discussed the Reynolds equation and boundary conditions related. Meanwhile, the details regarding hydrodynamic journal bearing, surface texturing, and wall slip applications are elaborate more in Section 2.4. Research gap and chapter summary are then presented to conclude the whole chapter.

2.2 Hydrodynamic Lubrication

Lubrication is essential to reduce/prevent the rate of wear and lowers the friction occurs. Hydrodynamic lubrication is used in the journal bearing which characterized by conformal surfaces as such there is the generation of positive pressure to support the normal load. The film is thick as such it prevents solid surfaces from touching each other. The clarification is explained by Szeri [22], Mitsui, [24], Hamrock [25], Schmid [26], Heywood [27], Becker [28], and many more as reference [36-38].

Hydrodynamic is known as the best lubrication in terms of friction and wear reduction. As for the features, hydrodynamic journal bearing consists of a journal and a bearing surface (sleeve) separated by a layer of a lubrication film. As refer at Figure 2.1, the loads are applied on the journal itself, causing a downwards displacement from the initial center location. The decrease of film thickness leads to the development of

positive pressure in which provides the cushioning effect when the bearing surfaces closer to each other.
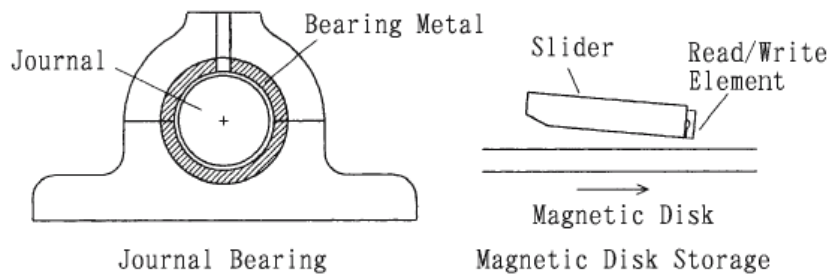
Figure 2.1: General illustration of hydrodynamic journal bearing [29].

The role of lubrication in different regimes can be seen in the Stribeck curve as shown in Figure 2.2. From the curve, the specific clarification towards the journal bearing is founded by Heywood [27], then De Kraker et al. [30] comes out with the calculations with respect to Stribeck curve. Meanwhile, the Stribeck curve has been used in hydrodynamic lubrication based on Siripuram and Stephens [31] to investigate the effect of asperity shape towards the friction coefficient. From the analysis, the asperity shape does not affect the coefficient of friction, but it is affected by cross section size.
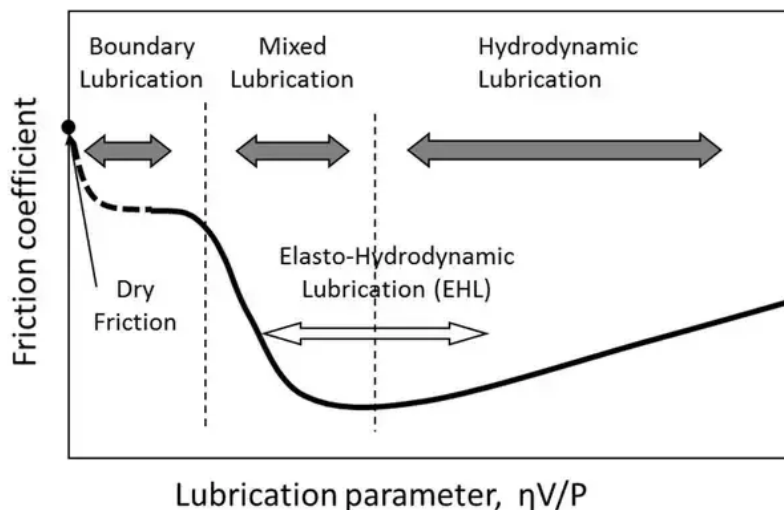
Figure 2.2: Stribeck curve diagram [29, 32].

2.3 Reynolds Equation in Hydrodynamic Journal Bearings

In previous theoretical work, Reynolds theory was introduced to simulate the outcome. However, some assumptions are required due to higher level of complexity of interface and its treatments. Reynolds introduced some assumptions with no noticeable difference with the actual condition, even though some other factors are unreal but it simplifies the analysis procedure. The assumptions made are:

1. The fluid is Newtonian, incompressible, has constant viscosity and the flow is laminar.
2. The lubricant at the liquid-solid region has perfect adhesion with the bearing surfaces.
3. Both rotating journal and sleeve is a rigid surface.
4. The pressure gradient and inertia towards the film thickness direction is negligible.
5. Pressure gradient at the radial clearance or film thickness is neglected as the clearance is too small.

From the Reynolds equation, the static characteristics can be determined based on the assumptions mentioned earlier [22]. The governing Equation (2.1) for this work is represented as:

$$\frac{\partial}{\partial x}\left[h^3 \frac{\partial p}{\partial x}\right] + \frac{\partial}{\partial z}\left[h^3 \frac{\partial p}{\partial z}\right] = 6\mu \left[U \frac{\partial h}{\partial x} + 2V\right] \tag{2.1}$$

Using and implementing boundary conditions, approximations, and theories are essential to ease and provides better numerical calculation as shown in Figure 2.3. In this research, Equation (2.1) is solved to acquire static oil film forces [22]. However, squeeze action is not considered as it is not within the scope of this research.

2.3.1 Boundary Conditions in Film Lubrication

Boundary conditions is necessary to solve the Reynolds equation. To simplify this, Figure 2.3 shows the classification of the boundary conditions. The classification of the boundary conditions are as follows;

a) *Reynolds Boundary Condition*

At position of $\theta = \pi + \delta$, the assumption made is that the oil film is neglected as the pressure and the pressure gradient are zero. Oil flow discontinuity at $\theta = \pi$ can be justified if using this boundary condition [1].

b) *Sommerfeld's Boundary Condition*

At this condition, the oil rupture is not calculated and the assumption made is that at $\theta = 0$ and $\theta = 2\pi$, the $p = 0$. The positive and negative pressures present are considered when using this boundary condition [5].

c) *Gumbel's Boundary Condition*

Like Sommerfeld's, the pressure is calculated without oil film rupture factor, but only the positive pressure is calculated. The negative pressure calculated will becomes zero at atmospheric pressure. This boundary condition is applicable when the bearing pressure is essentially high. The ranging point for this condition is $0 < \theta < \pi$, which is also known as Half-Sommerfeld boundary condition [5].
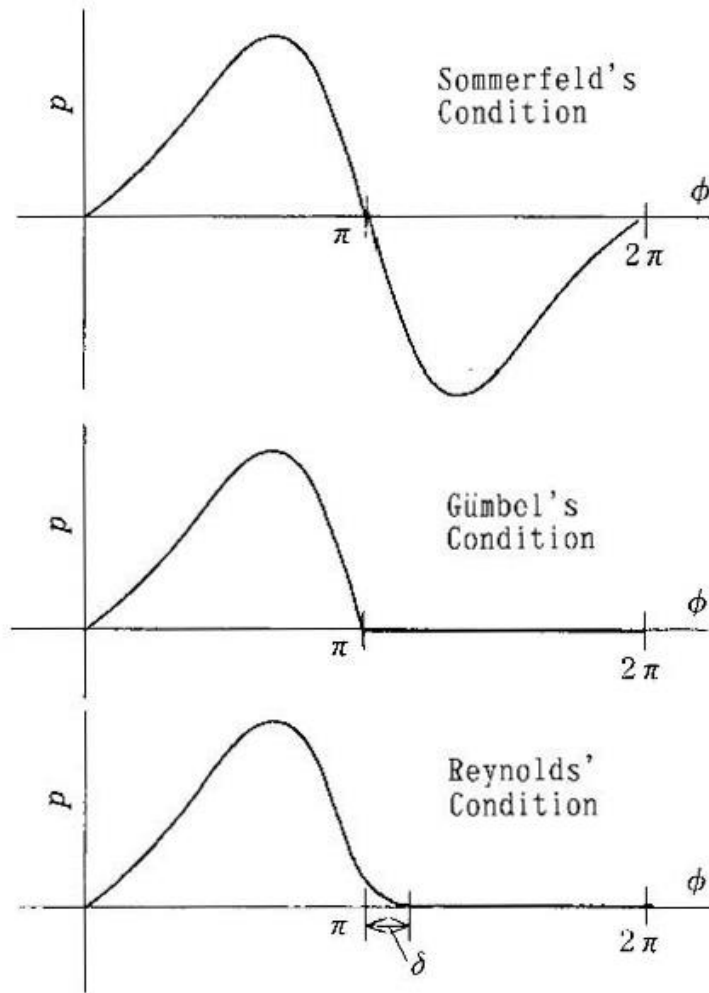
Figure 2.3: Types of boundary conditions in oil lubrication [29].

2.4 Hydrodynamic Journal Bearing

Hydrodynamic journal bearing is one of the most preferred bearing in real application compared to sliding and rolling element bearing. This is due to is advantage features in shock resistivity, long life, and its ability to absorb the vibration produced. These features come from the hydrodynamic pressure that produced to support the journal load inside the bearing as the load is directed normal to the journal. The cross-section of the full journal bearing is shown in Figure 2.3.

13
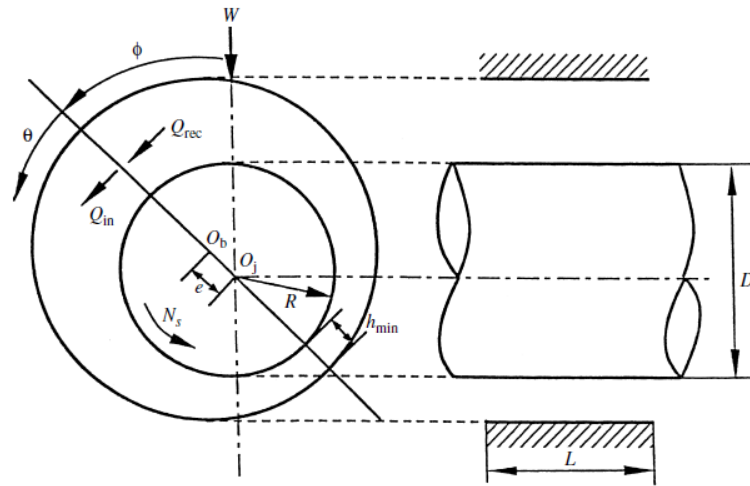
Figure 2.4: Journal bearing and its cross section [33].

In the mechanism of hydrodynamic journal bearing illustrated in Figure 2.4, the physical wedge mechanism caused hydrodynamic pressure distribution to occur [23, 37, 38]. Hydrodynamic lubrication consists of few characteristics in which:

1. The lubricant viscosity increases due to increase in pressure, in which occurs from the lubricant shear resistance.

2. As the speed increases, the thickness of fluid lubricant increases as well given that there is external load and lubricant viscosity.

3. Lubricant viscosity should be increased to attain high pressure with constant load.

4. Increased in viscosity leads to increase of lubricant friction.

5. For industrial bearings, 0.001 radian is the typical value for slope of solid surfaces.
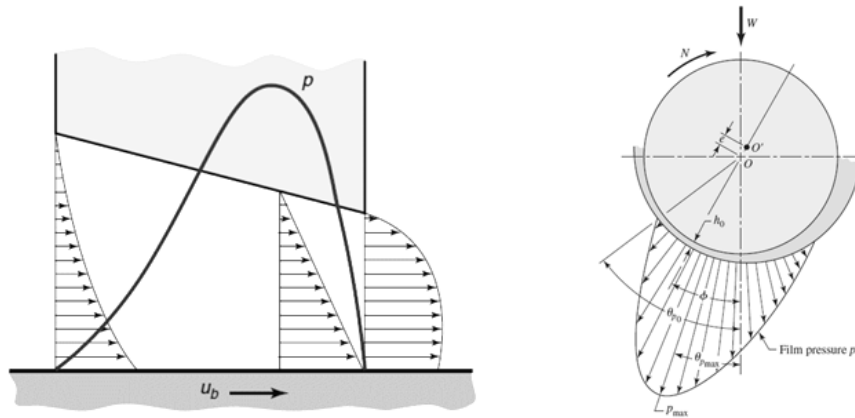
Figure 2.5: Wedge effect and pressure distribution of hydrodynamic journal bearing [30].

2.4.1 Classification of Journal Bearing

In hydrodynamic journal bearing design, there are three main groups that are classified based on its slenderness ratio. The slenderness ratio, or commonly known as L/D ratio is tabulated on Table 2.1 into long bearing, short bearing, and finite bearing. In this research however, the analysis only covers long and short journal bearing for the sake of convenience of the results obtained.

Table 2.1: Classification of hydrodynamic journal bearings [22,29,33].

Journal Bearing Subgroup	Slenderness Ratio
Long Bearing	$L/D \geq 2$
Short Bearing	$L/D = 0.25$
Finite Bearing	$0.25 < L/D < 1.5$

2.4.1.1 Long Journal Bearing (L/D ≥ 2)

Long journal bearing is defined as the slenderness ratio (L/D) is greater than 2 as shown in Figure 2.6 [1]. In this journal bearing characteristic based on Reynolds theory, the pressure distribution in circumferential direction is more significant compare to the pressure distribution in axial direction, which the pressure in axial direction can be neglected as shown in Equation (2.2) [22, 36]. In this case, the Reynolds boundary condition can be applied as mentioned previously.

$$\frac{\partial}{\partial x}\left[h^3 \frac{\partial p}{\partial x}\right] = 6\mu\left[U\frac{\partial h}{\partial x} + 2V\right] \tag{2.2}$$
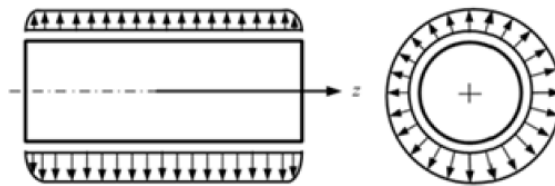
Figure 2.6: Long journal bearing [34].

2.4.1.2 Short Journal Bearing (L/D = 0.25)

For short journal bearing, the slenderness ratio is defined as L/D=0.25 as seen in Figure 2.7 [23]. Short journal bearing is classified when the length of the bearing is shorter than the diameter of the journal/shaft, which explains the low slenderness ratio. Compared to long journal bearing, the pressure at the axial direction is more significant than the pressure in circumferential direction based on short bearing theory and its approximations [35], which the circumferential pressure can be neglected as shown in Equation (2.3).

$$\frac{\partial}{\partial z}\left[h^3 \frac{\partial P}{\partial z}\right] = 6\mu\left[U\frac{\partial h}{\partial x} + 2V\right] \tag{2.3}$$

16
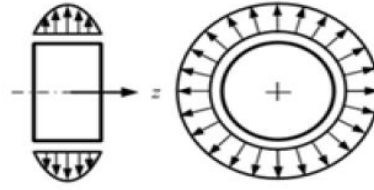
Figure 2.7: Short journal
bearing [34].

For hydrodynamic journal bearing is known with fixed bearing and rotating journal/shaft. At Figure 2.8, the hydrodynamic journal bearing is illustrated with a load carrying capacity noted as F, along the axis of the bearing. Pressure profiles are shown in circumferential and axial directions. Eccentricity effect presence due to an external force occurs on the journal surface, in which provides a convergent area between the bearing and the journal. In other case, the journal will be in concentric state and pressure profiles are unable to generate by the oil film. In general operation, the lubricant oil is pumped into the converging area when the journal rotates, thus generates a wedge action of the pressure profile. Cavitation effect occurs when the pressure drops back into the diverging area.
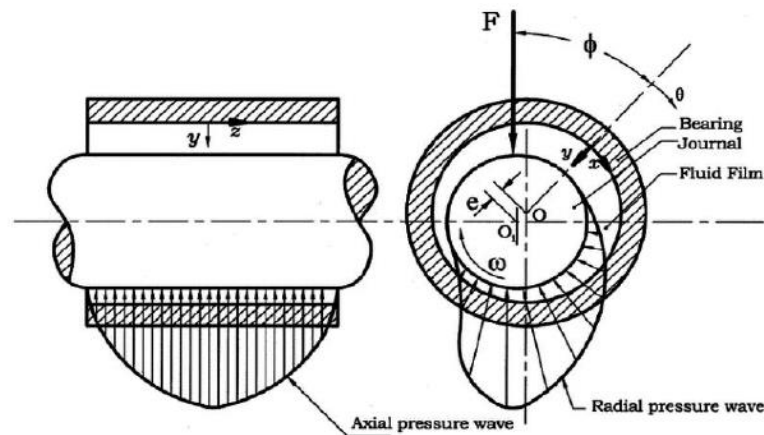
Figure 2.8: Load capacity with pressure profiles of axial and
circumferential directions [34].

17

2.4.2 Surface Texturing

Analysis of hydrodynamic journal bearing with texture surface is one of the most popular methods in improving its performance. It varies from the type of texture surface applied, surface texture location whether it is on the bearing surface or the journal itself, and many more. One of the most prominent research is done by Tonder [12]. His study regarding the effect of surface roughness on the load support shows that the presence of dimples or texture at the inlet of the sliding surface induced greater oil film pressure and load-carrying capacity. To extend his research, the effect of previous result is theoretically analyzed to prove that there is significant improvement at the inlet of sliding surface. In other case, Brizmer et. al. [14] acknowledged the effect of surface texture in improving sliding contacts. They analyzed the effect of micro-dimple on the parallel sliding surface by using laser surface texture (LST) technique which resulted it can provide support for load capacity. Some discoveries are found through numerical simulation in this research in which researchers can have better prediction in load support from the height ratio, textured segments, and the ratio of the bearing width to overall width. Partial texturing of regular micro-dimples resulted better load capacity provided that the journal bearing is operated at low eccentricity ratio ($\varepsilon < 0.3$). Even though partial texturing in low eccentricity operation provides higher load capacity, the stability of the journal bearing is affected in which will be crucial in long term operation. Meanwhile, full laser texturing provides better stability of the bearing, but it lowers the load capacity that the bearing can withstand, thus the selection of the parameter is required.

Another research that related to surface texturing is done by Shen et. al. [39], as the study is done towards the effect of dimple structures towards the load carrying capacity. The studies proved that dimple structures indeed change the load carrying capacity of hydrodynamic lubrication. The analysis is done with different dimple geometries, with different diameter and depth. Interestingly, the research is done in both numerical and experimental way to investigate how dimple structure affects the lubricant behavior. From the results, internal dimple structure greatly changes the load-carrying capacity of the hydrodynamic lubrication. Another observation that can be shown is that cylindrical dimples with rectangular cross-section resulted higher load capacity compared to cylindrical dimple with triangular cross-section. This is due to the

converging step shape in which enhanced pressure capacity of the structure. Other than that, larger dimple structures provided constant load capacity as compared to smaller dimple structures. The research also concluded that cylindrical shape provides better improvement in load capacity compared to other geometrical structures based on the comparisons made.
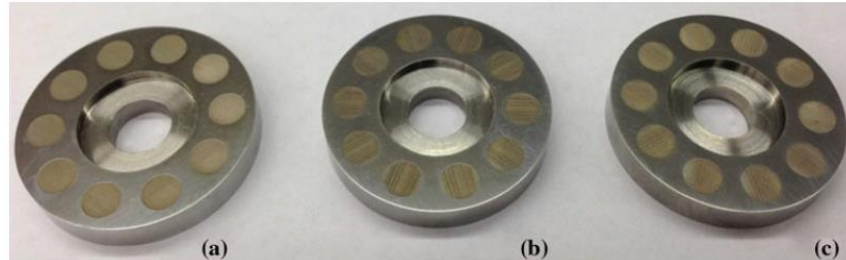
Figure 2.9: Specimen of large dimples; (a) R-shaped, (b) T2-shaped and (c) T1-shaped [39].

The analysis of surface texturing does not stop numerically and theoretically. Lu and Khonsari [40] in their research provided an experimental study of the dimple effect towards journal bearings by using machining and chemical etching technique. The research shows that specific parameters are required to achieve friction performance of journal bearings; namely amount of load, dimple size, shape, and depth. The etched dimple and machining samples can be seen at Figure 2.9. From the results, it is also shows that bearing surface with full etched dimples provide better frictional performance over partial etched dimples. Thus, another evidence is clear that surface texturing does not only improves load capacity, but also reduced hydrodynamic friction for better efficiency.

(a) Machined dimples   (b) Etched dimples
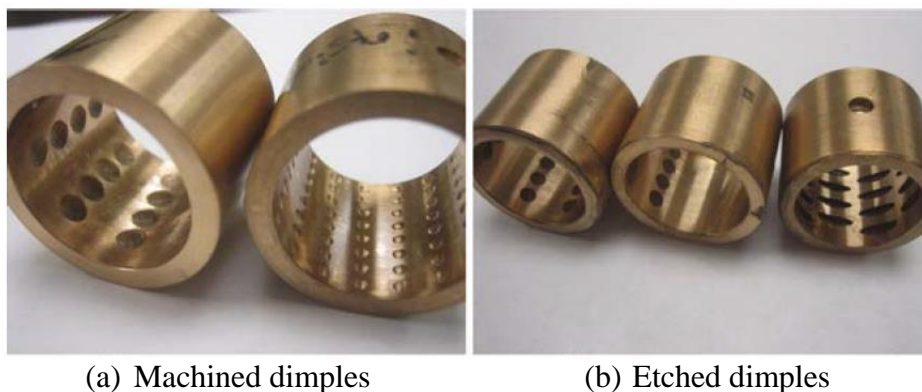
Figure 2.10: Samples of dimpled bushings [40].

The research mentioned above are some of the many examples of implementing surface texture to increase the hydrodynamic performance of journal bearings. Besides, it is also known and proved that partial texturing provides better performance of load capacity and friction reduction compared to full texturing method and also plain surface. Some of the related works done can be seen from Qiu and Khonsari [41], as they studied on the effect of surface texturing of the dimple shape towards the tribological performance. In this research, they used mass-conserving algorithm method to accommodate different surface roughness. From the results obtained, optimum size of dimple depth and its density could maximize the load-carrying capacity which is crucial during operation. Other characteristics of surface texturing such as partial texturing, texture region, orientation effect and shape effect are also discussed in this section [42-44].

In other discoveries, Cupillard et. al. [45] initially found that for low eccentricity ratio operation, the dimple depth needs to be less than the film thickness itself to ensure maximum performance. Later then, the work done is amended with some additional studies and also dimple configurations on the hydrodynamic journal bearing based from the research work done by Mishra et. al. [46]. In this research, the results were obtained in terms of load-carrying capacity and coefficient of friction by using CFD analysis integrated with numerical simulation. The analysis of the surface texturing effect in finite journal bearing is also extended by Kango and Sharma [47] by using non-Newtonian fluid, positive transverse, longitudinal roughness, and combined sinusoidal approach. In numerical analysis of non-Newtonian lubricant and surface texture, the modified Reynolds equation is solved by using finite difference method (FDM) to analyze bearing performances. From the results obtained, full wave roughness with transverse positive can maximize the load-carrying capacity and friction force when compared with other three values of roughness profiles. In addition, longitudinal roughness with sinusoidal profile is the best selection for friction reduction. Besides that, De Kraker et. al. [48] used governing Reynolds equation to study the surface texture effect in the fluid region. The analysis is done the investigate the dimple depth is greater than the minimum fluid film thickness in the fluid region towards the performance of journal bearing.

In different approach of the analysis of journal bearing performance, Kango et. al. [49, 50] analyzed the performance of finite journal bearing in which consist of various forms of surface texture and its location at the bearing surface. The analyzed is done by using FDM throughout governing Reynolds equation to determine the effect of surface texture towards bearings performance, in which proved that it improves bearing performance, regardless of the texture surface location at the bearing surface. Besides, Tala Ighil et. al. [51] has shown that proper surface texture configuration towards the contact surface can enhanced the journal bearing performances and characteristics. From various texture surface configurations, they found out that the lubricant film thickness has increased at the textured area. Even though the phenomenon occurred shows the significant effect towards the journal bearing, but applying surface texture towards the whole contact surface does not shows significant improvement. However, some progressive improvements can be seen through adequate texture size with regards to rotational speed of the bearing. In other approach, Tala Ighil et. al. [52] has studied the effect of the surface texture towards bearing performances. The comparison is done with and without the surface texture with respect to journal bearing characteristics and performances by using FDM as their numerical method. From the research, appropriate design of the texture surface geometry and its distribution greatly affects the minimum film thickness and maximum pressure. There are also various researches that enhanced the surface texturing to further improve the performance of the bearings specifically [74-82].

2.4.3 Boundary Slip

The assumption of the boundary condition in the Reynolds equation is that there is no-slip effect occurs between the two moving surfaces. However, based on the previous researchers done, the slip phenomenon did occur at molecularly smooth surface and micro-geometrical conditions [53-62]. The analysis of slip effect towards hydrodynamic lubrication begins when Spikes [56] conducted the investigation towards the half-wetted bearing. The Reynolds equation is modified to accommodate the slip phenomenon that occurs against the fixed surface. From the research, it is found that one-sided wall with slip surface could generates load support at critical shear stress.

The analysis also found that low friction value can be obtained at low convergence ratio bearings whereby the critical shear stress is zero. The second part of the Spikes' analysis concludes that slip phenomenon occurs at low shear stress which less than 10kPa or might possibly less than 1Pa [57]. In other research, Salant and Fortier [63, 64] extended the scope of the slip analysis in which by using a heterogeneous slip/no-slip surface configuration. The research shown that with proper surface pattern, the increase in load capacity and friction reduction can be achieved with zero critical shear stress. However, bearing instability will occur if the critical shear stress is nonzero. The research also compares the slip effect with the recess surface, resulted that the slip pattern act like a recess in which reducing the flow friction, but better even without the presence of the recess itself. Thus, the slip surface can be assumed to have the same capability in increasing load capacity and friction reduction.

Besides that, the interest in partial slip analysis is also brought up to investigate the effect towards the bearing characteristics. Rao [65] in his analysis investigates the effect of partial slip surface towards single-grooved slider and journal bearing by using Reynolds boundary condition. From the research, it is found that the partial slip condition on the slider bearing surface improves the dimensionless pressure distribution of the load applied, provided that the grooved surface further increase the improvements, meanwhile the partial slip on the journal bearing surface also improves the dimensionless pressure distribution. However, the results for both analyses also shown that the dimensionless shear stress is noticeably higher at the slip region, but decreases at the grooved region. The research is also supported the investigation done by Wu [66], in which the analysis is done with different eccentricity ratios at different slip regions. From the research findings, slip at the bearing surface has improve different advantages compared to plain bearing as the improvements is better at low eccentricity ratio. It is also found that location and slip zone size does affect the bearing characteristics. However, in different point of view, Wu and Ma [67] also raised some concerns regarding the abnormal behavior of the wall slip towards journal bearing performance. The parametric quadratic programming (PQP) method is used to investigate the wall slip problems. The results show that load capacity of the journal bearing decreases if two surfaces have the same lubricant with adhesion property. Other than that, hydrodynamic effect is also disappear and no-load support generated if the

wall slip is on opposite directions over lubricated surface. Besides, wall slip effect will be more complicated if both lubricated surface has different adhesion characteristics.

In different analysis of wall slip towards hydrodynamic lubrication, Lin et. al. [68] has done a numerical analysis on partial slip surface with shear flow towards slider bearing. The analysis only focused on the slider bearing to investigate the slip effect using numerical model. From the calculation made, wall slip surface on the slider bearing lowers the friction force, even though it was not caused by the location of slip zone. However, load capacity is affected by the location of slip zone, thus concludes that slip surface requires proper design in order to improve both load-carrying capacity and friction force. Aurelian et. al. [69] meanwhile investigate wall slip influences towards elastohydrodynamic journal bearing. By using finite element analysis, they found that wall slip surface provides better power loss compare to textured surface. However, both wall slip and textured surface does improve load-carrying capacity providing that the location of the wall slip/texture surface is properly designed. In addition, bearing performance could be decrease if texture surface or wall slip is wrongly selected. In overall, wall slip surface in hydrodynamic lubrication does improved the static performance, but some factors need to take into consideration such as bearing operating conditions, location of the wall slip on the surface, and type of bearing used.

2.4.4 Surface Texture with Slip Configuration

In another extend, researchers found that it is interesting to investigate the effect of wall slip and texture surface in one configuration in hydrodynamic lubrication. This is due to positive outcome obtained from the analysis done before. Tauviqirrahman et. al. [13] used modified Reynolds equation to investigate the surface configuration of slip and texture on a parallel sliding surface. From the analysis made, they found that wall slip condition gives better improvements towards pressure distribution compared to surface texturing. They also found that partial texturing contributes less improvement towards the load-carrying capacity, despite the surface texture is combined with a wall slip surface. They also agreed that partial texturing gives better improvements over full surface texturing. Rao et. al. [70] used different method which is narrow groove theory

(NGT) in analyzing parallel slider and concentric journal bearing with partially textured and slip surfaces. In their research, the surface configuration is analyzed using couple stress effect method, meanwhile one-dimensional analysis method based on modified Reynolds equation is used to identify the expression of dimensionless pressure and shear stress. Four parameters are measured in which the dimensionless texture length, ratio of land with slip to recess region, dimensionless recess depth, and also dimensionless slip coefficient. The analysis made shows that the slip with recess depth improves the dimensionless load capacity and coefficient of friction for both parallel slider and concentric journal bearings. It is also found that the improvement of partial texturing and slip depends on the slope parameter or eccentricity ratio, ranges from 0.0 to 0.3 respectively.

In different research, Rao et. al. [71] also investigates the effect of partially textured slip towards the load capacity in slider and journal bearing. The similar method is used which is NGT, which solely focused on the load capacity and pressure distribution. The results of the research show that the increase of texture with slip on land region improves the load capacity of the parallel slider and journal bearing. It is also concluded that texture surface and slip wall are the most significant factor in improving hydrodynamic performance of slider and journal bearings. The similar article is also presented which investigates the load carrying capacity improvement and reduction of friction coefficient [72, 73]. However, the method used for this approach is by using one-dimensional analysis of altered Reynolds equation. The method also proves that partially textured with slip on the bearing surface improves the dimensionless load capacity and reduces the friction coefficient. Surprisingly, the recess region shows better improvements over dimensionless slip parameter which different from the analysis mentioned previously. In overall, partial texturing with slip on the bearing surface carries great potential in improving hydrodynamic performance of journal bearing.

2.5 Summary of Literature Review

To simplify the extraction of information in the literature reviews, the critical sources are summarized in the form of tables for better representation of information and to identify the research gap as follows;

Table 2.2: Summary of literature reviews

Author	Method	Research Highlights
Tonder [12]	• Reynolds Equation	Generates hydrodynamic pressure and increase load capacity by roughing the plane inlet
Etsion [42]	• Reynolds • Experimental Study	Friction coefficient of LST lowered compared to plain bearing
Cupillard [45]	• Navier Stokes • CFD	Proved the analysis did by Tonder using CFD analysis
Tala-Ighil [51,52]	• Reynolds Equation • FDM	Location and shape of dimpled surface affected journal bearing performances
Brizmer [14]	• Theoretical Analysis	Theoretically analysed the potential of laser surface texturing (Full and Partial) in journal bearing
Kango [49,50]	• Numerical Model • Reynolds	Presence of micro-cavities enhance the journal bearing performance
Hamdavi [82]	• DuBois-Ocvirk • Reynolds Theory	Partially textured surface at the groove region improve the performance of short journal bearing
Shen & Khonsari [39]	• Reynolds • Mass-conserving analysis	Dimples internal structure directly affects the load carrying capacity of hydrodynamic lubrication
Craig [53]	• Experimental	The occurrence of partial boundary slip from the forces generated in an aqueous Newtonian fluid
Spikes [56,57]	• Modified Reynolds Equation	Analysed the slip surface application and lubrication model. (Extended Reynolds Equation)
Salant & Fortier [63,64]	• Reynolds Equation	Modified Reynolds equation to analyse the heterogenous slip/no-slip of slider bearing
Aurelian [69]	• FEM	FEM analysis on wall slip effect on fluid bearings
Rao [70-73]	• Reynolds Equation	Partial textured slip on grooved journal bearing improved the bearing performance at high eccentricity ratio
Tauviqirrahman [13]	• Reynolds Equation	Analysed the combination of texture and slip in a mathematical modelling of parallel sliding surface
Lin [68]	• Numerical Analysis • Double Parameters	Large area of texture and slip surface using double parameter method

2.6 Research Gap

Efficiency and performance of hydrodynamic journal bearing that operates in various conditions is one of the major concerns for the engineers. The high demand of hydrodynamic journal bearing to be used in the rotating systems requires better innovation improve its performance. These bearings are classified into long bearing and short bearing which based on their slenderness (L/D) ratio. Even though journal has lot of advantages over other types of bearing, but the concerns of lubrication and improving its characteristics further. As mentioned on the previous sub-sections, surface texturing, and wall slip surface are the most common method in improving the hydrodynamic performance of journal bearings. However, the performance of partially textured with slip surface on these three types of grooved journal bearings are not well mentioned and carried out in the literature. Hence, the new research in which implements the partially textured with slip surface towards the above-mentioned types of grooved journal bearing would be beneficial for the new studies.

2.7 Chapter Summary

This chapter covers the comprehensive overview of the lubrication, surface texturing, wall slip, and tribology literature. The discussion is made based on the most relevant scientific sources and research activities related in this area. It is also mentioned that the governing Reynolds equation with necessary modification and its boundary conditions towards the hydrodynamic journal bearing are discussed in detailed manner. Static characteristics such as load capacity and pressure distribution are introduced by using suitable figures and references obtained. In addition, surface texturing has been shown with different geometrical shapes and the wall slip is presented in various configurations. In general, it is interestingly found that both surface texturing and wall slip surface delivers a better performance for hydrodynamic journal bearings to operate at higher load capacities and better efficiency.

CHAPTER 3

METHODOLOGY

3.1 Overview

This chapter covers the methodology and approaches applied in this research study to achieve the research objectives. The methodology that will be discussed is the performance of surface texture with slip in hydrodynamic journal bearings. The equation that will be used is the governing Reynolds equation. To make the research convenience as the analysis involved two set of journal bearings: long bearing and short bearing, different theories are applied towards the governing Reynolds equation. From the sets of analysis made, the static characteristics in which comprises the load carrying capacity and pressure distribution are calculated. As for a reference, hydrodynamic journal bearing is noted as plain bearing when the entire surface has no surface texture and wall slip applied. In addition, the plain bearing model constructed were developed into hydrodynamic journal bearing with textured surface and wall slip models by applying texture length (θ_t), texture depth $(H_{g)}$, end texture width (θ_g), number of textures applied (n), and slip parameter (A) at different eccentricity ratios. At the end at this chapter, the numerical methods for proposed configuration of hydrodynamic journal bearings is proposed.

3.2 Research Design

To develop a comprehensive journal bearing model for long bearing and short bearing, appropriate procedures should be under attention. Figure 3.1 shows the overall procedure steps of methodology. The procedure begins with study of literature review and data re-modelling to construct the base model for further development. The following steps are explained in this procedure:

1. Initial step for the development of the model and evaluation of hydrodynamic journal bearings are based from the literature review and model programming for long bearing [72] and short bearing [81].

2. The plain bearing is used a baseline model for the hydrodynamic journal bearing proposed based on literature reviews.

3. The long and short bearing for hydrodynamic journal bearing models are developed to analyze the effect of surface texturing and wall slip towards performance of the bearing (load capacity, shear stress, pressure distribution, and coefficient of friction).

4. The validation is done by the comparison of the results obtained with the plain bearing model developed in Step 2 with the proposed hydrodynamic journal bearing model as referred at Step 3. The plain journal bearing model is taken as the validation benchmark as it is validated from previous literatures by duplicating the methods applied and comparing the results.

5. The final step of this procedure is presentation of the results obtained and the discussion for all the performance outcome of hydrodynamic journal bearings.

From the procedure steps mentioned above, Reynolds equation is required to develop the proposed journal bearing model. Reynolds equation is then modified accordingly for long and short bearing to accommodate hydrodynamic journal bearing model as summarized in Figure 3.2. From there, the performance analysis is carried out in which leads to the pressure distribution, load-carrying capacity, shear stress and friction coefficient required. The method used is discussed further in this chapter, meanwhile the Chapter 4 and 5 will further discussed about the results obtained, discussions and conclusions.
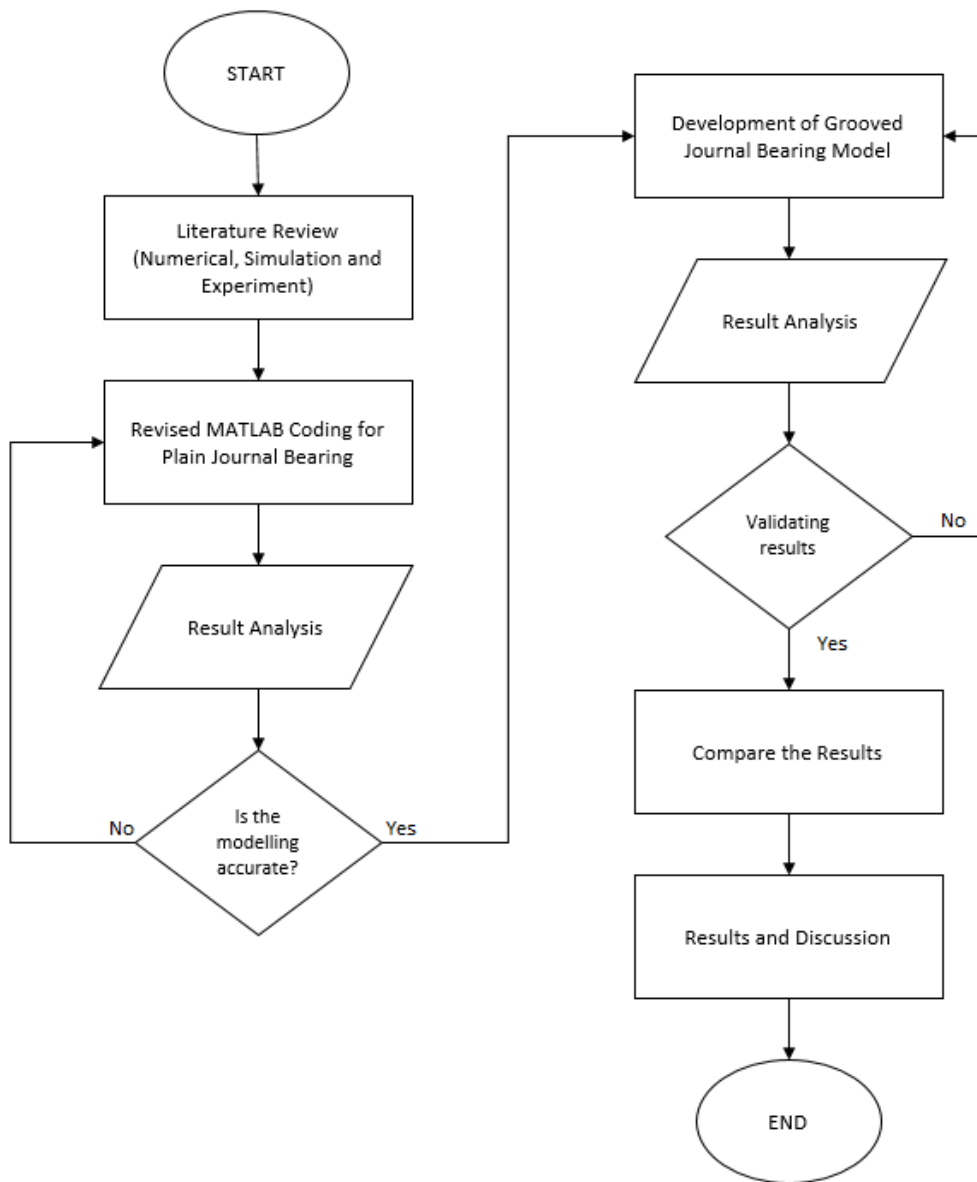
Figure 3.1: Research Flowchart.
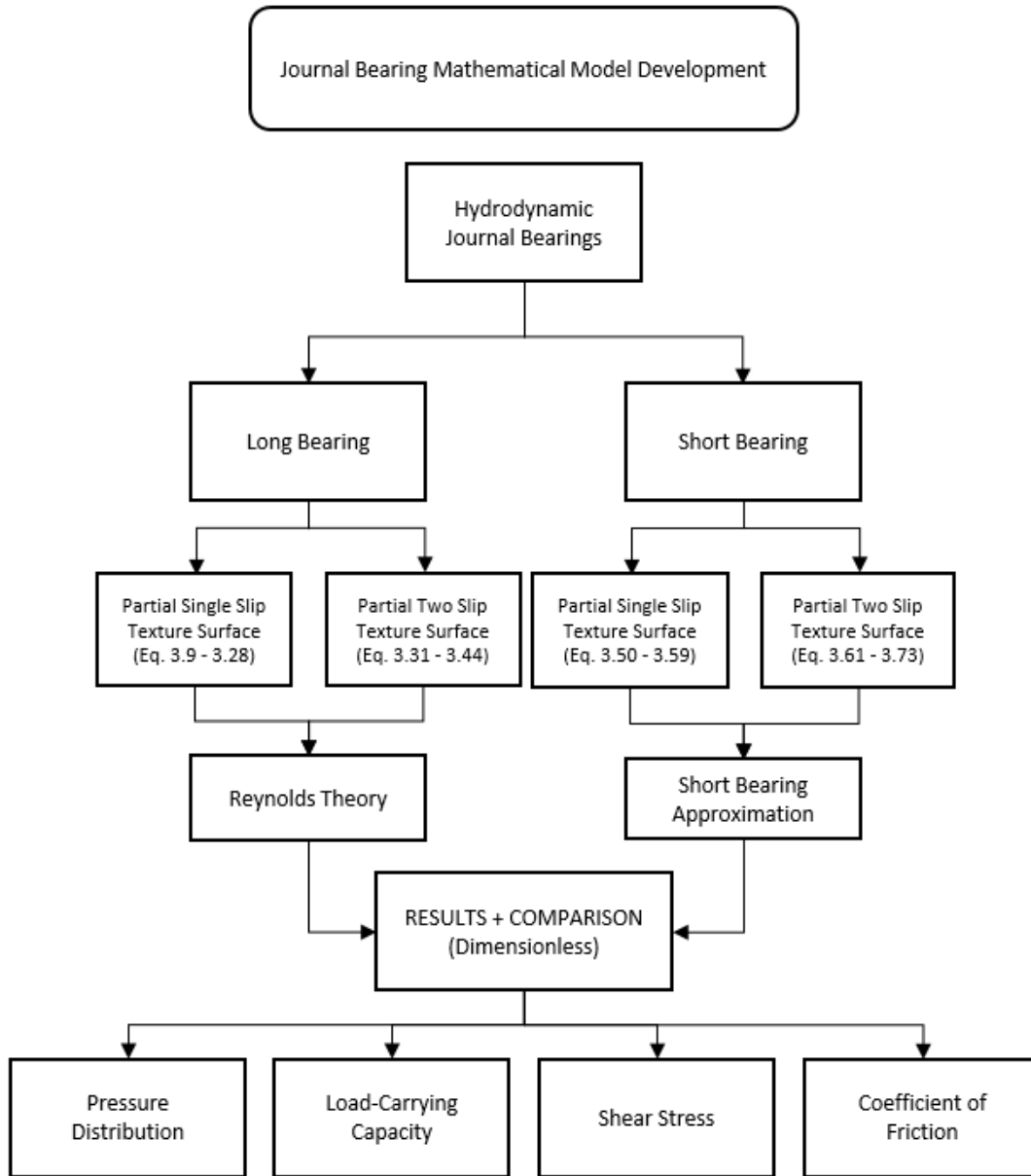
Figure 3.2: Procedure of developing the bearing model.

In this research, the developed model of journal bearing with single-slip partial textured surface is shown in Figure 3.3, and the Figure 3.4 shows the journal bearing with two-slip partial textured surface. The textured region (θ_t) consist of alternate land applied with slip and recess sections with no slip, in which has following parameters; slip to no-slip ratio magnitude (γ), textured region length (θ_t), number of slip region (n), texture depth (H_g), and end texture length (θ_g). The following parameters is varied into sets of values shown below:

1. The slip to no-slip ratio magnitude is set to values of 0.2, 0.5, and 0.6.

2. Textured region length is set into values ranging from 40º and 120º

3. Number of slip region is set into 2, 4, and 6 in every analysis respectively.

4. The texture depth is set in three different value, 0.2, 0.5, and 0.6 while the fixed texture width, (θ_g) is fixed to 150º of the starting point to the end of the circumferential length (180º).

For load capacity and friction coefficient analysis, the eccentricities ratio (ε) of the operated journal bearings are ranging from 0.1 to 0.8, while the eccentricity ratio is set to 0.1 for pressure distribution and shear stress analysis. The parameters range of values are selected based on average range used from previous research such as Tauviqirrahman et. al. [13], Hamdavi et. al. [81], and Rao et. al. [70-73] to reduce the complexity of the comparison and validation of data obtained.
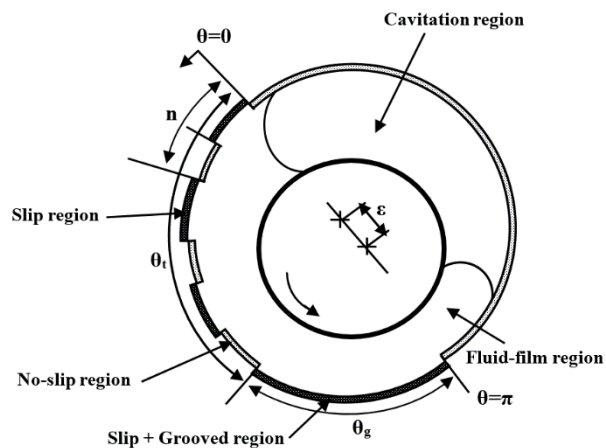
Figure 3.3: Grooved journal bearing with single-slip partial texture model.
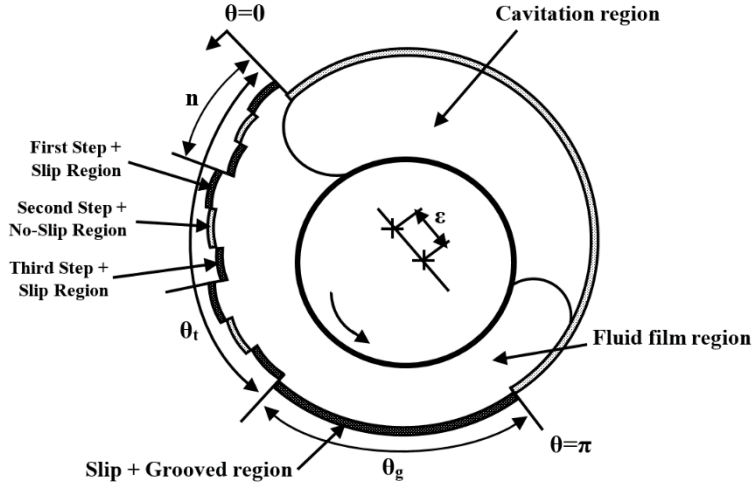
Figure 3.4: Grooved journal bearing with two-slip partial
texture model.

3.3 Long Journal Bearing

Long journal bearing is defined as the bearing is described as 'infinitely long'. In this description, the circumferential pressure is greater compared to the axial pressure. Figure 3.4 shows the schematic diagram of the long journal bearing, in which the bearing length (L) is longer than the journal bearing diameter (D). Thus, expression of the slenderness ratio is shown in $L > D$.

3.3.1 Partial Single-slip Texture Surface

From the Figure 3.3, the textured region θ_t consist of successive slip at the recess sections and no-slip at the land sections on the bearing surface. The angular length of the slip at recess region is known as $\theta_{1,2} - \theta_{1,1} = \cdots = \theta_{n,2} - \theta_{n,1} = \theta_s$, meanwhile the angular length of the no-slip with land region is marked as $\theta_{1,3} - \theta_{1,2} = \cdots = \theta_{n,3} - \theta_{n,2} = \theta_n$. At the end of the textured region θ_t, the end textured region is applied with slip surface in which marked as $\theta_g - \theta_t$.

The momentum equation of the pressure in the journal bearing is shown in Equation (3.1) is in the function of sliding direction of x-axis;

$$\frac{dp}{dx} = \mu \frac{d^2u}{dy^2} \qquad (3.1)$$

Navier slip boundary conditions are applied on θ_s and $\theta_g - \theta_t$, meanwhile no-slip conditions are applied on the other part of the plain surface. Thus, the boundary conditions for velocity at the journal and bearing surface are;

At $y = 0$, $u = U$ and at point $y = h$, $u = -\alpha\mu \frac{du}{dy}$ $\qquad (3.2)$

Equation (3.2) is then integrated at x-direction for velocity component, thus providing boundary conditions in Equation (3.3);

$$u = \frac{1}{2\mu}\left[y^2 - \frac{yh(h + 2\alpha\mu)}{h + \alpha\mu}\right]\frac{dp}{dx} + U\left(1 - \frac{y}{h + \alpha\mu}\right) \qquad (3.3)$$

The continuity equation across the film is show in Equation (3.4);

$$q_x = \int_0^h u \, dy \qquad (3.4)$$

By integrating the continuity equation and substitute from Equation (3.3) into Equation (3.4), the partial slip surface is formed into classical Reynolds equation;

$$\frac{d}{dx}\left[\frac{h^3(h + 4\alpha\mu)}{12\mu(h + \alpha\mu)}\frac{dp}{dx}\right] = \frac{U}{2}\frac{d}{dx}\left[\frac{h(h + 2\alpha\mu)}{(h + \alpha\mu)}\right] \qquad (3.5)$$

From Equation (3.5), the dimensionless form of partial slip surface in modified Reynolds equation is;

$$\frac{d}{d\theta}\left[\frac{H^3(H + 4A)}{12\mu(H + A)}\frac{dp}{dx}\right] = \frac{1}{2}\frac{d}{d\theta}\left[\frac{H(H + 2A)}{(H + A)}\right] \qquad (3.6)$$

Taken into consideration that the texture region θ_t and end texture region θ_g consist of dimensionless film thickness in which expressed as $H' = H + H_g$, which;

$$H = (1 + \varepsilon \cos \theta) \tag{3.7}$$

From the Figure, the boundary conditions of the slip and no slip at textured region are defined respectively;

$$P|_{\theta=0} = 0, P|_{\theta=\theta_{1,2}} = P_{1,2} \quad \text{and} \quad P|_{\theta=\theta_{1,3}} = P_{1,3} \tag{3.8}$$

Equation (3.6) obtained earlier is then integrated with respect to the dimensionless pressure profiles of the slip and no-slip regions respectively, resulting new sets of equation below;

$$\frac{dP}{d\theta}\left(0 \le \theta \le \theta_{1,2}\right) = \frac{6(H' + 2A)}{H'^2(H' + 4A)} - \frac{12(H' + A)Q}{H'^3(H' + 4A)} \tag{3.9}$$

$$\frac{dP}{d\theta}\left(\theta_{1,2} \le \theta \le \theta_{1,3}\right) = \frac{6}{H^2} - \frac{12Q}{H^3} \tag{3.10}$$

From the boundary conditions identified in Equation (3.8), both Equation (3.9) and Equation (3.10) is then integrated together with respect to boundary conditions mentioned, obtaining a series of dimensionless pressure for slip and no-slip region, respectively;

$$P\left(0 \le \theta \le \theta_{1,2}\right) = P|_{\theta=0} + 6 \int_0^{\theta_{1,2}} \frac{(H'+2A)}{H'^2(H'+4A)} d\theta -$$
$$12Q \int_0^{\theta_{1,2}} \frac{(H'+A)}{H'^3(H'+4A)} d\theta \tag{3.11}$$

$$P(\theta_2 \le \theta \le \theta_3) = P|_{\theta=\theta_{1,2}} + 6 \int_{\theta_{1,2}}^{\theta_{1,3}} \frac{1}{H^2} d\theta - 12Q \int_{\theta_{1,2}}^{\theta_{1,3}} \frac{1}{H^3} d\theta \tag{3.12}$$

In terms of different number of regions involved n, the boundary conditions for θ_s and θ_n sections are defined as;

$$P|_{\theta=\theta_{n,1}} = P_{\theta=\theta_{n-1,3}}, P|_{\theta=\theta_{n,2}} = P_{n,2} \quad \text{and} \quad P|_{\theta=\theta_{n,3}} = P_{n,3} \tag{3.13}$$

From the newly defined boundary conditions in different number of regions parameter, Equation (3.6) is then integrated in which yields the dimensionless pressure with slip and no slip profiles for number of regions n;

$$P\left(\theta_{n,1} \leq \theta \leq \theta_{n,2}\right) = P_{\theta=\theta_{n-1,3}} + 6 \int_{\theta_{n,1}}^{\theta_{n,2}} \frac{(H'+2A)}{H'^2(H'+4A)} d\theta -$$
$$12Q \int_{\theta_{n,1}}^{\theta_{n,2}} \frac{(H'+A)}{H'^3(H'+4A)} d\theta$$

(3.14)

$$P\left(\theta_{n,2} \leq \theta \leq \theta_{n,3}\right) = P|_{\theta=\theta_{n,2}} + 6 \int_{\theta_{n,2}}^{\theta_{n,3}} \frac{1}{H^2} d\theta - 12Q \int_{\theta_{n,2}}^{\theta_{n,3}} \frac{1}{H^3} d\theta$$

(3.15)

At the end section $\theta_g - \theta_t$, since the profile is similar with recess with slip region, therefore the boundary conditions and the pressure profiles are similar.

$$P|_{\theta=\theta_t} = P_{\theta_t} \quad \text{and} \quad P|_{\theta=\theta_g} = P_{\theta_g}$$

(3.16)

$$P\left(\theta_t \leq \theta \leq \theta_g\right) = P_{\theta=\theta_t} + 6 \int_{\theta_t}^{\theta_g} \frac{(H'+2A)}{H'^2(H'+4A)} d\theta -$$
$$12Q \int_{\theta_t}^{\theta_g} \frac{(H'+A)}{H'^3(H'+4A)} d\theta$$

(3.17)

The dimensionless pressure throughout and perpendicular to the centre line obtained from Equation (3.14), (3.15), and (3.17) is further undergo an integration that gives the dimensionless radial and tangential load carrying capacity;

$$W_\varepsilon = -\left[\int_{\theta_{n,1}}^{\theta_{n,2}} P \cos\theta \, d\theta + \int_{\theta_{n,2}}^{\theta_{n,3}} P \cos\theta \, d\theta + \right.$$
$$\left. \int_{\theta_{n,3}}^{\theta_{n,4}} P \cos\theta \, d\theta + \cdots + \int_{\theta_t}^{\theta_g} P \cos\theta \, d\theta \right]$$

(3.18)

$$W_\emptyset = \left[\int_{\theta_{n,1}}^{\theta_{n,2}} P \sin\theta \, d\theta + \int_{\theta_{n,2}}^{\theta_{n,3}} P \sin\theta \, d\theta + \right.$$
$$\left. \int_{\theta_{n,3}}^{\theta_{n,4}} P \sin\theta \, d\theta + \cdots + \int_{\theta_t}^{\theta_g} P \sin\theta \, d\theta \right]$$

(3.19)

Both radial and tangential load carrying capacity is then can be used to obtain the dimensionless load-carrying capacity intended for the research;

$$W = \sqrt{W_\varepsilon^2 + W_\emptyset^2} \qquad (3.20)$$

The shear stress is originally expressed as;

$$\tau_{xy} = -\mu \frac{du}{dy} \qquad (3.21)$$

For the journal bearing at $y = 0$, the shear stress defined in Equation (3.21) is then become;

$$\tau_{xy}|_{y=0} = \frac{1}{2}\left[\frac{h(h + 2\alpha\mu)}{h + \alpha\mu}\right]\frac{dp}{dx} + \frac{\mu U}{h + \alpha\mu} \qquad (3.22)$$

From the expression in Equation (3.22), the non-dimensional form of shear stress is obtained for the sake of convenience of the outcome;

$$\Pi|_{y=0} = \frac{1}{2}\left[\frac{H(H + 2A)}{H + A}\right]\frac{dP}{d\theta} + \frac{1}{H + A} \qquad (3.23)$$

Therefore, the non-dimensional shear stress for each surface regions defined accordingly as follows;

$$\Pi\big(\theta_{n,1} \leq \theta \leq \theta_{n,2}\big) = -\frac{6Q(H' + 2A)}{H'^2(H' + 4A)} + \frac{4(H' + 3A)}{H'(H' + 4A)} \qquad (3.24)$$

$$\Pi\big(\theta_{n,2} \leq \theta \leq \theta_{n,3}\big) = -\frac{6Q}{H^2} + \frac{4}{H} \qquad (3.25)$$

$$\Pi\big(\theta_t \leq \theta \leq \theta_g\big) = -\frac{6Q(H' + 2A)}{H'^2(H' + 4A)} + \frac{4(H' + 3A)}{H'(H' + 4A)} \qquad (3.26)$$

To obtain the coefficient of friction, C_f, the friction force, F is required by integrating the shear stress along the bearing surface. Then, the friction force obtained is divided by load capacity to obtain friction coefficient as shown;

$$F = \int_0^{\theta_r} \Pi \, d\theta \qquad (3.27)$$

$$C_f = \left(\frac{R}{C}\right)\frac{f}{w} = \frac{F}{W} \tag{3.28}$$

3.3.2 Partial Two-slip Texture Surface

For the partial two-slip texture configuration as shown in Figure 3.4, the method of analysis is the same as partial single-slip texture. However, the noticeable difference is the additional surface region in between in which expressed below. The angular length of the first step with slip region is known as $\theta_{1,2} - \theta_{1,1} = \cdots = \theta_{n,2} - \theta_{n,1} = \theta_{r1}$, meanwhile the angular length of the second step without slip region is marked as $\theta_{1,3} - \theta_{1,2} = \cdots = \theta_{n,3} - \theta_{n,2} = \theta_{r2}$, and the angular length at third step with slip is defined as $\theta_{1,4} - \theta_{1,3} = \cdots = \theta_{n,4} - \theta_{n,3} = \theta_n$. At the end of the textured region θ_t, the end textured region is applied with slip surface in which marked as $\theta_g - \theta_t$.

The boundary conditions of each surface feature at textured and end textured region are defined respectively;

$$P|_{\theta=0} = 0,\ P|_{\theta=\theta_{n-1,2}} = P_{n,2}\ ,\ P|_{\theta=\theta_{n,3}} = P_{n,3}\ ,P|_{\theta=\theta_{n,4}} = P_{n,4} \tag{3.29}$$

$$P|_{\theta=\theta_t} = P_{\theta_t}\ \text{ and }\ P|_{\theta=\theta_g} = P_{\theta_g}$$

The film thickness at first step and second step recess areas are H' and H'' respectively where;

$$H = (1 + \varepsilon\ cos\theta),\ H' = H + H_g\ \text{and}\ H'' = H + \frac{1}{2}H_g \tag{3.30}$$

From the conditions defined above, the dimensionless pressure profile of the textured region, θ_t are define from the equation below;

$$\frac{dP}{d\theta}\left(\theta_{n,1} \le \theta \le \theta_{n,2}\right) = \frac{6(H' + 2A)}{H'^2(H' + 4A)} - \frac{12(H' + A)Q}{H'^3(H' + 4A)} \tag{3.31}$$

$$\frac{dP}{d\theta}(\theta_{n,2} \leq \theta \leq \theta_{n,3}) = \frac{6}{H''^2} - \frac{12Q}{H''^3} \tag{3.32}$$

$$\frac{dP}{d\theta}(\theta_{n,3} \leq \theta \leq \theta_{n,4}) = \frac{6(H+2A)}{H^2(H+4A)} - \frac{12Q(H+A)}{H^3(H+4A)} \tag{3.33}$$

Equations (3.31), (3.32), and (3.33) is then integrated together with respect to boundary conditions mentioned in Equation (3.29), obtaining a series of dimensionless pressure for slip and no-slip region, respectively;

$$P(\theta_{n,1} \leq \theta \leq \theta_{n,2}) = P|_{\theta=0} + 6 \int_0^{\theta_{n,2}} \frac{(H'+2A)}{H'^2(H'+4A)} d\theta - \\ 12Q \int_0^{\theta_{n,2}} \frac{(H'+A)}{H'^3(H'+4A)} d\theta \tag{3.34}$$

$$P(\theta_{n,2} \leq \theta \leq \theta_{n,3}) = P|_{\theta=\theta_{1,2}} + 6 \int_{\theta_{n,2}}^{\theta_{n,3}} \frac{1}{H''^2} d\theta - 12Q \int_{\theta_{n,2}}^{\theta_{n,3}} \frac{1}{H''^3} d\theta \tag{3.35}$$

$$P(\theta_{n,3} \leq \theta \leq \theta_{n,4}) = P|_{\theta=\theta_{1,3}} + 6 \int_{\theta_{n,3}}^{\theta_{n,4}} \frac{(H+2A)}{H^2(H+4A)} d\theta - \\ 12Q \int_{\theta_{n,3}}^{\theta_{n,4}} \frac{(H+A)}{H^3(H+4A)} d\theta \tag{3.36}$$

$$P(\theta_t \leq \theta \leq \theta_g) = P_{\theta=\theta_t} + 6 \int_{\theta_t}^{\theta_g} \frac{(H'+2A)}{H'^2(H'+4A)} d\theta - \\ 12Q \int_{\theta_t}^{\theta_g} \frac{(H'+A)}{H'^3(H'+4A)} d\theta \tag{3.37}$$

From the expressions above, the dimensionless radial and tangential load carrying capacity are obtained together;

$$W_\varepsilon = - \left[\int_{\theta_{n,1}}^{\theta_{n,2}} P \cos\theta \, d\theta + \int_{\theta_{n,2}}^{\theta_{n,3}} P \cos\theta \, d\theta + \\ \int_{\theta_{n,3}}^{\theta_{n,4}} P \cos\theta \, d\theta + \cdots + \int_{\theta_t}^{\theta_g} P \cos\theta \, d\theta \right] \tag{3.38}$$

$$W_\emptyset = \left[\int_{\theta_{n,1}}^{\theta_{n,2}} P \sin\theta \, d\theta + \int_{\theta_{n,2}}^{\theta_{n,3}} P \sin\theta \, d\theta + \\ \int_{\theta_{n,3}}^{\theta_{n,4}} P \sin\theta \, d\theta + \cdots + \int_{\theta_t}^{\theta_g} P \sin\theta \, d\theta \right] \tag{3.39}$$

Then the dimensionless load carrying capacity is calculated;

38

$$W = \sqrt{W_\varepsilon^2 + W_\phi^2} \qquad (3.40)$$

The non-dimensional shear stress for partial two-slip texture surface at each surface regions are defined respectively;

$$\Pi\big(\theta_{n,1} \le \theta \le \theta_{n,2}\big) = -\frac{6Q(H' + 2A)}{H'^2(H' + 4A)} + \frac{4(H' + 3A)}{H'(H' + 4A)} \qquad (3.41)$$

$$\Pi\big(\theta_{n,2} \le \theta \le \theta_{n,3}\big) = -\frac{6Q}{H''^2} + \frac{4}{H''} \qquad (3.42)$$

$$\Pi\big(\theta_{n,3} \le \theta \le \theta_{n,4}\big) = -\frac{6Q(H + 2A)}{H^2(H + 4A)} + \frac{4(H + 3A)}{H(H + 4A)} \qquad (3.43)$$

$$\Pi\big(\theta_t \le \theta \le \theta_g\big) = -\frac{6Q(H' + 2A)}{H'^2(H' + 4A)} + \frac{4(H' + 3A)}{H'(H' + 4A)} \qquad (3.44)$$

Similar method from Equation (3.27) and (3.28) are applied to obtain the friction force, F and the coefficient of friction, C_f.

3.4 Short Journal Bearing

Compared to long journal bearing, short journal bearing is defined when the length of the bearing (L) is lower than the diameter of the journal (D). In this condition, the short bearing approximation of Dubois and Ocvirk is applied for steady state condition in which known as the journal axes is parallel to bearing axes. To obtain the expressions required for short journal bearing, the modified Reynolds equation and Half-Sommerfeld boundary condition is used. The results obtained is validated from the plain bearing done by Rao [82], with the same operating conditions.

The Dubois-Ocvirk short bearing approximation applied on the modified Reynolds equation for short journal bearing is expressed as;

$$\frac{\partial}{\partial z}\left(h^3 \frac{\partial}{\partial z}\right) = 6\mu U \frac{\partial h}{\partial x} \qquad (3.45)$$

The film thickness H and H' can be expressed as;

$$H = 1 + \varepsilon \cos \theta \text{ and } H' = H_g + H \tag{3.46}$$

In Half-Sommerfeld boundary conditions, the respective assumption is considered;

$$p = 0 \text{ at } z = \pm \frac{L}{2}$$

Equation (3.34) is the integrated twice with respect to z and by applying boundary conditions at Equation (3.46), the pressure is known as;

$$p = \frac{3\mu\omega}{h^3} \frac{dh}{d\theta}\left(z^2 - \frac{L^2}{4}\right) \tag{3.47}$$

From the short bearing approximation method, the pressure profiles for slip and no slip are derived respectively;

$$P_1 = 12 \left(\frac{L}{D}\right)^2 \left(\frac{1 + 2A}{1 + 4A}\right)\left(\frac{1}{H^3}\right)\frac{\partial H}{\partial \theta}\left(z^2 - \frac{1}{4}\right) \tag{3.48}$$

$$P_2 = \left(\frac{12}{H^3}\right)\left(\frac{L}{D}\right)^2 \frac{\partial H}{\partial \theta}\left(z^2 - \frac{1}{4}\right) \tag{3.49}$$

3.4.1 Partial Single-slip Texture Surface

In these expressions derived, the coordinate system is located at the middle along the bearing length L. By applying the expression of film thickness in Equation (3.35) and neglecting the diverging wedge pressure, the pressure profile $(z = 0)$ at the slip $P(\theta_{n,1} \leq \theta \leq \theta_{n,2})$ and no-slip region $P(\theta_{n,2} \leq \theta \leq \theta_{n,3})$, and the end textured region $(\theta_t \leq \theta \leq \theta_g)$ is known as P_1, P_2, and P_g respectively.

$$P_1 = 3 \left(\frac{L}{D}\right)^2 \left(\frac{1 + 2A}{1 + 4A}\right)\left(\frac{1}{H'^3}\right)\frac{\partial H}{\partial \theta} \tag{3.50}$$

$$P_2 = \left(\frac{12}{H^3}\right)\left(\frac{L}{D}\right)^2 \frac{\partial H}{\partial \theta}\left(\frac{1}{4}\right) \tag{3.51}$$

$$P_g = 3 \left(\frac{L}{D}\right)^2 \left(\frac{1 + 2A}{1 + 4A}\right)\left(\frac{1}{H'^3}\right)\frac{\partial H}{\partial \theta} \tag{3.52}$$

40

Considering the journal is in equilibrium, the load-carrying capacity can be obtained by determining radial and tangential load capacity for each pressure profile defined earlier;

$$F_\varepsilon = \iint P_o \cos\theta \ dz \ d\theta \tag{3.53}$$

$$F_\emptyset = \iint P_o \sin\theta \ dz \ d\theta \tag{3.54}$$

Thus, the dimensionless load capacity of short journal bearing can be computed;

$$W = \sqrt{F_\varepsilon{}^2 + F_\emptyset{}^2} \tag{3.55}$$

To determine the dimensionless shear stress of journal bearing, the expressions from Equation (3.22) is used as the condition of journal bearing is still the same. However, the assumption made is the flow due to pressure gradient in x-direction is neglected, which the shear stress for short bearing is further simplified.

$$\frac{dP}{d\theta} = 0 \tag{3.56}$$

$$\Pi_1 = \frac{6Q(H' + 2A)}{H'^2(H' + 4A)} \tag{3.57}$$

$$\Pi_2 = \frac{6Q}{H^2} \tag{3.58}$$

$$\Pi_g = \frac{6Q(H' + 2A)}{H'^2(H' + 4A)} \tag{3.59}$$

As the dimensionless shear stress for each surface region are defined, the coefficient of friction C_f can be derived by using similar approach from the long journal bearing analysis in Equation (3.27) and (3.28).

3.4.2 Partial Two-slip Texture Surface

For partial two-slip texture surface, the method and derivation process are still similar as before. The only addition with respect to extra depth on texture length θ_t is applied in which the film thickness is the same with Equation (3.30).

$$H = (1 + \varepsilon \cos\theta), \ H' = H + H_g \text{ and } H'' = H + \frac{1}{2}H_g \qquad (3.60)$$

From the defined film thickness in Equation (3.58), the pressure profiles are defined accordingly to comprehend the configuration showed in Figure 3.4.

$$P_1 = 3\left(\frac{L}{D}\right)^2 \left(\frac{1 + 2A}{1 + 4A}\right)\left(\frac{1}{H'^3}\right)\frac{\partial H}{\partial \theta} \qquad (3.61)$$

$$P_2 = \left(\frac{12}{H''^3}\right)\left(\frac{L}{D}\right)^2 \frac{\partial H}{\partial \theta}\left(z^2 - \frac{1}{4}\right) \qquad (3.62)$$

$$P_3 = 3\left(\frac{L}{D}\right)^2 \left(\frac{1 + 2A}{1 + 4A}\right)\left(\frac{1}{H^3}\right)\frac{\partial H}{\partial \theta} \qquad (3.63)$$

$$P_g = 3\left(\frac{L}{D}\right)^2 \left(\frac{1 + 2A}{1 + 4A}\right)\left(\frac{1}{H'^3}\right)\frac{\partial H}{\partial \theta} \qquad (3.64)$$

Then, the radial and tangential load carrying capacity are computed together like Equation (3.51) and (3.52). Therefore, the dimensionless load capacity is derived in which similar with Equation (3.53);

$$F_\varepsilon = \iint P_o \cos\theta \ dz \ d\theta \qquad (3.65)$$

$$F_\emptyset = \iint P_o \sin\theta \ dz \ d\theta \qquad (3.66)$$

$$W = \sqrt{F_\varepsilon^2 + F_\emptyset^2} \qquad (3.67)$$

The dimensionless shear stress is then defined for partial two-slip texture surface;

$$\Pi_1 = \frac{6Q(H' + 2A)}{H'^2(H' + 4A)} \qquad (3.68)$$

$$\Pi_2 = \frac{6Q}{H''^2} \tag{3.69}$$

$$\Pi_3 = \frac{6Q(H + 2A)}{H^2(H + 4A)} \tag{3.70}$$

$$\Pi_g = \frac{6Q(H' + 2A)}{H'^2(H' + 4A)} \tag{3.71}$$

Lastly, the coefficient of friction, C_f is defined in which similar with Equation (3.27) and (3.28).

$$F = \int_0^{\theta_r} \Pi \, d\theta \tag{3.72}$$

$$C_f = \left(\frac{R}{C}\right)\frac{f}{w} = \frac{F}{W} \tag{3.73}$$

3.5 Validation of Results from Previous Data

The validation of the results is done by re-modelling of the previous research by previous authors such as Rao [70-73]. The method is extracted and then the simulation is reconducted to validate the similarity of the results produced. However, due, to the differences in terms of derivation of equations, terms, initial values and technique applied in the MATLAB, the results obtained are not as accurate compared to the original article. However, the trend of the graphs obtained shows the similarities which support the validation of the methods and results obtained. Figure 3.5 and 3.6 shows the comparison of the results obtained with the results from the research article from Rao [73]. The similarities of the results obtained enabled the progress of the research flowchart to the development of grooved journal bearing with partial texture and slip surface to be carried out.
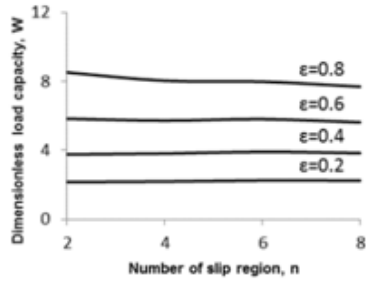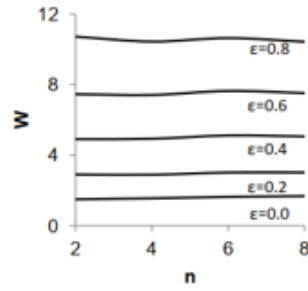
Figure 3.5: Validation and comparison of results obtained (left) for number of slip region with Rao (right) [73].
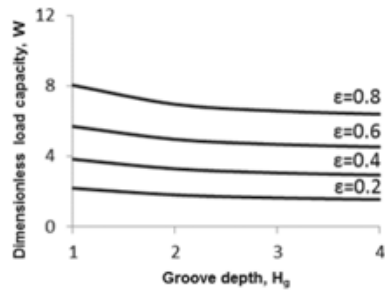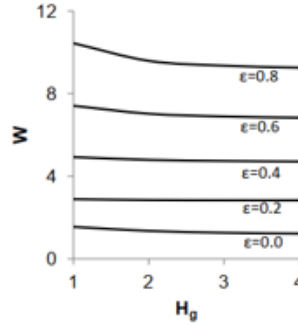
Figure 3.6: Validation and comparison of results obtained (left) for groove depth with Rao (right) [73].

3.6 Chapter Summary

The numerical model is constructed according to long and short journal bearings, together with partial single-slip texture surface and partial two-slip texture surface configurations. The model is then simulated in MATLAB software, according to sets of variables selected and parameters mentioned. The numerical simulation shows the outcome of the analysis required for further analysis. The results of the whole analysis are recorded, plotted, and discussed in the next chapter.

CHAPTER 4

RESULTS AND DISCUSSION

4.1 Overview

This chapter consists of two main sections, in which the first section, Section 4.2 discusses the analysis of a long hydrodynamic journal bearing and its performance compared with a plain journal bearing. Meanwhile, Section 4.3 discusses short hydrodynamic journal bearing, together with its comparison with a plain hydrodynamic journal bearing. Both long and short bearing analyses are presented with dimensionless load carrying capacity, dimensionless shear stress, friction coefficient, and pressure distribution, respectively. The summary of the entire results obtained is then discussed in Section 4.4.

4.2 Long Hydrodynamic Journal Bearing

In this section, the results for hydrodynamic journal bearings are presented. The results consist of dimensionless load carrying capacity, dimensionless shear stress, friction coefficient, and pressure distribution. The parameters involved in the analysis are mentioned later in the sub-section, of which some of the parameters were fixed to reduce the analysis complexity due to various parameters changed, such as the end texture length, θ_g, was set to 150º, the slip coefficient magnitude was set to 1, and the standardised texture depth was set to 0.5 unless mentioned otherwise. The values were selected based from the previous research that using within the same range [13, 70-73, 81], thus providing a good platform for results comparison and validation of data. The results presented for the plain and partial slip textured surfaces of the hydrodynamic journal bearings were based on the slenderness ratio (L/D) of 2.

4.2.1 Pressure Distribution

The results of the dimensionless pressure distribution of the partial single-slip textured surface, partial two-slip textured surface, and the plain hydrodynamic journal bearing are presented in Figures 4.1, 4.2, 4.3, and 4.4. These figures show the effect of the applied partial slip texture on the hydrodynamic film pressure of the journal bearing with four different sets of parameters, namely, the slip to no slip ratio, γ; texture length, θ_t; number of texture regions applied, n; and texture depth, H_g. For these results, the eccentricity ratio, ε, was set to 0.1 and the pressure distribution profiles were plotted at the circumferential bearing angle.

In general, the applied partial-slip textured surface on the journal bearing showed significant improvements compared to the plain bearing. It has been shown that the applied partial-slip texture increased the pressure distribution along the circumferential angle of 0º to 180º. One noticeable pattern of the pressure distribution was that the pressure changed according to the surface texture characteristics, which can be seen from all figures, in which the change of the number of textured region fluctuated the graph pattern with respect to it. In addition, the pressure fluctuations ended at the texture length of 120º. Then, the pressure read the changes across the fixed-end textured regions, θ_g, which showed overall improvement for all of the parameters from 120º to 180º compared to plain bearing. The changes of the parameters from all the figures showed that the applied partial texture with a slip surface changed the behaviour of the lubrication film and effect of convergence. As seen in the plain bearing, the hydrodynamic pressure achieved its maximum value at 95º. Meanwhile, applying the partial-slip texture configuration changed the pattern from a bell-curved shape with the plain bearing to an incremental graph pattern, which was maximised at the end section at 155º, due to the complex surface features along the bearing surface.

However, applying the partial single-slip texture and partial two-slip texture provided significant differences as well. Based on Figures 4.1, 4.2, 4.3, and 4.4, applying an additional wall slip condition of the textured surface resulted in better pressure improvements compared to the single-slip condition. By using a plain bearing as the reference, the percentage's increase and decrease were calculated. From Figure

4.1, the partial two-slip textured surface had an improvement of 160.1% -for $\gamma = 0.6$ and 121.7% for $\gamma = 0.2$. There was also a minor increase of pressure distribution for the partial single-slip surface which resulted in a decrease of 1.82% for $\gamma = 0.2$ and an increase for the partial single-slip of 52.6% for $\gamma = 0.6$. Besides that, altering the texture length, θ_t, in Figure 4.2, showed the improvement of 125.5% at $\theta_t = 40^o$ and 31.5% at $\theta_t = 120^o$ for the partial single-slip. For the partial two-slip textured surface, a 166.2% performance improvement was obtained from $\theta_t = 40^o$ and a 136.9% improvement was attainable for $\theta_t = 120^o$. These results also show that the partial two-slip textured configuration provided better performance compared to the single-slip texture and the plain bearing.

From Figure 4.3, the changes of the number of textured regions resulted in several improvements for both surface configurations, especially the partial two-slip configuration. For the partial single-slip textured surface, the hydrodynamic pressure increased by 36.4% in average compared to the plain bearing. Meanwhile, applying the partial two-slip textured surface increased the average pressure performance by 136.7%. Changing the number of textured regions, however, did not result in significant differences, as the peak pressure attained was roughly similar in the same configuration. For the last parameter, which was the texture depth in Figure 4.4, applying the partial two-slip textured surface greatly increased the pressure performance by 141.7% for $H_g = 0.8$ and 117.2% for $H_g = 0.2$. On the other hand, the results from applying the partial single-slip textured surface with the same parameters show 18.2% increase for $H_g = 0.8$ and a 42.9% increase of performance for $H_g = 0.2$. The results from Figure 4.4 show that increasing the texture depth improved the maximum hydrodynamic pressure for the applied journal bearing compared to the plain bearing.
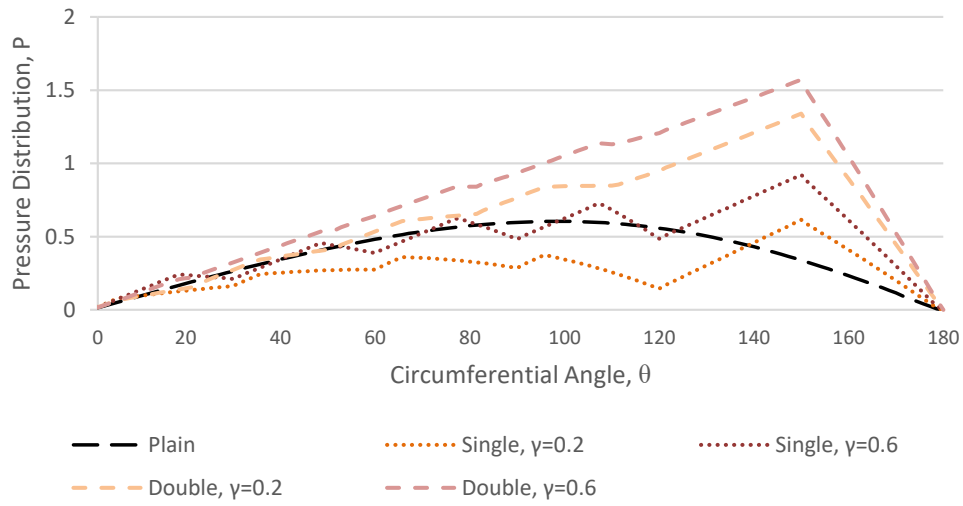
Figure 4.1: Dimensionless pressure distributions for γ=0.2 and γ=0.6 with single and double-slip partial textures at ε=0.1.
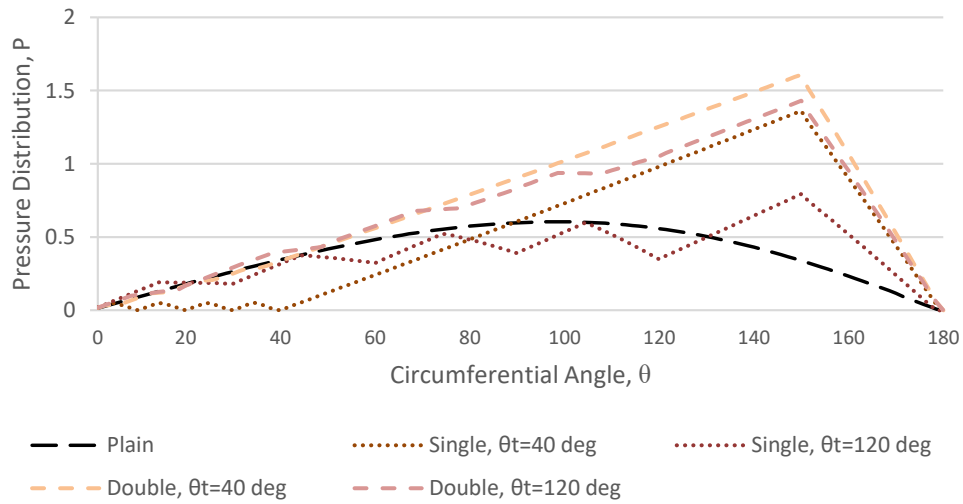
Figure 4.2: Dimensionless pressure distributions for n=2 and n=6 with single and double-slip partial textures at ε=0.1.
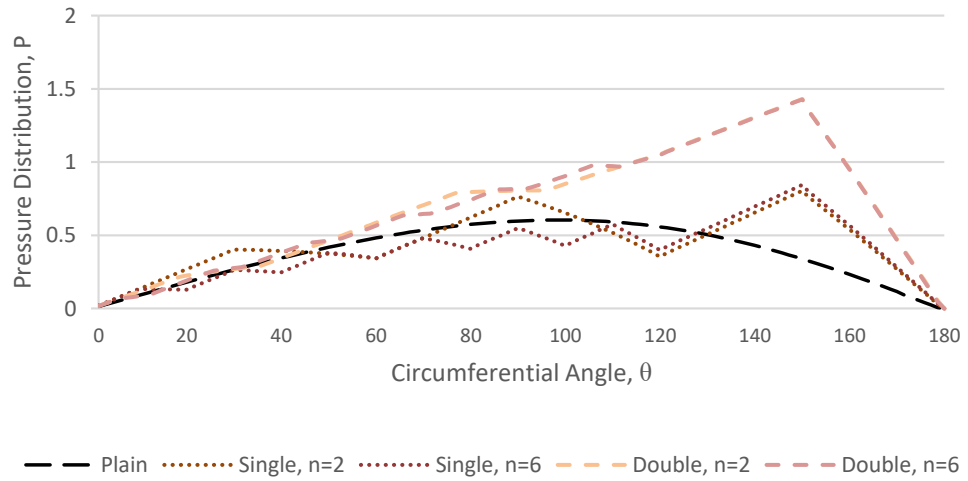
Figure 4.3: Dimensionless pressure distributions for $\theta_t=40^\circ$ and $\theta_t=120^\circ$ with single and double-slip partial textures at $\varepsilon=0.1$.
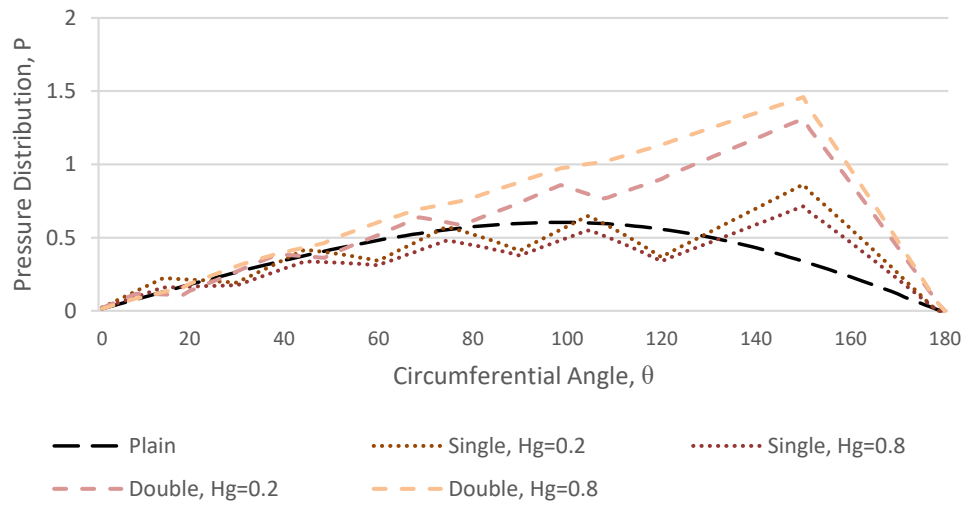
Figure 4.4: Dimensionless pressure distributions for $H_g=0.2$ and $H_g=0.8$ with single and double-slip partial textures at $\varepsilon=0.1$.

4.2.2 Dimensionless Load Carrying Capacity

The dimensionless load carrying capacities for the partial single-slip textured surface, partial two-slip textured surface and plain bearing are presented in Figures 4.5, 4.6, 4.7, and 4.8. In these figures, four parameters were analysed, namely slip to no slip ratio, γ; texture length, θ_t; number of textured regions applied, n; and texture depth, H_g. The magnitudes of the load capacities were analysed with respect to the eccentricity ratios ranging from 0 to 0.8. In summary, the dimensionless load carrying capacity is a derivation from the hydrodynamic pressure, thus it is directly related to each other. From all the figures mentioned, applying the partial single-slip textured and partial two-slip textured surfaces resulted in lower performances in the high eccentricity ranges compared to the plain bearing. However, most of the proposed configurations, especially partial two-slip textured surfaces resulted good improvements at the eccentricity ratio of 0.1, which was the low operating condition. The overall analysis showed that most of the applied configurations had better load capacities at low eccentricity ratios, which is essential for a low operating speed. Therefore, for this section, the performance analysis focuses on the eccentricity ratio of 0.1 only. From Figure 4.5, which analysed the slip to no slip ratio magnitude, γ, applying the partial two-slip textured surface provided better performance than the plain bearing as compared to the partial single-slip textured surface. The percentage difference at $\varepsilon=0.1$ for the single-slip was a 34.2% decrease for $\gamma=0.2$ and 17.2% for $\gamma=0.6$. Meanwhile, applying the two-slip on the partial textured surface showed a greater performance improvement of 73.1% for $\gamma=0.2$ and a 104.4% performance increase for $\gamma=0.6$. However, increasing the eccentricity ratio greater than 0.3 resulted in a performance drop for both configurations compared to the plain journal bearing. On the other hand, Figure 4.6 shows the dimensionless load capacity with respect to texture length, θ_t. Similar with previous data, the performance improvement was detected at $\varepsilon=0.1$, for which applying the single-slip increased the maximum load capacity by 51.2% for $\theta_t=40°$ and a slight decrease of 4% for $\theta_t=120°$ respectively. Meanwhile, for the two-slip partial texture surface, the performance improvement was much greater at 101.8% for $\theta_t=40°$ and 80.7% for $\theta_t=120°$, respectively.

Figure 4.7 shows the effect of applying different numbers of textured regions onto the bearing surfaces on the load carrying capacity. Applying the two-slip partial texture showed better load capacity compared to the single-slip with noticeable improvement compared to the plain bearing at ε=0.1. The partial two-slip textured surface handled the load capacity well at the eccentricity ratios from 0.1 to 0.3. In terms of performance difference compared to the plain bearing at ε=0.1, the results show a 9.8% improved performance at n=2 and a 0.1% improvement at n=6, respectively, for the partial single-slip textured surface. For the partial two-slip texture surface, the results show better improvement in the maximum load capacity of 79.9% at both n=2 and n=6, respectively. The solid reasoning for the higher percentage reduction is that, increasing the number of textured regions increased the complexity of the bearing surface, thus resulting in a higher fluid flow resistance, which thus reduced the load capacity that could be achieved in the high eccentricity range. In Figure 4.8, the graph shows the performance of the load capacity towards the texture depth. Looking at the maximum load capacity at the high eccentricity ratio, increasing the texture depth reduced the load capacity of the journal bearing, despite it performing better in the low eccentricity range from 0.1 to 0.3. In terms of percentage difference, the single-slip partial texture surface with a texture depth of 0.2 had a slight performance increase of 3.7%, whilst increasing the depth to 0.8 lowered the performance by 10.8%. On the other hand, the partial single-slip textured surface with the texture depth of 0.2 showed a 60.1% improvement over the plain bearing whilst the texture depth of 0.8 showed an 89.8% performance improvement with the same comparison.
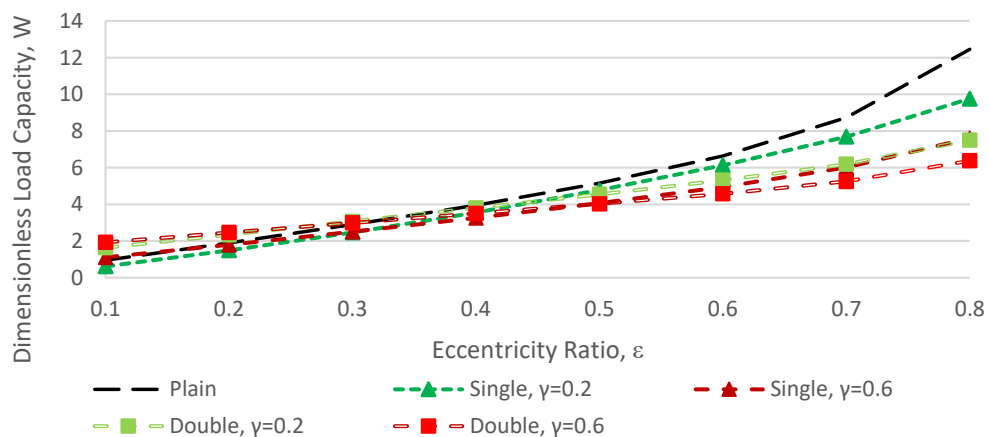
Figure 4.5: Dimensionless load carrying capacities for γ=0.2 and γ=0.6 with single and double-slip partial textures at $0.1<\varepsilon<0.8$.
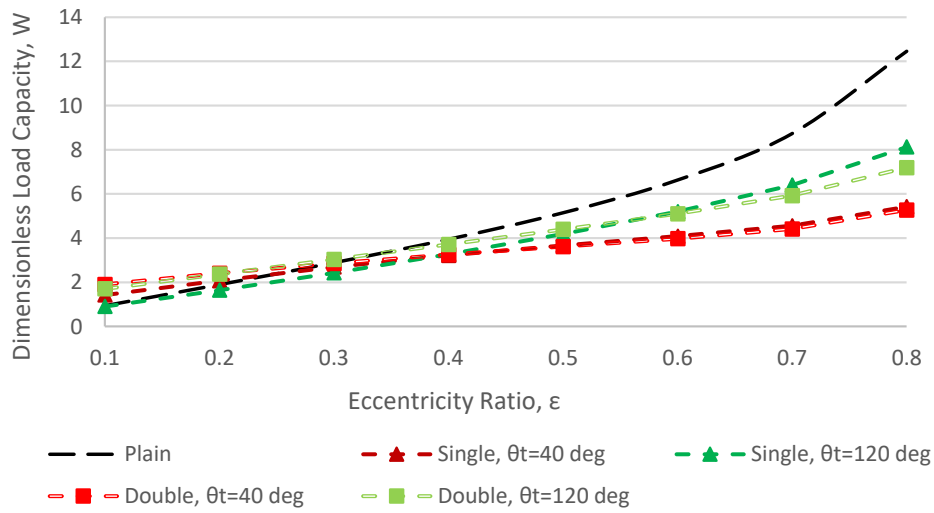
Figure 4.6: Dimensionless load carrying capacities for $\theta_t=40^o$ and $\theta_t=120^o$ with single and double-slip partial textures at $0.1<\boldsymbol{\varepsilon}<0.8$.

Figure 4.7: Dimensionless load carrying capacities for n=2 and n=6 with single and double-slip partial textures at $0.1<\varepsilon<0.8$.
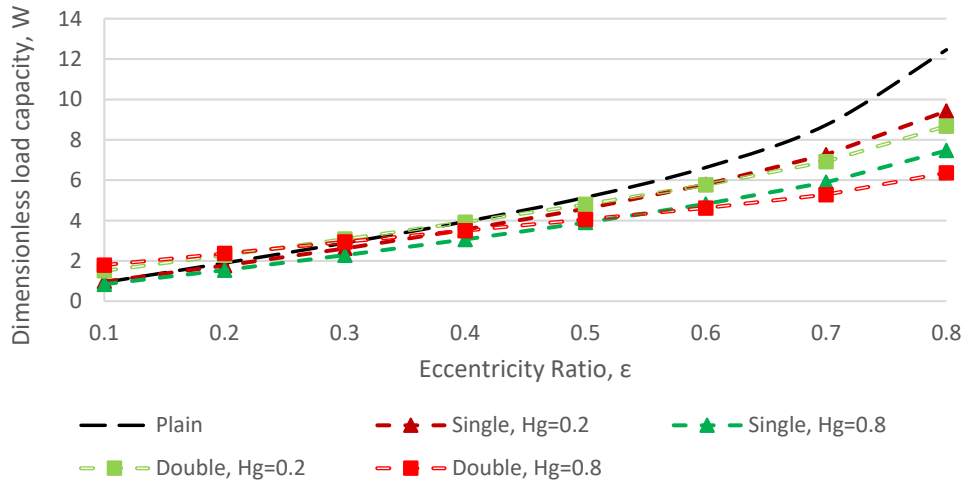
Figure 4.8: Dimensionless load carrying capacities for $H_g=0.2$ and $H_g=0.8$ with single and double-slip partial textures at $0.1<\varepsilon<0.8$.

4.2.3 Dimensionless Shear Stress

Another set of results extracted from the analysis was the dimensionless shear stress. Shear stress was crucial in order to determine the flow resistivity of the fluid film across the convergent region of the journal bearing. As for comparison, the dimensionless shear stress values for the plain bearings were included as well. Figures 4.9, 4.10, 4.11, and 4.12 show the dimensionless shear stress for the partial single-slip textured and partial two-slip textured surfaces, with respect to different sets of parameters similar with the previous discussion. For the sake of convenience, the dimensionless form was applied in this case with the eccentricity ratio of 0.1. From Figure 4.9, it can be seen that applying the two-slip on the partial texture surface did increase the shear stress on the journal bearing, regardless of different slip to no slip ratio parameters, γ, being applied. In addition, it was expected that, due to the complex features of the partial two-slip textured surface configuration, the shear stress generated was greatly increased. In terms of percentage difference compared to the plain bearing, by using the maximum shear stress achieved, applying the two-slips increased the shear stress by a whopping 196.3% at $\gamma=0.2$ and 188% at $\gamma=0.6$. However, the single-slip partial texture surface increased the shear stress by only a small margin of 9.9% at $\gamma=0.2$

and 4.2% at γ=0.6. In other words, increasing the surface complexity will definitely increase the shear stress exerted in the fluid film region. In Figure 4.10, the texture length parameter, θ_t, was used to see the effect on the shear stress. From the rough observation, the two-slip partial texture surface had a higher shear stress compared to the single-slip textured surface due to the same reason. It is agreed that the surface topography of the bearing surface is important when trying to minimise the shear stress effect generated in the hydrodynamic journal bearing. In this case, the shear stress increased by 185.5% at θ_t=40° and 194% at θ_t=120° for the partial two-slip surface, which was not a good result when considering real applications. In another case, the single-slip textured configuration recorded a 4.1% shear stress reduction at θ_t=40° and a 6% increase for θ_t=120°. These outcomes show the capability of the single-slip partial texture surface in minimising the shear stress effect on the journal bearing despite having a complex surface configuration.

In another two sets of parameters, which were the number of textured regions, n and texture depth, H_g, as shown in Figures 4.11 and 4.12, similar observations discussed earlier in Figures 4.9 and 4.10. In Figure 4.11, the partial two-slip textured configuration recorded a 194.1% increase in the shear stress at n=2 and a 193.9% increment at n=6 when compared to the plain journal bearing. Other than that, there was a small increase of 6.5% of the shear stress at n=2 and 5.9% for n=6, which was considerably small. In another case, the partial two-slip textured surface recorded a 172.3% increase in the maximum shear stress at H_g=0.2 and a 210% increment at H_g=0.8 in Figure 4.12, thus proving that condition of increasing the texture depth on more complex surfaces reduces the journal bearing performance in several factors. In the partial single-slip configuration, it could be seen that the surface configuration increased 5.8% of the shear stress at H_g=0.2 and 1.3% at H_g=0.8.
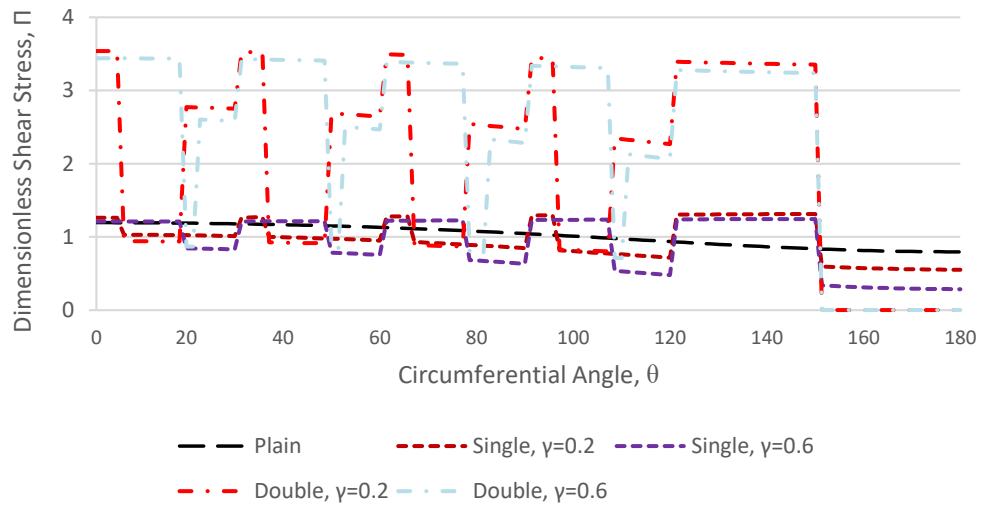
Figure 4.9: Dimensionless shear stress values for γ=0.2 and γ=0.6 with single and double-slip partial textures at ε=0.1.
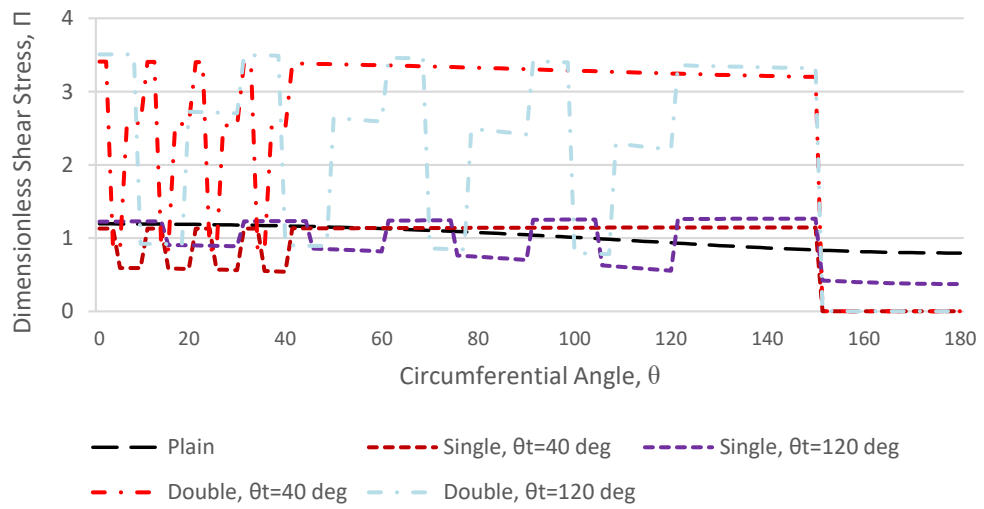
Figure 4.10: Dimensionless shear stress values for θ_t=40° and θ_t=120° with single and double-slip partial textures at ε=0.1.
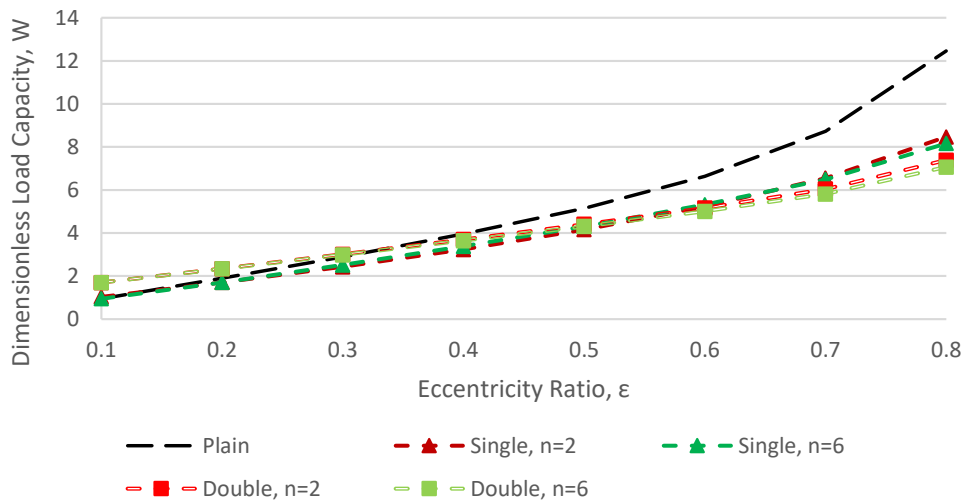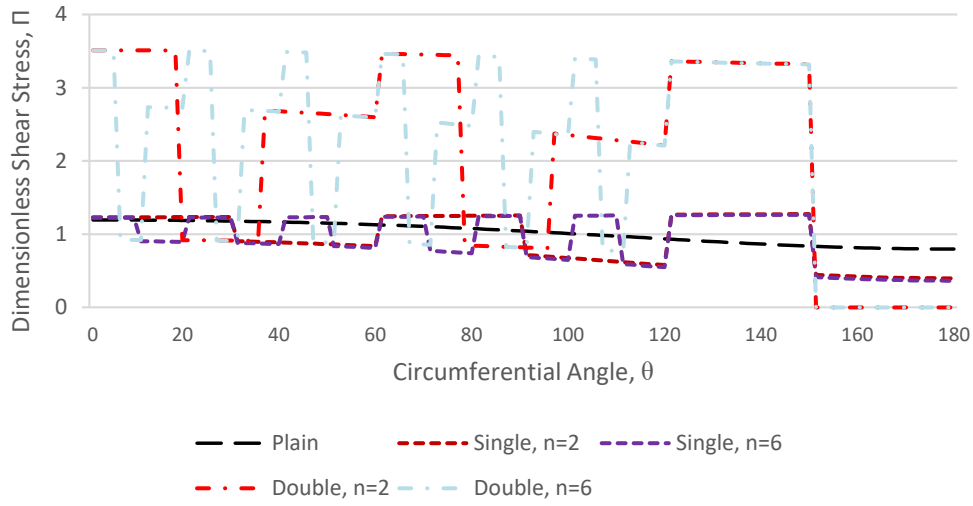
Figure 4.11: Dimensionless shear stress values for n=2 and n=6 with single and double-slip partial textures at ε=0.1.
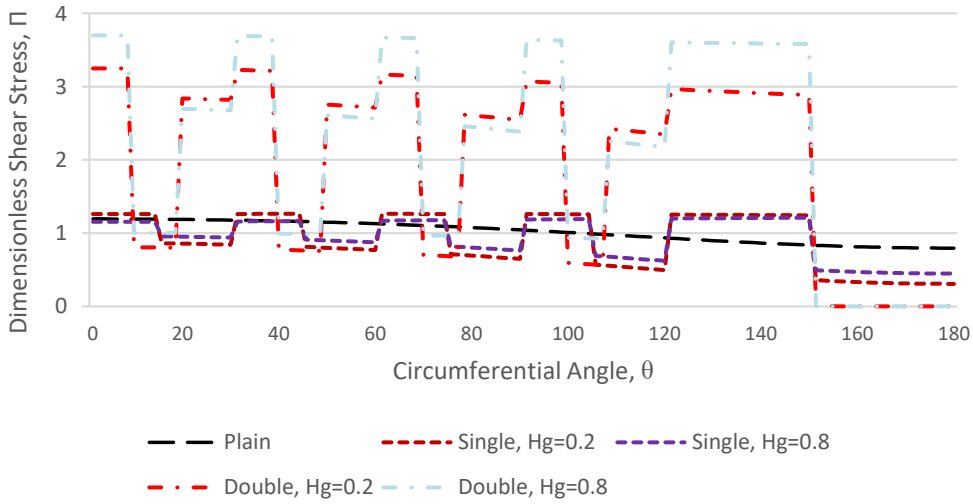
Figure 4.12: Dimensionless shear stress values for H_g=0.2 and H_g=0.8 with single and double-slip partial textures at ε=0.1.

4.2.4 Friction Coefficient

Another result that was extracted from the analysis was the coefficient of friction, C_f. The friction coefficient was obtained from the friction force, which was integrated from the dimensionless shear stress, Π; then, it was divided by the dimensionless load capacity, W, obtained in the previous discussion. The parameters applied were similar, with respect to the eccentricity ratios ranging from 0.1 to 0.8 as shown in Figures 4.13, 4.14, 4.15, and 4.16. From the rough observation from all the figures, it can be seen that the partial single-slip texture in both configurations had noticeable low friction coefficients at the low eccentricity ratios compared to the partial two-slip texture surface and plain journal bearing, therefore, the improvements at the low eccentricity ratio will be discussed in this section. In Figure 4.13, the partial single-slip textured surface with $\gamma=0.2$ had a lower friction coefficient at $\varepsilon=0.1$, whilst the friction coefficient at $\gamma=0.6$ initiated a slightly higher value compared to the plain bearing. However, as the eccentricity ratio increased, the friction coefficient tended to have a small decrement, resulting in a higher value when compared to the plain bearing. The partial single-slip texture had a 44.6% increase in the friction coefficient at $\gamma=0.2$ and a 22.3% decrease in the friction coefficient at $\gamma=0.6$. Meanwhile for the partial two-slip textured surface, the $\gamma=0.2$ produced a 874.6% higher friction coefficient and a 1037.3% increase in the friction coefficient at $\gamma=0.6$. Thus, these results show that the partial two-slip textured configuration produced a higher friction coefficient and the partial single-slip textured surface is a better option in minimising the friction coefficient effect at a low eccentricity ratio. On the other hand, a similar pattern can be seen in Figure 4.14, which represents using the texture length as the variable along with the eccentricity ratios. From the graph, the partial single-slip texture with the texture length of 40° had a lower friction coefficient at 42.9% when the eccentricity ratio ranged from 0.1 to 0.3. Meanwhile, at $\theta_t=120°$, it showed noticeable improvement with a 4.2% friction reduction at $\varepsilon=0.1$. Whilst, for the partial two-slip texture, it can be seen that the friction coefficient increased by a whopping 1108.2% for $\theta_t=40°$ and 938.7% at $\theta_t=120°$, which supports the previous reasoning mentioned in the dimensionless shear stress.

Looking at the next parameter, which is the number of textured regions, n, shown in Figure 4.15, the graph trend does not deviate much for the two-slip partial texture surface, which on average produced a 960.9% increment for $n=2$ and $n=6$ over the plain journal bearing. On the other hand, the partial single-slip reduced it significantly with a 11.5% on average for $n=2$ and $n=6$ at the eccentricity ratio of 0.1. In Figure 4.16, the increasing texture depth showed a higher friction coefficient, which agreed with the outcome discussed in the previous sub-section. As for the percentage difference, the partial single-slip texture surface recorded a 13.5% decrease in the friction coefficient for H_g=0.2 and a small increase of 3.3% at H_g=0.8 at the eccentricity ratio of 0.1. In another case, the partial two-slip textured surface recorded a 1014.2% increase in the friction coefficient at H_g=0.2 and a 928.2% increase for H_g=0.8. These results show that increasing the complexity of the surface texture and slip on the journal bearing surface reduced the performance by a big margin, which need to be take into consideration.
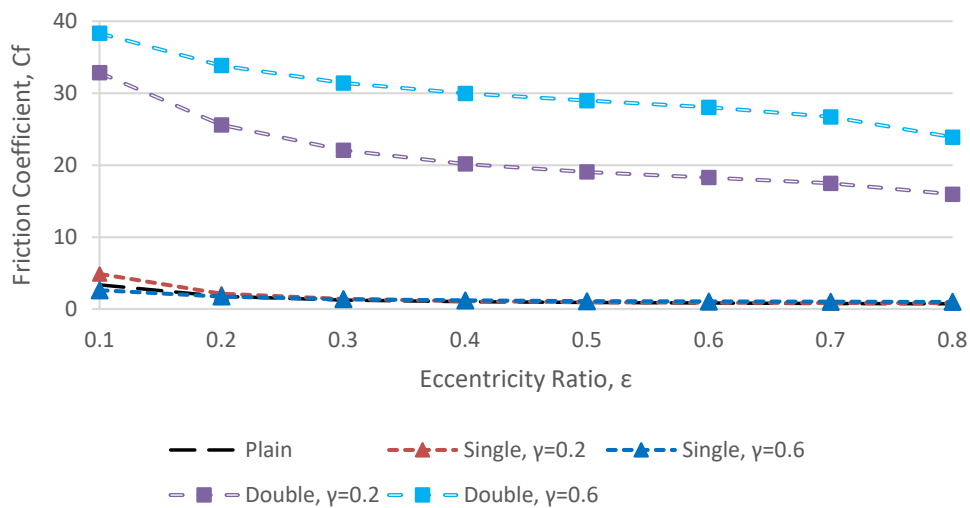
Figure 4.13: Friction coefficients for γ=0.2 and γ=0.6 with single and double-slip partial textures at 0.1<ε<0.8.
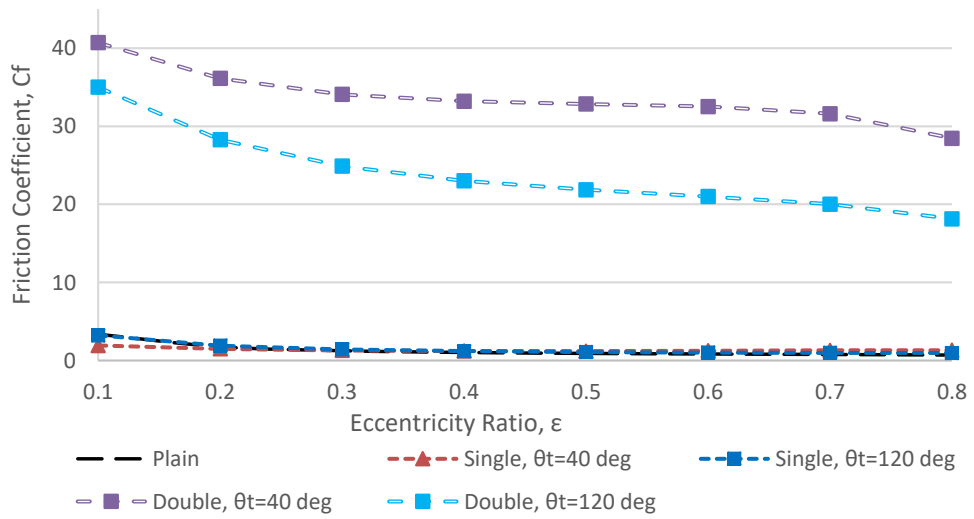
Figure 4.14: Friction coefficients for $\theta_t=40^o$ and $\theta_t=120^o$ with single and double-slip partial textures at $0.1<\varepsilon<0.8$.
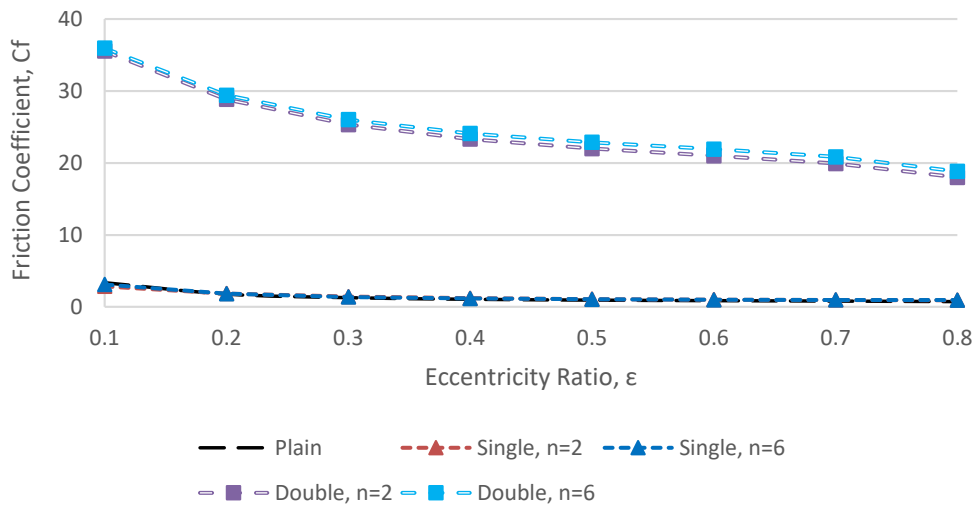
Figure 4.15: Friction coefficients for n=2 and n=6 with single and double-slip partial textures at $0.1<\varepsilon<0.8$.
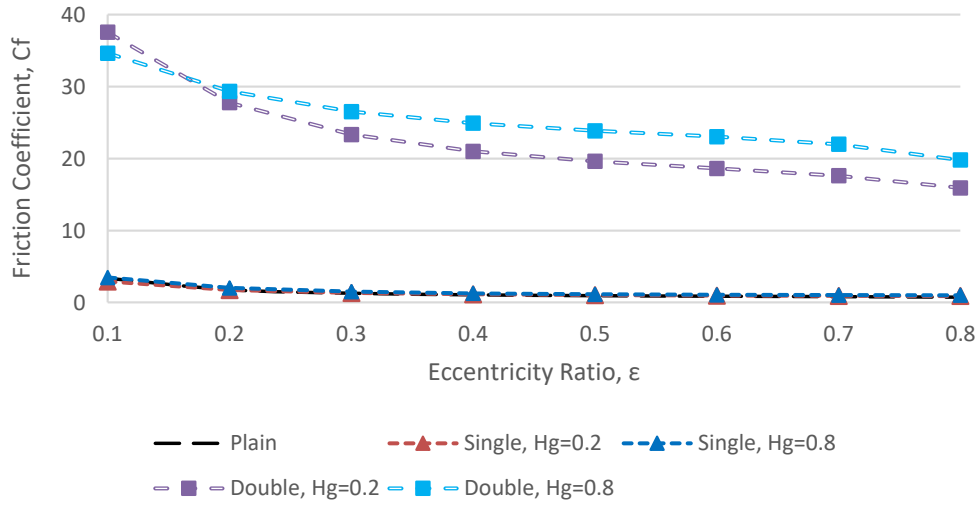
Figure 4.16: Friction coefficients for H_g=0.2 and H_g=0.8 with single and double-slip partial textures at $0.1<\varepsilon<0.8$.

4.3 Short Hydrodynamic Journal Bearing

In this section, the results are obtained for the partial texture with slip on a short hydrodynamic journal bearing, with slenderness ratio (L/D) of 0.25.

4.3.1 Pressure Distribution

The dimensionless pressure distributions for the partial texture with slip for a short journal bearing and plain journal bearing are shown in Figures 4.17, 4.18, 4.19, and 4.20. Similar to the long hydrodynamic journal bearing, the parameters used were slip to no slip ratio, γ; texture length, θ_t; number of texture regions applied, n; and texture depth, H_g. In addition, the eccentricity ratio, ε, was set to 0.1, and the pressure distribution profiles have been plotted at the circumferential bearing angle. Figure 4.17 shows the pressure profiles for the partial texture with slip and the plain journal bearing, which illustrates that the partial texture with both the single and double-slip had lower pressures at the textured regions. This was due to the phenomenon of the hydrodynamic pressure, which developed due to the convergent effect on the plain journal bearing; but due to the presence of the partial texture and slip, it increased the fluid film thickness,

which reduced the hydrodynamic pressure. Increasing the slip to no slip ratio magnitude shifted the pressure to a higher circumferential angle and maintained the maximum pressure as compared to the plain bearing; meanwhile, applying the partial two-slip with texture reduced the hydrodynamic pressure by 40% for both values.

From Figure 4.18, a similar observation can be seen with slightly different factors. For the partial single-slip texture, applying a low texture length, θ_t, reduced the hydrodynamic pressure by 40% at θ_t=40º, whilst increasing θ_t to 120 degrees maintained the maximum pressure distribution. A similar observation and inference can be deduced with that partial two-slip texture; 40% of the maximum pressure decreased at θ_t=40º and θ_t=120º. From these recorded observations, reducing the texture length, θ_t, and applying the partial two-slip textured surface did affect the maximum hydrodynamic pressure of the short journal bearing.

Application of the number of textured region parameters, n, can be observed in Figure 4.19. Looking forward to the partial single-slip texture with respect to the plain bearing, increasing the number of textured regions increased the frequency of the hydrodynamic pressure along the circumferential angle. This was due to the changes of the fluid film thickness along the textured region of the circumferential angle, thus reducing the hydrodynamic pressure at the particular textured sections. However, there was no reduction in the maximum hydrodynamic pressure recorded when compared to the plain bearing. Moving on to the partial two-slip textured surface, it was the same prediction as with previous parameters; whereby, applying additional texture depth reduced the hydrodynamic pressure significantly, which saw a 40% reduction in the maximum pressure recorded compared to the plain journal bearing for both values of 2 and 6.

Figure 4.20 shows the effect of changing the texture depth, H_g, along the bearing surface on the hydrodynamic pressure distribution. In the partial single-slip texture, the pressure remained the same at H_g=0.2 and H_g=0.8. However, the partial two-slip texture recorded a 25% pressure reduction at H_g=0.2 and a 40% reduction at H_g=0.8. This explains the effect of increasing the texture depth, which increased the fluid film thickness thus significantly reducing the hydrodynamic pressure.
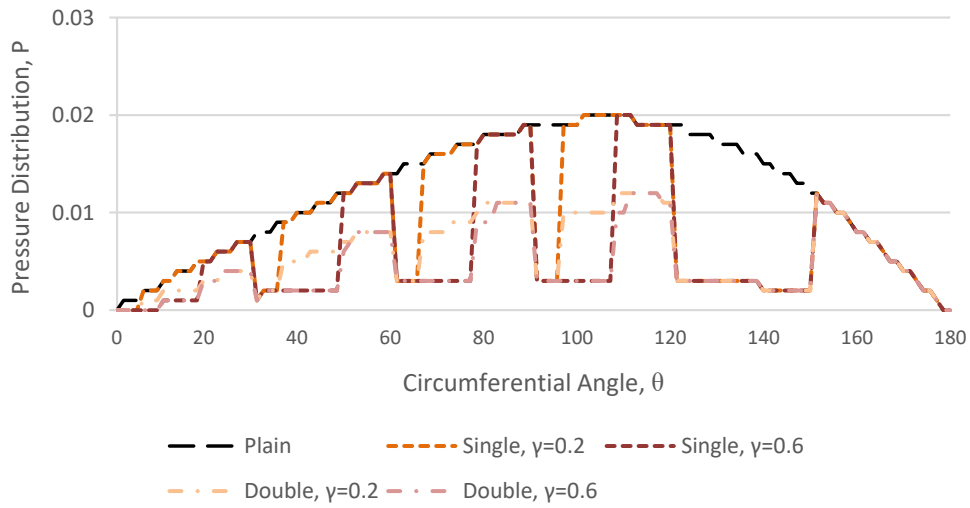
Figure 4.17: Dimensionless pressure distribution for γ=0.2 and γ=0.6 with single and double slip partial texture at ε=0.1.
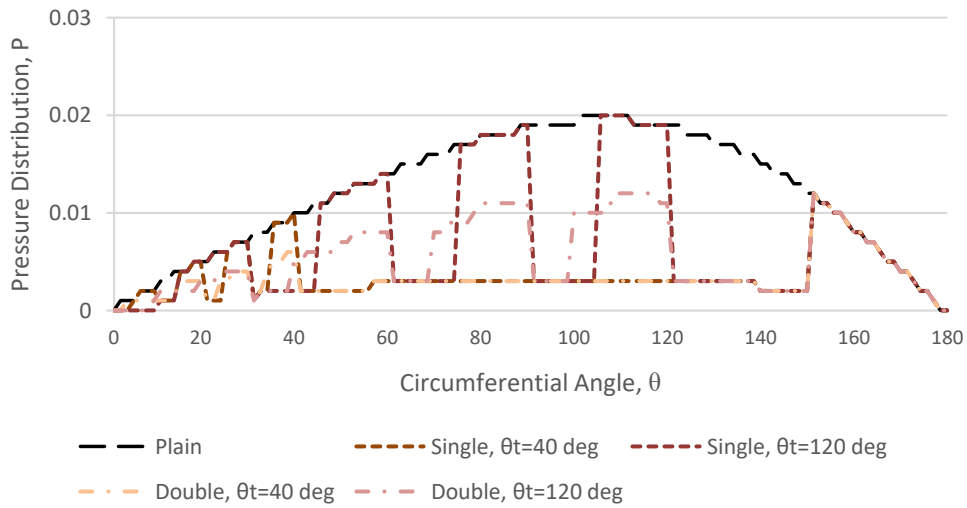
Figure 4.18: Dimensionless pressure distributions for θ_t=40° and θ_t=120° with single and double-slip partial textures at ε=0.1.
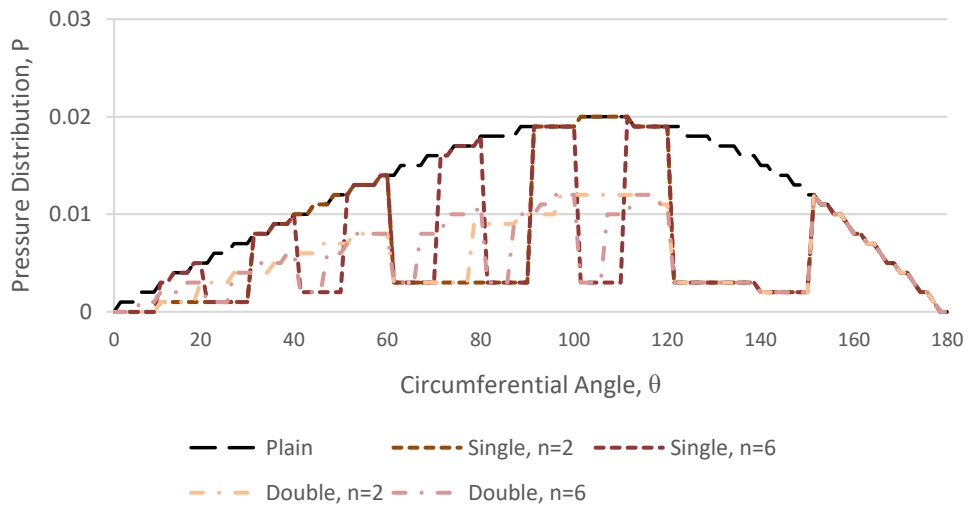
Figure 4.19: Dimensionless pressure distributions for n=2 and n=6 with single and double-slip partial textures at ε=0.1.
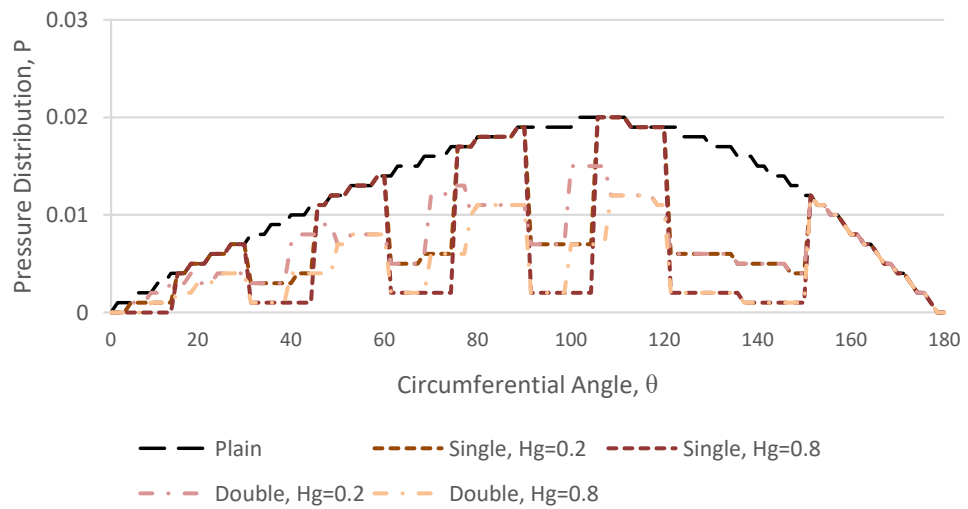
Figure 4.20: Dimensionless pressure distributions for H_g=0.2 and H_g =0.8 with single and double-slip partial textures at ε=0.1.

4.3.2 Dimensionless Load Carrying Capacity

The dimensionless load carrying capacities for the short plain, partial single-slip texture surface, and partial two-slip textured surface of hydrodynamic journal bearings are shown in Figures 4.21, 4.22, 4.23, and 4.24. The graphs have been plotted with respect to the eccentricity ratio, ε, ranging from 0.1 to 0.8 with similar parameters conducted as previously.

In the Figure 4.21, the graph illustrates the effect of the slip to no slip ratio magnitude, γ, on the load capacity. Compared to the plain journal bearing, applying both the partial single and two-slip textured surfaces greatly reduced the load capacity. This was due to the calculation of the short bearing, which did not consider the pressure gradient from the short bearing approximation theory. These results also proved that the partial texture with two-slip had a lower load capacity compared to the single-slip as the complexity of the surface increased. Applying the partial texture with the slip resulted in a steady and small increase in the load capacity compared to the plain bearing as the difference gap became bigger as the ε ratio increased to 0.8. It is also shown that the lower slip to no slip ratio, γ, produced better results compared to the higher γ. In terms of percentage difference compared to the plain bearing at the eccentricity ratio of 0.1, the partial single-slip texture recorded a 27.9% reduction for $\gamma=0.2$ and a 51.2% reduction in the load capacity at $\gamma=0.6$. Meanwhile, for the partial two-slip textured surface, the load capacity performance dropped by 60% in average.

Figure 4.22 shows the texture length's, θ_t, effect on the load capacity. In this graph, it shows that a longer texture length, θ_t, produced a better load capacity over the eccentricity ratio. However, as the eccentricity ratio increased, the difference between the applied texture and slip to the plain bearing increased as well. This also led to the deduction that the increase in the eccentricity ratio reduced the effect of the applied texture on the hydrodynamic pressure, thus directly affecting the outcome of the load capacity. In terms of the percentage drop of the performance, applying $\theta_t=40^\circ$ for both the partial texture single and two-slip showed an average decrease of 76%; meanwhile, for $\theta_t=120^\circ$, both the partial texture with one and two-slip surfaces showed an average of 51.3% decrease in performance at the 0.1 eccentricity ratio.

Figure 4.23 shows the effect of the number of textured regions, n, applied over the load capacity performance. In the graph, there is only a very small difference that is noticeable between single-slip and two-slip configurations. The partial single-slip texture had a better load capacity over the two-slip configuration, with fewer textured regions resulting in a significantly higher load capacity compared to the higher number of textured regions. The lower number of textured regions significantly reduced the effect of the pressure magnitude drop along the circumferential angle, thus resulting in a slightly higher load capacity, overall. However, the performance still decreased when compared to the plain bearing with a total at the 0.1 eccentricity ratio of, 41.3% and a 55.7% load capacity drop at n=0.2 for the single-slip and two-slip partial textures, respectively. There were, also decreases of 46.3% and 57.7% at n=0.8 for the partial single-slip texture and partial two-slip textures, respectively.

The effect of the texture depth in the partial texture with slip at the 0.1 eccentricity ratio is illustrated in Figure 4.24. From the graph, a significant observation can be recorded from H_g=0.2 and H_g=0.8 for one-slip and two-slip, respectively. From the results, applying the lower texture depth of 0.2 showed that a better load capacity was produced compared to a higher texture depth of 0.8. The same reasoning as with the dimensionless pressure distribution directly affected the load capacity at the same time, which led to a significant difference between the two calculated texture depths. Applying H_g=0.2 for the partial single-slip, however, showed a 35.8% decrease over the plain bearing, and a 45.3% decrease for the partial two-slip texture with a similar comparison. On the other hand, the texture depth, H_g, of 0.8 recorded a 49.3% decrease in the load capacity for the partial single-slip. The partial two-slip texture, meanwhile, recorded 57.2% decrease in load capacity performance compared to the plain bearing.
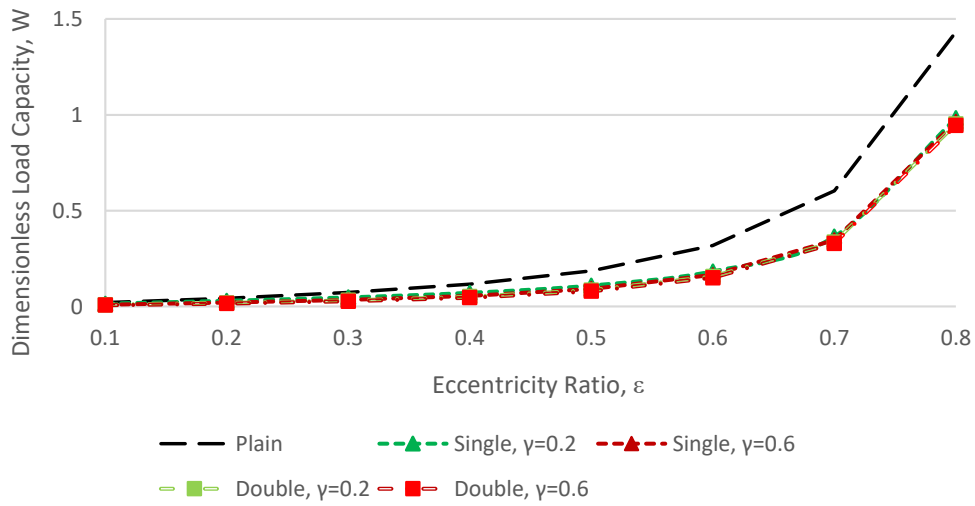
Figure 4.21: Dimensionless load carrying capacities for γ=0.2 and γ=0.6 with single and double-slip partial textures at 0.1<ε<0.8.
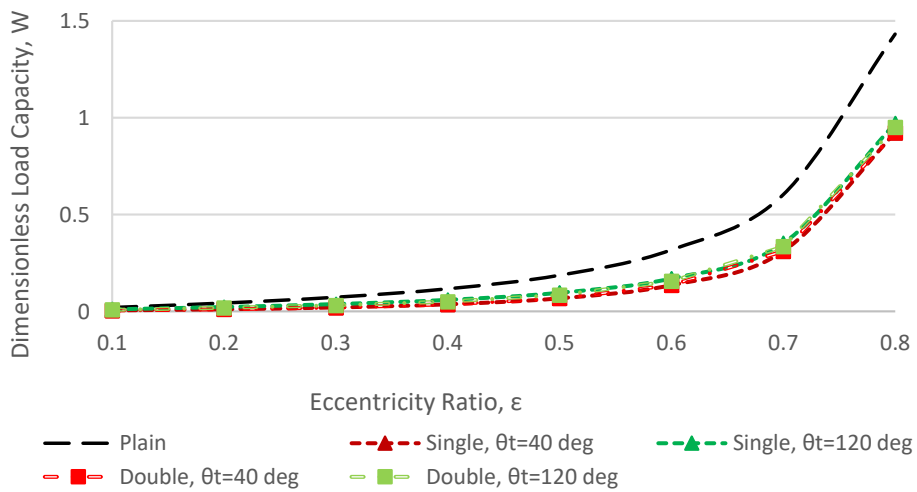
Figure 4.22: Dimensionless load carrying capacities for θ_t=40° and θ_t=120° with single and double-slip partial textures at 0.1<ε<0.8.
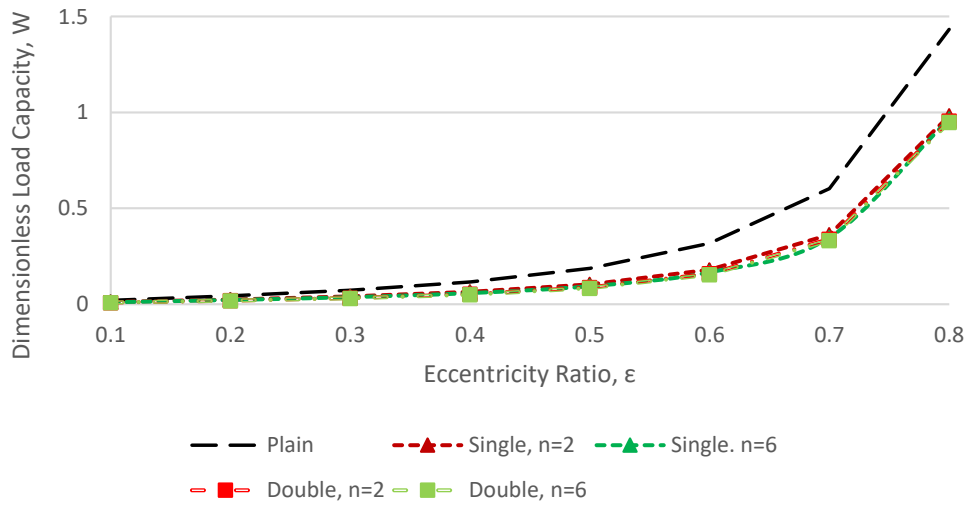
Figure 4.23: Dimensionless load carrying capacities for n=2 and n=6 with single and double-slip partial textures at $0.1<\varepsilon<0.8$.
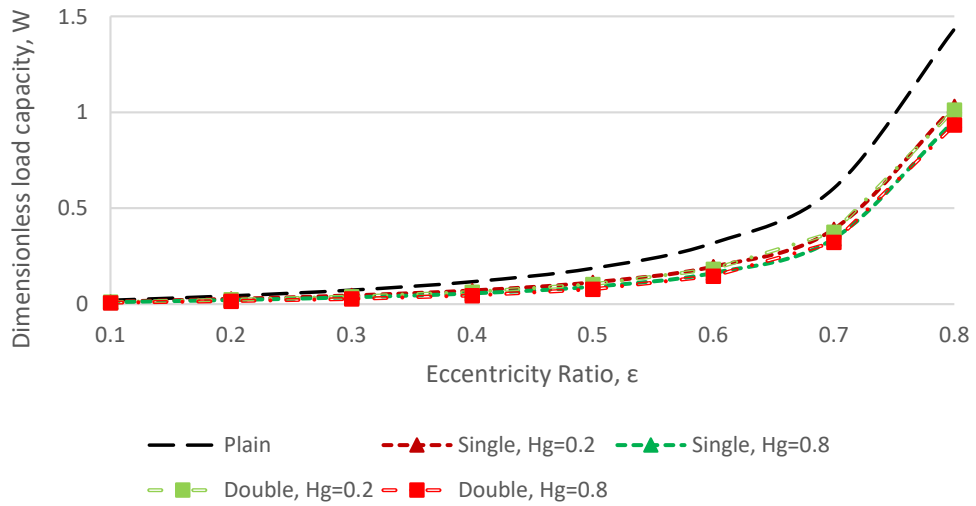
Figure 4.24: Dimensionless load carrying capacities for H_g=0.2 and H_g=0.8 with single and double-slip partial textures at $0.1<\varepsilon<0.8$.

4.3.3 Dimensionless Shear Stress

The outcomes for the dimensionless shear stress are shown in Figures 4.25, 4.26, 4.27, and 4.28, with similar parameters along similar circumferential angles, ranging from 0° to 180°. Figure 4.25 shows the dimensionless shear stress for slip to no slip ratio magnitudes, γ, with the plain bearing added for performance reference. From the graph, shear stress was produced higher for the partial two-slip texture configuration compared to the single-slip configuration. Changing γ only extended the maximum shear stress at the new position on the circumferential angle, but it did not change the maximum or minimum shear stress produced for both the single and two-slip configurations. In terms of the maximum shear stress achieved, the partial two-slip texture produced higher shear stress compared to the partial single-slip texture. This was due to the difference in the film thickness along the circumferential angle, which was greater for the partial two-slip configuration, thus resulting in higher readings. Applying the partial single-slip texture, however, increased the shear stress by 53.7% compared to the plain bearing for both slip to no slip ratio magnitudes, γ, applied; and the partial two-slip texture, meanwhile, showed an 84.8% increase for similar γ values over the plain bearing performance.

On the next graph in Figure 4.26, it shows the dimensionless shear stress performance with different texture lengths, θ_t. Similar to the previous case, varying θ_t did not change the maximum and minimum shear stress values produced in the same configuration. The obvious observation that can be recorded is that the shear stress produced was more frequent at lower circumferential angles for $\theta_t=40^\circ$, which occurred, particularly, in the range of 0° to 50°. Applying the higher θ_t of 120° evenly distributed the shear stress in the range of 0° to 120° along the circumferential angle. As the maximum shear stress achieved was the same for the same configurations with different θ_t, both results showed a 53.7% shear stress increase over the plain bearing for the partial single- slip textured surface, and 73.6% and 84.8% increases for $\theta_t=40^\circ$ and $\theta_t=120^\circ$, respectively, for the partial two-slip textured surface. There was a slightly higher shear stress produced at $\theta_t=120^\circ$; at the 120° circumferential angle, the graph shows a slight increase in the gradient over the circumferential angle. Thus, the results obtained are not the same as $\theta_t=40^\circ$. Moving on to the next graph shown in Figure 4.27,

the change in the number of textured regions similarly produced the same observations and results as recorded in Figure 4.26. In the graph, it shows that increasing the number of textured regions only increased the frequency of the shear stress produced along the circumferential angle. Moreover, the maximum and minimum shear stress readings remained the same for the respective configurations, in which the partial two-slip textured surface still produced a higher maximum shear stress compared to the partial single-slip and the plain bearing. From the graph, it can be seen that both numbers of textured regions for the partial two-slip textured surface increased the shear stress by 84.8% compared to the plain bearing, and at the same time, the partial single-slip texture produced 53.7% higher shear stress over the plain bearing, which was greater compared to the two-slip configuration.

The last parameter investigated was the varying texture depth towards the dimensionless shear stress as shown in Figure 4.28. The graph shows that the partial two-slip surface showed similar maximum shear stress as in Figures 4.26 and 4.27, which was an 84.8% increase in the shear stress over the plain bearing. However, the shear stress reading for the partial single-slip configuration showed that the lower texture depth of H_g=0.2 produced higher shear stress compared to H_g=0.2. With the maximum shear stress value of 1.898, it represents an increase of 70.8% over the plain bearing for H_g=0.2; meanwhile, for H_g=0.8, the maximum shear stress recorded along the circumferential angle was 1.584, which was a 42.6% increment over the plain bearing. This might be due to the changes in the fluid film thickness and texture region over the circumferential length located at 120°, which exerted higher shear stress at H_g=0.2.
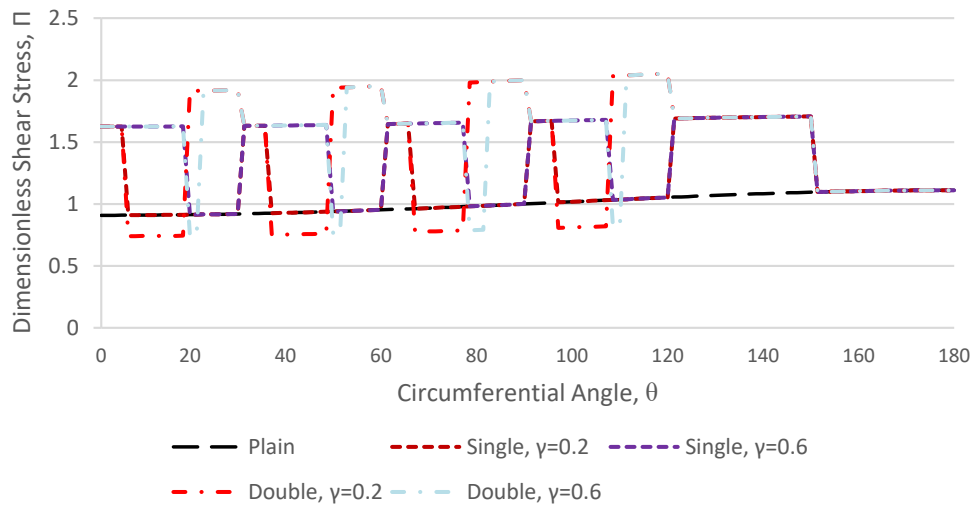
Figure 4.25: Dimensionless shear stress values for γ=0.2 and γ=0.6 with single and double-slip partial textures at ε=0.1.
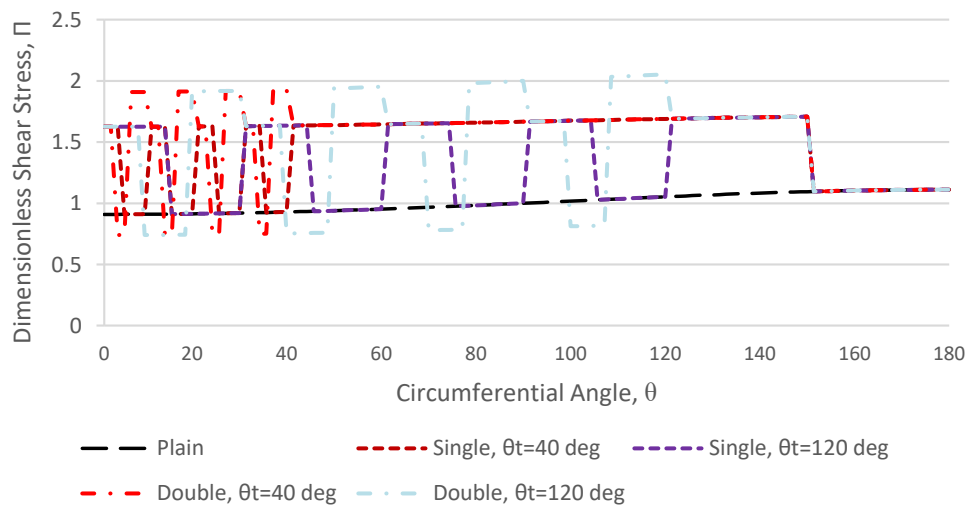
Figure 4.26: Dimensionless shear stress values for θ_t=40º and θ_t =120º with single and double-slip partial textures at ε=0.1.
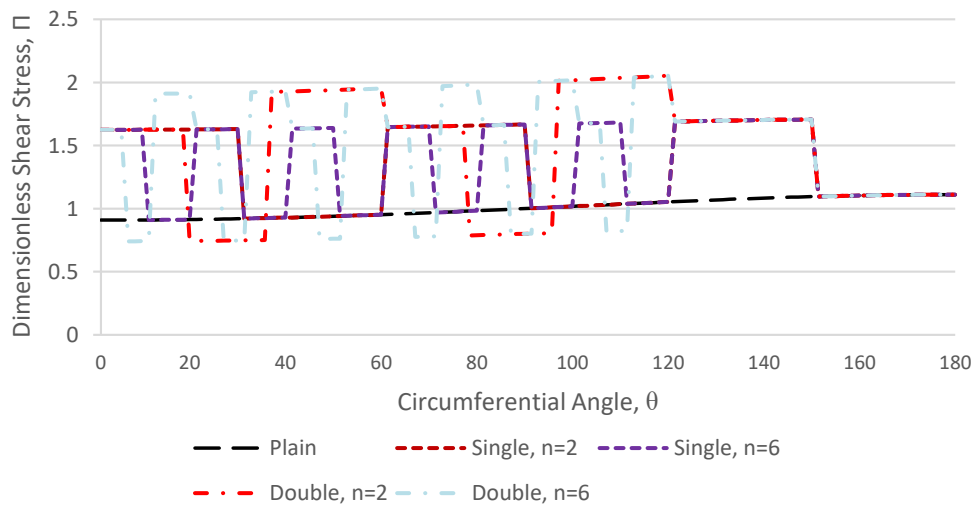
Figure 4.27: Dimensionless shear stress values for n=2 and n=6 with single and double-slip partial textures at ε=0.1.
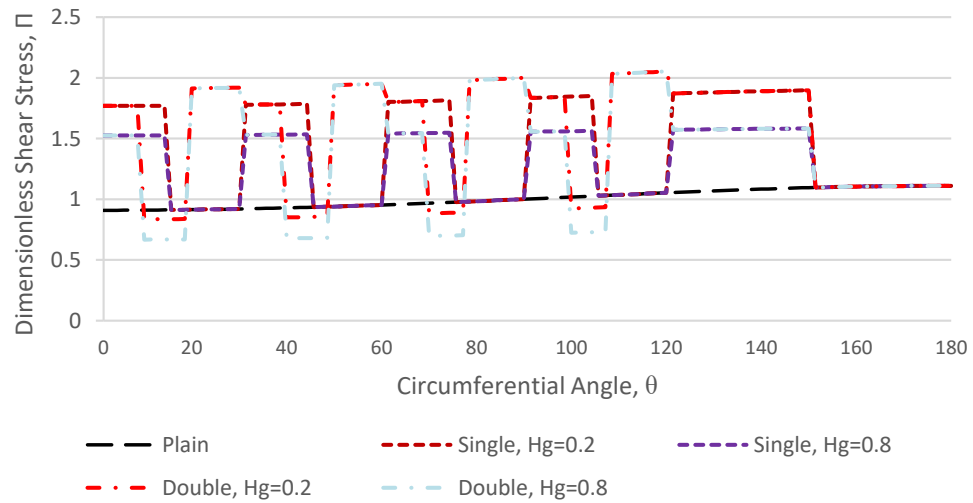
Figure 4.28: Dimensionless shear stress values for H_g=0.2 and H_g=0.8 with single and double-slip partial textures at ε=0.1.

4.3.4 Friction Coefficient

The results for the coefficient of friction, C_f, for the short hydrodynamic journal bearing are shown in Figures 4.29, 4.30, 4.31, and 4.32. Using similar parameters as previously, the results were directly affected by the dimensionless shear stress on the previous section as mentioned in Chapter 3. The results also show the comparison of the plain bearing for benchmarking purposes to find whether applying the partial texture with slip improved the performance of the journal bearing. Figure 4.29 shows the friction coefficients, C_f, for the slip to no slip ratio magnitude, γ, of 0.2 and 0.6 for both surface configurations, with eccentricity ratios, ε, ranging from 0.1 to 0.8. From the results, it can be seen that the partial single-slip texture had a lower C_f compared to the partial two-slip textured surface. However, the plain bearing performance in the C_f was no match for both configurations mentioned. It is also shown that the C_f value was very much greater at the low eccentricity ratios, ranging from 0.1 to 0.5 before the C_f value gap between the configurations got closer. Therefore, both configurations are preferable at higher eccentricity ratios, which demand high speed and heavy operations to reduce the increase of the friction coefficient. In terms of percentage difference, the results show a whopping 214.1% and 345.5% increase in the C_f for γ=0.2 and γ=0.6 for the partial two-slip texture surface respectively. Meanwhile, the partial single-slip texture showed an increase of 65.8% for γ=0.2 and 183.3% for γ=0.6 in the C_f performance over the plain bearing. This was due to the high values recorded at the 0.1 eccentricity ratio as the bearing had to work much harder on the textured and slip surface.

Figure 4.30 shows the friction coefficient performance over the texture length, θ_t. From the results, the partial single-slip texture increased the friction coefficient by 523.5% over the plain bearing. This was due to the compressed textured region at the initial bearing's circumferential length thus providing more tense surface texture on it, resulting a higher C_f at the 0.1 eccentricity ratio. However, increasing the texture length reduced the friction coefficient due to the surface texture being distributed more evenly along the circumferential angle. The results recorded a 143.2% increase in the C_f for θ_t=120°. On the other hand, the partial two-slip texture recorded the highest friction coefficient with a 553.9% C_f increase for θ_t=40° and a 243.6% increase in friction

coefficient for θ_t=120°. The next analysis was made by varying the number of textured regions, n, towards the friction coefficient as shown in Figure 4.31. From the graph, reducing the number of textured regions helped to lower the C_f value when compared with the partial texture with slip configurations. However, the C_f increased was too high to be considered, which was 128.2% for n=2 and 148% for n=6 in the partial single-slip texture over the plain bearing. The partial two-slip texture, on the other hand, recorded a 230.7% for n=2 and a 247.6% for n=6 increase in the C_f value compared to the plain bearing. A similar reason can be deduced for this in that, the C_f value was the highest at the low eccentricity ratio, and the C_f value inversed exponentially as the eccentricity ratio increased.

The last parameter in the friction coefficient analysis was varying the texture depth, H_g, as shown in Figure 4.32. The graph pattern and trends are the same as Figure 4.31, where the C_f shows an inversed exponential as the eccentricity ratio increased. In addition, the partial single-slip texture showed lower C_f values compared to the partial two-slip texture at low eccentricity ranged from 0.1 to 0.3 before the effect of the lower texture depth kicked in. At the high eccentricity ratio, the lower H_g of 0.2 reduced the friction coefficient significantly, even though it could not compete with the plain bearing benchmark. By using the lowest C_f value recorded, the partial single-slip texture showed an increase of 120.9% for H_g=0.2 and 151.8% for H_g=0.8 when compared to the plain bearing. Meanwhile, the partial two-slip textured surface configuration showed 183.3% increase in the C_f for H_g=0.2 and a 285.6% increase in the C_f for H_g=0.8. Overall, these results showed that the applied partial texture with slip show slightly better results at the high eccentricity ratio as the friction coefficient reduced dramatically.
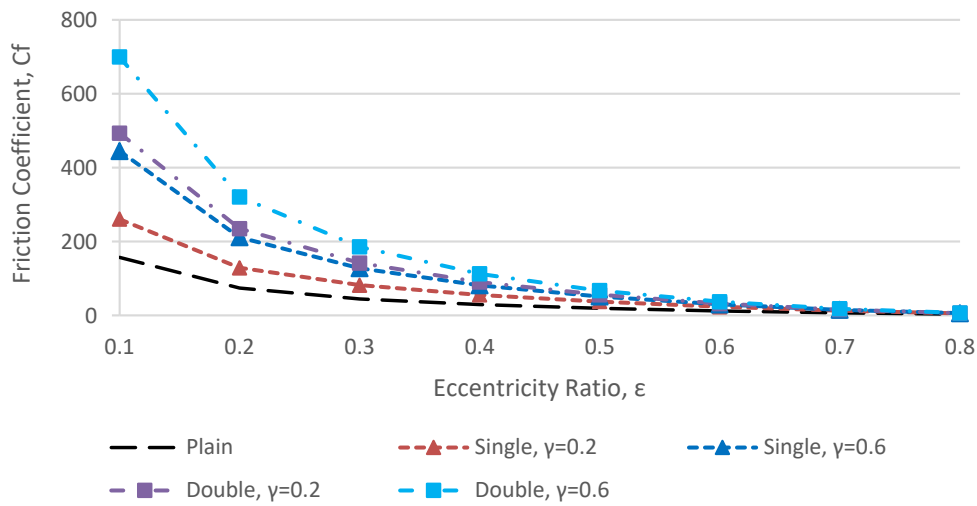
Figure 4.29: Friction coefficients for γ=0.2 and γ=0.6 with single and double-slip partial textures at 0.1<ε<0.8.
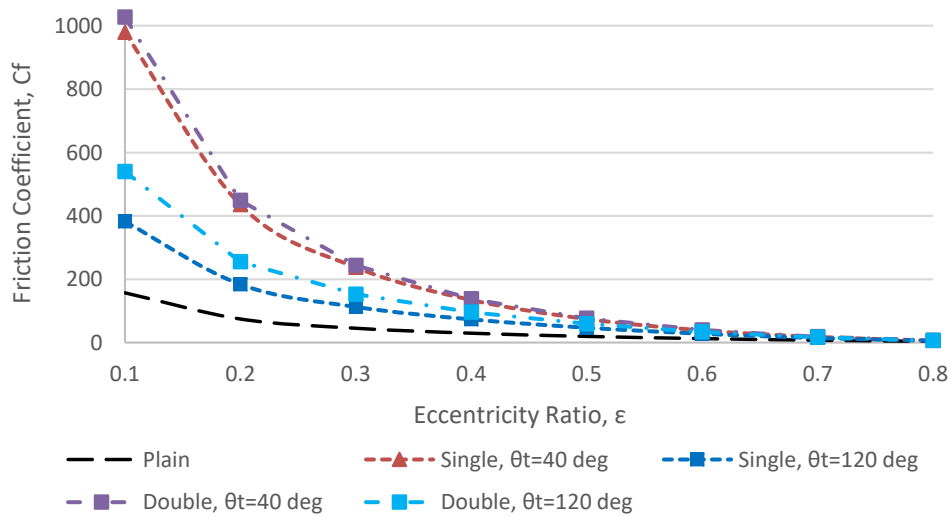
Figure 4.30: Friction coefficients for θ_t=40º and θ_t=120º with single and double-slip partial textures at 0.1<ε<0.8.
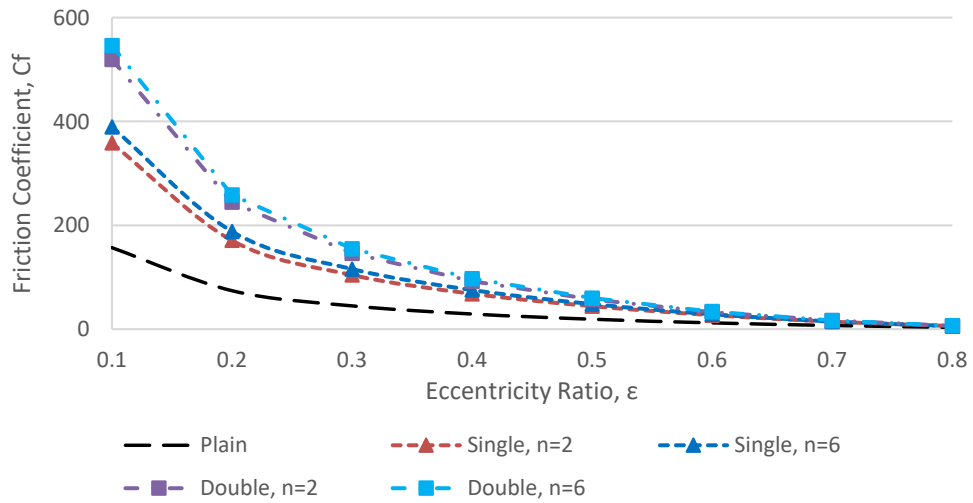
Figure 4.31: Friction coefficients for n=2 and n=6 with single and double-slip partial textures at 0.1<ε<0.8.
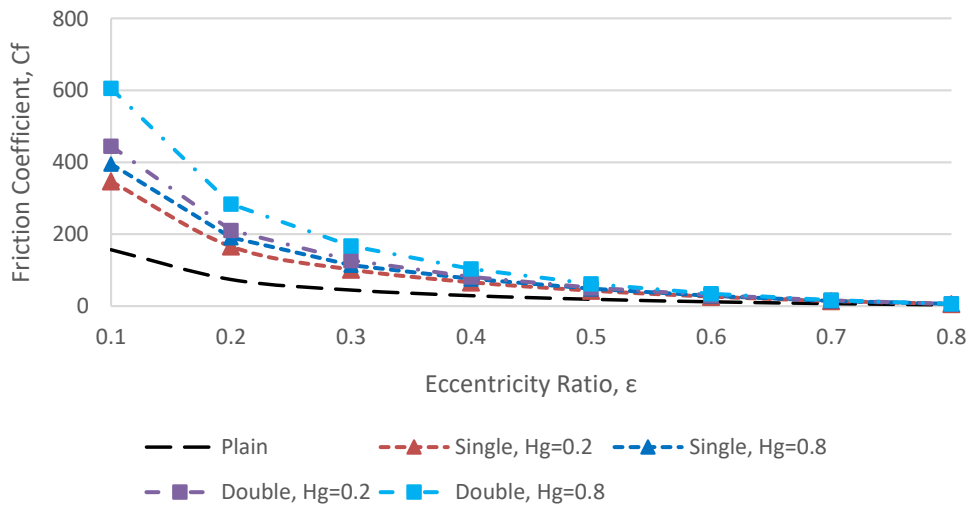
Figure 4.32: Friction coefficients for H_g=0.2 and H_g=0.8 with single and double-slip partial textures at 0.1<ε<0.8.

4.3.5 Discussion of the Performance Analysis

This section discusses the obtained results for the long and short hydrodynamic journal bearings. The reasoning behind the increase and decrease of the performance magnitude parameters is mentioned according to the long and short bearing, respectively, as follows.

4.3.5.1 Long Journal Bearing

Applying the partial texture with slip on the hydrodynamic journal bearings showed the pressure was significantly higher, with up to 196% improvement when compared to the plain bearing. The results obtained were due to the modified Reynolds equation that included the circumferential pressure which was constantly changing along the bearing's textured surface. The equation also involved the integration parameter of the fluid film lubrication. Adding additional slip on the second configuration also increased the performance magnitude of the journal bearing, especially at the low eccentricity ratio. These results also affected the outcome of the load carrying capacity, in which the load capacity was better at the 0.1 eccentricity ratio. However, the drawback was that adding the additional slip increased the shear stress and friction coefficient greatly compared to the plain bearing, which needs to be taken into consideration. As the bearing surface was applied with the partial texture with slip, it was predicted that the surface would increase the friction coefficient of the journal bearing. Even though the increase in the friction coefficient was obtained, the percentage was quite minimal for the single-slip textured configuration, but not for the configuration of the two-slip partial texture surface as mentioned. In summary, Table 4.1 shows the performance summary of the pressure distribution and dimensionless shear stress analyses along the circumferential angle; whilst Table 4.2 shows the summary of the bearing analysis in the load capacity and friction coefficient at the 0.1 eccentricity ratio.

Table 4.1: Performance summary of long hydrodynamic journal bearing with respect to circumferential angle.

Configuration		Parameters	Value	Performance % (+/-)
Pressure Distribution	Plain	-	0.604	-
	Partial Single-slip Texture Surface	$\gamma=0.2$	0.615	+1.82
		$\gamma=0.6$	0.922	+52.6
		$\theta_t=40$	1.362	+125.5
		$\theta_t=120$	0.794	+31.5
		n=2	0.804	+33.1
		n=6	0.844	+39.7
		$H_g=0.2$	0.863	+42.9
		$H_g=0.8$	0.714	+18.2
	Partial Two-slip Texture Surface	$\gamma=0.2$	1.339	+121.7
		$\gamma=0.6$	1.571	+160.1
		$\theta_t=40$	1.608	+166.2
		$\theta_t=120$	1.431	+136.9
		n=2	1.431	+136.9
		n=6	1.428	+136.4
		$H_g=0.2$	1.312	+117.2
		$H_g=0.8$	1.460	+141.7
Dimensionless Shear Stress	Plain	-	1.194	-
	Partial Single-slip Texture Surface	$\gamma=0.2$	1.312	+9.9
		$\gamma=0.6$	1.244	+4.2
		$\theta_t=40$	1.145	-4.1
		$\theta_t=120$	1.266	+6.0
		n=2	1.272	+6.5
		n=6	1.264	+5.9
		$H_g=0.2$	1.263	+5.8
		$H_g=0.8$	1.209	+1.3
	Partial Two-slip Texture Surface	$\gamma=0.2$	3.538	+196.3
		$\gamma=0.6$	3.439	+188.0
		$\theta_t=40$	3.409	+185.5
		$\theta_t=120$	3.510	+194.0
		n=2	3.512	+194.1
		n=6	3.509	+193.9
		$H_g=0.2$	3.251	+172.3
		$H_g=0.8$	3.701	+210.0

Table 4.2: Performance summary of long hydrodynamic journal bearing with 0.1 eccentricity ratio.

	Configuration	Parameters	Critical Point @Eccentricity = 0.1	Performance % (+/-)
	Plain	-	0.944	-
Dimensionless Load Carrying Capacity	Partial Single-slip Texture Surface	$\gamma=0.2$	0.621	-34.2
		$\gamma=0.6$	1.107	+17.2
		$\theta_t=40$	1.428	+51.2
		$\theta_t=120$	0.907	-4.0
		n=2	1.037	+9.8
		n=6	0.946	+0.1
		$H_g=0.2$	0.979	+3.7
		$H_g=0.8$	0.842	-10.8
	Partial Two-slip Texture Surface	$\gamma=0.2$	1.635	+73.1
		$\gamma=0.6$	1.930	+104.4
		$\theta_t=40$	1.906	+101.8
		$\theta_t=120$	1.706	+80.7
		n=2	1.699	+79.9
		n=6	1.699	+79.9
		$H_g=0.2$	1.512	+60.1
		$H_g=0.8$	1.792	+89.8
	Plain	-	3.369	-
Friction Coefficient	Partial Single-slip Texture Surface	$\gamma=0.2$	4.873	+44.6
		$\gamma=0.6$	2.619	-22.3
		$\theta_t=40$	1.925	-42.9
		$\theta_t=120$	3.226	-4.2
		n=2	2.855	-15.3
		n=6	3.112	-7.63
		$H_g=0.2$	2.915	-13.5
		$H_g=0.8$	3.479	+3.3
	Partial Two-slip Texture Surface	$\gamma=0.2$	32.835	+874.6
		$\gamma=0.6$	38.317	+1037.3
		$\theta_t=40$	40.704	+1108.2
		$\theta_t=120$	34.994	+938.7
		n=2	35.544	+955.0
		n=6	35.942	+966.8
		$H_g=0.2$	37.539	+1014.2
		$H_g=0.8$	34.640	+928.2

4.3.5.2 Short Journal Bearing

Applying texture with slip on a short journal bearing did not bring any improvement for this analysis compared to the plain bearing. The main reason behind this is that the Reynolds equation only considered the axial direction; thus, the x-direction calculation was neglected. These derivations greatly affected the denominator of the equation where the pressure and film thickness were located, resulting in lower magnitudes of the hydrodynamic pressure. Even though there was a solution to increase the load capacity magnitude, which would reduce the film thickness by minimizing the texture depth, it was found that a thin film thickness is not convenient for normal operating conditions. In addition, the low pressure magnitude produced directly showed that the load capacity was expected to be lower as well. Similar to the dimensionless shear stress and friction coefficient, applying the surface texture increased the shear stress and friction coefficient. This was due to the surface topography of the bearing's textured surface, where the film thickness changed along the circumferential angle; thus, it required more force to overcome the increased friction and stress. In addition, the surface complexity on the partial two-slip textured configuration showed a tremendously large percentage margin compared to the plain bearing, which is something that must not be considered at all. Interestingly, reducing the texture length, θ_t, on the partial single-slip showed small improvement as the textured region was compressed, providing more of the plain surface along the circumferential angle, resulting in lower shear stress at the particular parameter. To summarise the short bearing analysis, Tables 4.3 and 4.4 show the percentage difference in performance at the circumferential angle and eccentricity ratio of 0.1, respectively.

Table 4.3: Performance summary of short hydrodynamic journal bearing with respect to circumferential angle.

	Configuration	Parameters	Value	Performance % (+/-)
Pressure Distribution	Plain	-	0.020	-
	Partial Single-slip Texture Surface	$\gamma=0.2$	0.020	0.0
		$\gamma=0.6$	0.020	0.0
		$\theta_t=40$	0.012	-40.0
		$\theta_t=120$	0.020	0.0
		n=2	0.020	0.0
		n=6	0.020	0.0
		$H_g=0.2$	0.020	0.0
		$H_g=0.8$	0.020	0.0
	Partial Two-slip Texture Surface	$\gamma=0.2$	0.012	-40.0
		$\gamma=0.6$	0.012	-40.0
		$\theta_t=40$	0.012	-40.0
		$\theta_t=120$	0.012	-40.0
		n=2	0.012	-40.0
		n=6	0.012	-40.0
		$H_g=0.2$	0.015	-25.0
		$H_g=0.8$	0.012	-40.0
Dimensionless Shear Stress	Plain	-	1.111	-
	Partial Single-slip Texture Surface	$\gamma=0.2$	1.708	+53.7
		$\gamma=0.6$	1.708	+53.7
		$\theta_t=40$	1.708	+53.7
		$\theta_t=120$	1.708	+53.7
		n=2	1.708	+53.7
		n=6	1.708	+53.7
		$H_g=0.2$	1.898	+70.8
		$H_g=0.8$	1.584	+42.6
	Partial Two-slip Texture Surface	$\gamma=0.2$	2.053	+84.8
		$\gamma=0.6$	2.053	+84.8
		$\theta_t=40$	1.929	+73.6
		$\theta_t=120$	2.053	+84.8
		n=2	2.053	+84.8
		n=6	2.053	+84.8
		$H_g=0.2$	2.053	+84.8
		$H_g=0.8$	2.053	+84.8

Table 4.4: Performance summary of short hydrodynamic journal bearing with 0.1 eccentricity ratio.

	Configuration	Parameters	Critical Point @Eccentricity = 0.1	Performance % (+/-)
Dimensionless Load Carrying Capacity	Plain	-	0.0201	-
	Partial Single-slip Texture Surface	$\gamma=0.2$	0.0145	-27.9
		$\gamma=0.6$	0.0098	-51.2
		$\theta_t=40$	0.0048	-76.1
		$\theta_t=120$	0.0110	-45.3
		n=2	0.0118	-41.3
		n=6	0.0108	-46.3
		$H_g=0.2$	0.0129	-35.8
		$H_g=0.8$	0.0102	-49.3
	Partial Two-slip Texture Surface	$\gamma=0.2$	0.0090	-55.2
		$\gamma=0.6$	0.0071	-64.7
		$\theta_t=40$	0.0047	-76.6
		$\theta_t=120$	0.0086	-57.2
		n=2	0.0089	-55.7
		n=6	0.0085	-57.7
		$H_g=0.2$	0.0110	-45.3
		$H_g=0.8$	0.0086	-57.2
Friction Coefficient	Plain	-	157.1	-
	Partial Single-slip Texture Surface	$\gamma=0.2$	260.5	+65.8
		$\gamma=0.6$	445.0	+183.3
		$\theta_t=40$	979.6	+523.5
		$\theta_t=120$	382.1	+143.2
		n=2	358.6	+128.2
		n=6	389.6	+148.0
		$H_g=0.2$	347.0	+120.9
		$H_g=0.8$	395.6	+151.8
	Partial Two-slip Texture Surface	$\gamma=0.2$	493.5	+214.1
		$\gamma=0.6$	699.7	+345.5
		$\theta_t=40$	1027	+553.9
		$\theta_t=120$	539.9	+243.6
		n=2	519.6	+230.7
		n=6	546.2	+247.6
		$H_g=0.2$	445.0	+183.3
		$H_g=0.8$	605.8	+285.6

4.4 Chapter Summary

In this chapter, the results from the various parameters for the long and short hydrodynamic journal bearings were illustrated, explained, and compared with a hydrodynamic plain journal bearing. The first section discussed the long hydrodynamic journal bearing, which involved the pressure distribution, load carrying capacity, dimensionless shear stress, and friction coefficient. The next section discussed the short hydrodynamic journal bearing with the same parameters in comparison with a plain bearing.

CHAPTER 5

CONCLUSION AND RECOMMENDATIONS

5.1 Overview

This chapter shows the major findings and important remarks related to this research work. The purpose of this study has been to investigate the effect of partial texture with slip towards the performance of hydrodynamic journal bearings. The major research tasks and findings are shown in Section 5.2. Meanwhile, Section 5.3 shows the recommendation for the future work.

5.2 Summary of the Research Tasks and Major Findings

Various investigations have been carried out throughout the research study and analysis. In the beginning, a detailed literature review was extracted to focus on the texture and slip effect on the hydrodynamic journal bearings and its applications. The important aspect was to improve the performance of the hydrodynamic journal bearing at a low eccentricity ratio by applying and modifying the bearing's surface with partial texture and slip in order to enhance the journal bearing's characteristics. Besides that, new models for long and short bearings were developed which represented the proposed surface configurations; they were then compared with a plain bearing, which acted as a performance benchmark. The developed model of the partial texture with slip created by using the modified Reynolds equation was then simulated by using MATLAB software to determine the performance capabilities at a specific range of eccentricity ratios and circumferential angle lengths on the bearing's surface.

This research has achieved its aim and objectives mentioned previously in Section 1.4, and further explanation can be seen as follows;

- Numerical methods were derived for both long and short hydrodynamic journal bearings. The derivations were based on the Reynolds equation by applying proper boundary conditions and approximations, which made according to the partial texture with slip surface configurations proposed for the journal bearing. This approach allows for further analysis of different texture locations and shapes by other researchers in the next level of research.

- The equation with respect to partial texture with slip surface configuration for long and short journal bearings were derived, respectively. The derived equations were then simulated by using parameters selected based on the literature review to determine the performance outcome with comparison to the plain journal bearing.

- The results show that long journal bearings have potential in improving the performance of journal bearings in terms of pressure distribution, load capacity, shear stress, and friction coefficient at a low eccentricity ratio. However, the short journal bearing did not show any potential improvement by applying the partial texture with slip configuration based on the results obtained.

In conclusion, a long journal bearing with partial texture and a slip surface has some positive impact in improving the performance of the journal bearing at a low eccentricity ratio compared to plain bearings. The short bearing meanwhile does not contribute to any performance increase at the same configuration.

5.3 Optimal Configurations for Hydrodynamic Journal Bearing

From the results obtained, the optimal surface configurations can be obtained mainly for long journal bearing. This is due to the negative feedbacks obtained from the analysis of the short journal bearing. For the long journal bearing, the optimal partial texture and slip surface can be simplified as follows:

84

- Increasing slip to no slip ratio magnitude, γ improved the load capacity by 17% for single slip, 104% for double slip, reduced the friction coefficient by 22% for single slip, and increased the pressure distribution by 52% and 160% for single slip and double slip respectively.

- Reducing the texture length, θ_t increased the load capacity to 51% and 101% for single and double slip respectively, reduced friction coefficient by 42% for single slip only, increased the pressure distribution by 125% for single slip and 166% for double slip surface, and reduced shear stress by 4% for single slip only.

- Reducing the number of textured region, n increased the load capacity by 9% for single slip, and 80% for double slip surface. It also reduced the friction coefficient by 15% for single slip surface only, while increased the pressure distribution by 33% and 137% for single and double slip respectively.

- Reducing texture depth, H_g improved the load capacity to 3.7% for single slip and 60% for double slip surface. It also reduced the friction coefficient for single slip surface by 13%, with addition of increased pressure distribution for single slip by 43% and 117% for double slip.

The optimal results obtained above can be used as a reference to extend this research in experimental and CFD analysis.

5.4 Reliability Concerns

Although the results obtained can be used as the main reference for the extension of the research, the reliability concerns of the journal bearing with applied surface configurations should be taken into account as well. For example, even though the pressure distribution of the applied surface configurations of the journal bearing increased, the durability and reliability of the journal bearing itself are still questionable as several factors are not included in the analysis such as materials, surrounding factors

and many more. Therefore, additional research should be carried out to determine the reliability of the journal bearing with applied surface configurations by using either experimental analysis or CFD analysis to further support the results obtained in this research.

5.5 Summary of Contributions

In summary, this research has contributed in terms of the capabilities of the journal bearings to be improved in various performance factors by using partial texture with slip surface. Performance increased achieved from the long journal bearings can be obtained by using various parameters available. However, this research also showed that there are also reductions in performance obtained towards the short journal bearing which requires further verification by using different methods and approach.

5.6 Recommendation of Future Works

From the analysis and research carried out, some studies and analyses can be extended further as follows:

1. The current research study can be used to study the effect on the dynamic characteristics of the journal bearing's performance, such as stability, attitude angle, damping coefficient, and stiffness coefficient.

2. The current study can be used to analyse the fluid flow across the bearing's surface by using the computational fluid dynamics (CFD) method to contribute more precise and accurate results.

3. The current study can also be extended as part of an experimental analysis to determine the real-life performance with real-life operating conditions. The research can also be extended to analyse the same configuration but with different texture shapes in the experimental analysis.

APPENDIX A

LIST OF PUBLICATIONS

- **Faez K.M.**, Hamdavi S., Rao T.V.V.L.N., Ya H.H., (2016). "An Analytical Investigation of the Grooved Journal Bearing Performance with Slip/No-Slip Texture Bearing." Journal of Engineering and Applied Sciences **11**(22): 12990-12993.

- **Faez K.M.**, Hamdavi S., Rao T.V.V.L.N., Ya H.H., Norani M. Mohamed (2017). "Performance Analysis of Long Grooved Journal Bearing with Slip, No-Slip and Slip/No-Slip Textured Surface Configurations." Journal of Engineering and Applied Sciences **12**(20): 5794-5798.

- **Faez K.M.**, Hamdavi S., Rao T.V.V.L.N., Ya H.H., Norani M. Mohamed (2018). "Performance Analysis of Grooved Hydrodynamic Journal Bearing with Multi-Depth Textured Surface." International Journal of Vehicle Structures & Systems **10**(2): 142-145

Other Related Publications

- Hamdavi, S., Rao T.V.V.L.N., Masdi M., **Faez K.M.**, Ya H.H., (2017). "Linear Stability Analysis of Short Journal Bearing with an Axial Groove." Materialwissenschaft und Werkstofftechnik **48**(3-4): 210-217.

- Hamdavi S., Ya H.H., Rao T.V.V.L.N., **Faez K.M.**, (2016). "An Analytical Approach to Investigate the Effect of Grooved Surface on Short Journal Bearing's Performance." Journal of Engineering and Applied Sciences **11**(20): 12045-12049.

- Hamdavi S., Ya H.H., Rao T.V.V.L.N., **Faez K.M.**, (2016). "Effect of Surface Texturing on Hydrodynamic Performance of Journal Bearings" Journal of Engineering and Applied Sciences **11**(01): 172-176.

BIBLIOGRAPHY

[1] T. Someya, J. Mitsui, J. Esaki, S. Saito, Y. Kanemitsu, T. Iwatsubo, et al., *Journal-bearing databook:* Springer Science & Business Media, 2013.

[2] B. Tower, "Research committee on friction second report on friction experiments," *Proceedings of the institution of mechanical engineers,* vol. 36, pp. 58-70, 1885.

[3] O. Reynolds, "On the theory of lubrication and its application to Mr. Beauchamp Tower's experiments, including an experimental determination of the viscosity of olive oil," *Proceedings of the Royal Society of London*, vol. 40, pp. 191-203, 1886.

[4] B. Tower, "First report on friction experiments," *Proceedings of the institution of mechanical engineers*, vol. 34, pp. 632-659, 1883.

[5] A. Sommerfeld, "The hydrodynamic theory of lubrication friction," *Z. Math. Phys*, vol. 50, pp. 97-155, 1904.

[6] N. P. Petroff and L. Wurzel, *Neue theorie der reibung*: L. Voss, 1887.

[7] T. Someya, J. Mitsui, J. Esaki, S. Saito, Y. Kanemitsu, T. Iwatsubo, et al., *Journal-bearing databook:* Springer Science & Business Media, 2013.

[8] B. Tower, "Research committee on friction second report on friction experiments," *Proceedings of the institution of mechanical engineers,* vol. 36, pp. 58-70, 1885.

[9] X. Wang and S. Hsu, "An integrated surface technology for friction control: a new paradigm effects of geometric shapes on friction," in *The 4th China International Symposium on Tribology*. Xi'an, 2004, pp. 12-20.

[10] D. Dowson, *History of tribology:* Addison-Wesley Longman Limited, 1979.

[11] G. Stachowiak and P. Podsiadlo, "3-D characterization, optimization, and classification of textured surfaces," *Tribology Letters*, vol. 32, pp. 13-21, 2008.

[12] K. Tonder, "Inlet roughness tribodevices dynamic coefficients and leakage," *Tribology International*, vol. 34, pp. 847–852, 2001.

[13] M. Tauviqirrahman, R. Ismail, J. Jamari, and D. Schipper, "A study of surface texturing and boundary slip on improving the load support of lubricated parallel sliding contacts," *Acta mechanica*, vol. 224, pp. 365-381, 2013.

[14] V. Brizmer and Y. Kligerman, "A laser surface textured journal bearing," *Journal of Tribology*, vol. 134, p. 031702, 2012.

[15] N. Tala-Ighil and M. Fillon, "A numerical investigation of both thermal and texturing surface effects on the journal bearings static characteristics," *Tribology International*, vol. 90, pp. 228-239, 2015.

[16] C. L. M. H. Navier. M´emoire sur les lois du mouvement des fluides. *M´emoires de l'Acad´emie Royale des Sciences de l'Institut de France*, vol. 6, pp. 389–440, 1823.

[17] J. C. Maxwell. On stresses in rarefied gases arising from inequalities of temperature. *Phil. Trans. Roy. Soc. Lond.*, vol. 170, pp. 231–256, 1879.

[18] E. Lauga, M. Brenner, and H. Stone, "Microfluidics: the no-slip boundary condition," *Springer handbook of experimental fluid mechanics*, pp. 1219-1240, 2007.

[19] C. Neto, D. R. Evans, E. Bonaccurso, H. J. Butt, and V. S. Craig, "Boundary slip in Newtonian liquids: a review of experimental studies," *Reports on Progress in Physics*, vol. 68, pp. 2859, 2005.

[20] M. A. Day, "The no-slip condition of fluid dynamics," *Erkenntnis*, vol. 33, pp. 285-296, 1990.

[21] D. Dowson and C. Taylor, "Cavitation in bearings," *Annual Review of Fluid Mechanics*, vol. 11, pp. 35-65, 1979.

[22] A. Z. Szeri, *Fluid film lubrication:* Cambridge University Press, 2010.

[23] G. B. DuBois and F. W. Ocvirk, "Analytical derivation and experimental evaluation of short-bearing approximation for full journal bearings," *US Government Printing Office Washington*, 1953.

[24] J. Mitsui, "Method of calculation for bearing characteristics," *Journal Bearing Databook, T. Someya, Editor, Springer Verlag, Berlin Heidelberg*, pp. 231- 240, 1988.

[25] B. J. Hamrock, S. R. Schmid, and B. O. Jacobson, *Fundamentals of Fluid Film Lubrication*: CRC press, 2004.

[26] S. R. Schmid, B. J. Hamrock, and B. O. Jacobson, "Fundamentals of Machine Elements: SI Version," *CRC Press*, 2014.

[27] J. B. Heywood, "Internal combustion engine fundamentals," vol. 930, *Mcgrawhill New York*, 1988.

[28] E. P. Becker, "Trends in tribological materials and engine technology," *Tribology International*, vol. 37, pp. 569-575, 2004.

[29] Y. Hori, "Hydrodynamic lubrication," *Springer Science & Business Media*, 2006.

[30] A. de Kraker, R. A. van Ostayen, and D. J. Rixen, "Calculation of Stribeck curves for (water) lubricated journal bearings," *Tribology International*, vol. 40, pp. 459-469, 2007.

[31] R. B. Siripuram and L. S. Stephens, "Effect of deterministic asperity geometry on hydrodynamic lubrication," *Journal of tribology*, vol. 126, pp. 527-534, 2004.

[32] Y. Kondo, T. Koyama, and S. Sasaki. "Tribological properties of ionic Liquids." *Ionic liquids-New aspects for the future*. InTech, 2013.

[33] M. M. Khonsari and E. R. Booser, "Applied tribology: bearing design and lubrication," *John Wiley & Sons*, vol. 12, 2008.

[34] R. Tiwari, "A brief history and state of the art of rotordynamics," Department of Mechanical Engineering, *Indian Institute of Technology Guwahati*, vol. 781039, 2008.

[35] J. Fedor, "Half Sommerfeld approximation for finite journal bearings," *Journal of Basic Engineering*, vol. 85, pp. 435-438, 1963.

[36] O. Pinkus and B. Sternlicht, "Theory of hydrodynamic lubrication," *McGrawHill*, 1961.

[37] A. Harnoy, "Bearing design in machinery: engineering tribology and lubrication," *CRC press*, 2002.

[38] J. Lund and K. Thomsen, "A calculation method and data for the dynamic coefficients of oil-lubricated journal bearings," *Topics in Fluid Film Bearing and Rotor Bearing System Design and Optimization, ASME, New York*, pp. 1- 28, 1978.

[39] C. Shen and M. M. Khonsari, "Effect of dimple's internal structure on hydrodynamic lubrication," *Tribology Letters*, vol. 52, pp. 415-430, 2013.

[40] X. Lu, and M. M. Khonsari, "An experimental investigation of dimple effect on the stribeck curve of journal bearings," *Tribology Letters*, vol. 27, pp. 169, 2007.

[41] Y. Qiu and M. Khonsari, "Performance analysis of full-film textured surfaces with consideration of roughness effects," *Journal of tribology*, vol. 133, p. 021704, 2011.

[42] I. Etsion, G. Halperin, V. Brizmer, and Y. Kligerman, "Experimental investigation of laser surface textured parallel thrust bearings," *Tribology Letters*, vol. 17, 2003.

[43] A. Kovalchenko, O. Ajayi, A. Erdemir, G. Fenske, and I. Etsion, "The effect of laser surface texturing on transitions in lubrication regimes during unidirectional sliding contact," *Tribology International*, vol. 38, pp. 219-225, 2005.

[44] V. G. Marian, D. Gabriel, G. Knoll, and S. Filippone, "Theoretical and Experimental Analysis of a Laser Textured Thrust Bearing," *Tribology Letters*, vol. 44, pp. 335-343, 2011.

[45] S. Cupillard, S. Glavatskih, and M. Cervantes, "Computational fluid dynamics analysis of a journal bearing with surface texturing," *Proceedings of the Institution of Mechanical Engineers, Part J: Journal of Engineering Tribology*, vol. 222, pp. 97-107, 2008.

[46] S. Mishra, A. Choudhury, and S. Sahu, "CFD investigation of influences of reverse textures on bearing surface of a journal bearing," *Journal of Applied Fluid Mechanics*, vol. 7, pp. 395-399, 2014.

[47] S. Kango and R. K. Sharma, "Studies on the influence of surface texture on the performance of hydrodynamic journal bearing using power law model," *International Journal of Surface Science and Engineering*, vol. 4, pp. 505-524, 2010.

[48] A. de Kraker, R. A. van Ostayen, A. Van Beek, and D. J. Rixen, "A multiscale method modeling surface texture effects," *Journal of tribology*, vol. 129, pp. 221-230, 2007.

[49] S. Kango, D. Singh, and R. Sharma, "Numerical investigation on the influence of surface texture on the performance of hydrodynamic journal bearing," *Meccanica*, vol. 47, pp. 469-482, 2012.

[50] S. Kango, R. Sharma, and R. Pandey, "Comparative analysis of textured and grooved hydrodynamic journal bearing," *Proceedings of the Institution of*

Mechanical Engineers, Part J: Journal of Engineering Tribology, vol. 228, pp. 82-95, 2014.

[51] N. Tala-Ighil, M. Fillon, and P. Maspeyrot, "Effect of textured area on the performances of a hydrodynamic journal bearing," *Tribology International*, vol. 44, pp. 211-219, 2011.

[52] N. Tala-Ighil and M. Fillon, "Surface texturing effect comparative analysis in the hydrodynamic journal bearings," *Mechanics & Industry*, vol. 16, p. 302, 2015.

[53] V. S. Craig, C. Neto, and D. R. Williams, "Shear-dependent boundary slip in an aqueous Newtonian liquid," *Physical review letters*, vol. 87, pp. 054504, 2001.

[54] Y. Zhu, and S. Granick, "Rate-dependent slip of Newtonian liquid at smooth surfaces," *Physical review letters*, vol. 87, pp. 096105, 2001.

[55] Y. Zhu, and S. Granick, "Limits of the hydrodynamic no-slip boundary condition," *Physical review letters*, vol. 88, pp. 106102, 2002.

[56] H. A. Spikes, "The half-wetted bearing. Part 1: extended Reynolds equation," *Proceedings of the Institution of Mechanical Engineers, Part J: Journal of Engineering Tribology*, vol. 217, pp. 1-14, 2003.

[57] H. A. Spikes, "The half-wetted bearing. Part 2: potential application in low load contacts," *Proceedings of the Institution of Mechanical Engineers, Part J: Journal of Engineering Tribology*, vol. 217, pp. 15-26, 2003.

[58] C. Neto, D. R. Evans, E. Bonaccurso, H. J. Butt, and V. S. Craig, "Boundary slip in Newtonian liquids: a review of experimental studies," *Reports on Progress in Physics*, vol. 68, pp. 2859, 2005.

[59] M. A. Day, "The no-slip condition of fluid dynamics," *Erkenntnis*, vol. 33, pp. 285-296, 1990.

[60] E. Lauga, M. Brenner, and H. Stone, "Microfluidics: the no-slip boundary condition," *Springer handbook of experimental fluid mechanics*, pp. 1219-1240, 2007.

[61] C. L. M. H. Navier. Mémoire sur les lois du mouvement des fluides. *Mémoires de l'Académie Royale des Sciences de l'Institut de France*, vol. 6, pp. 389–440, 1823.

[62] C. W. Wu, G. J. Ma, P. Zhou, and C. D. Wu, "Low friction and high load support capacity of slider bearing with a mixed slip surface," *Journal of Tribology*, vol. 128, pp. 904-907, 2006.

[63] R. F. Salant, and A. E. Fortier, "Numerical analysis of a slider bearing with a heterogeneous slip/no-slip surface," *Tribology Transactions*, vol. 47, pp. 328-334, 2004.

[64] R. F. Salant, and A. E. Fortier, "Numerical analysis of a journal bearing with a heterogeneous slip/no-slip surface," *Journal of Tribology*, vol. 127, pp. 820-825, 2005.

[65] T. V. V. L. N., Rao, "Analysis of single-grooved slider and journal bearing with partial slip surface," *Journal of tribology*, vol. 132, pp. 014501, 2010.

[66] C. Wu, (2008), "Performance of hydrodynamic lubrication journal bearing with a slippage surface," *Industrial Lubrication and Tribology*, vol. 60, pp. 293-298, 2008.

[67] C. W. Wu, and G. J. Ma, "Abnormal behavior of a hydrodynamic lubrication journal bearing caused by wall slip," *Tribology international*, vol. 38, pp. 492-499, 2005.

[68] Q. Lin, Z. Wei, and Y. Tang, "Numerical study on shear flow in sliding bearing with partial slip surface," *Procedia CIRP*, vol. 3, pp. 197-202, 2012.

[69] F. Aurelian, M. Patrick, and H. Mohamed, "Wall slip effects in (elasto) hydrodynamic journal bearings," *Tribology International*, vol. 44, pp. 868-877, 2011.

[70] T. V. V. L. N. Rao, A. M. A. Rani, T. Nagarajan, and F. M. Hashim, "Load Capacity of Partially Textured Slip Parallel Slider and Concentric Journal Bearing using Narrow Groove Theory," *Procedia Engineering*, vol. 68, pp. 63-69, 2013.

[71] T. V. V. L. N. Rao, A. M. A. Rani, T. Nagarajan, and F. M. Hashim, "Analysis of couple stress fluid lubricated partially textured slip slider and journal bearing using narrow groove theory," *Tribology International*, vol. 69, pp. 1-9, 2014.

[72] T. V. V. L. N. Rao, A. M. A. Rani, T. Nagarajan, and F. M. Hashim, "Analysis of slider and journal bearing using partially textured slip surface," *Tribology International*, vol. 56, pp. 121-128, 2012.

[73] T. V. V. L. N. Rao, A. M. A. Rani, T. Nagarajan, and F. M. Hashim, "Analysis of Grooved Journal Bearing with Partial Slip Surface," *Proceedings of Regional Tribology Conference 2011: RTC2011*, Malaysian Tribology Society, vol. 6, pp. 183-190, 2011.

[74] T. Ibatan, M. Uddin, and M. Chowdhury, "Recent development on surface texturing in enhancing tribological performance of bearing sliders," *Surface and Coatings Technology*, vol. 272, pp. 102-120, 2015.

[75] C. Ma and H. Zhu, "An optimum design model for textured surface with elliptical-shape dimples under hydrodynamic lubrication," *Tribology International*, vol. 44, pp. 987-995, 2011.

[76] I. Etsion and L. Burstein, "A model for mechanical seals with regular microsurface structure," *Tribology Transactions*, vol. 39, pp. 677-683, 1996.

[77] M. Qiu, B. R. Minson, and B. Raeymaekers, "The effect of texture shape on the friction coefficient and stiffness of gas-lubricated parallel slider bearings," *Tribology International*, vol. 67, pp. 278-288, 2013.

[78] W. Tang, Y. Zhou, H. Zhu, and H. Yang, "The effect of surface texturing on reducing the friction and wear of steel under lubricated sliding contact," *Applied surface science*, vol. 273, pp. 199-204, 2013.

[79] D. Sfyris and A. Chasalevris, "An exact analytical solution of the Reynolds equation for the finite journal bearing lubrication," *Tribology International*, vol. 55, pp. 46-58, 2012.

[80] F. Meng, T. Davis, J. Cao, Q. J. Wang, D. Hua, and J. Liu, "Study on effect of dimples on friction of parallel surfaces under different sliding conditions," *Applied surface science*, vol. 256, pp. 2863-2875, 2010.

[81] S. Hamdavi, H. H. Ya, T. V. V. L. N. Rao, and K. M. Faez, "An Analytical Approach to Investigate the Effect of Grooved Surface On Short Journal Bearing's Performance," *Journal of Engineering and Applied Sciences*, vol. 11, pp. 12045-12049, 2016.

[82] J. Rao, "History of rotating machinery dynamics," *Springer Science & Business Media*, vol. 20, 2011.

[83] L. De Chiffre, H. Kunzmann, G. Peggs, and D. Lucca, "Surfaces in precision engineering, microengineering and nanotechnology," *CIRP Annals-Manufacturing Technology*, vol. 52, pp. 561-577, 2003.

[84] D. Falconnet, G. Csucs, H. M. Grandin, and M. Textor, "Surface engineering approaches to micropattern surfaces for cell-based assays," *Biomaterials*, vol. 27, pp. 3044-3063, 2006.

[85] A. Bruzzone, H. Costa, P. Lonardo, and D. Lucca, "Advances in engineered surfaces for functional performance," *CIRP Annals-Manufacturing Technology*, vol. 57, pp. 750-769, 2008.

[86] A. del Campo and E. Arzt, "Fabrication approaches for generating complex micro-and nanopatterns on polymeric surfaces*," Chemical reviews*, vol. 108, pp. 911-945, 2008.

[87] D. G. Coblas, A. Fatu, A. Maoui, and M. Hajjam, "Manufacturing textured surfaces: State of art and recent developments," *Proceedings of the Institution 158 of Mechanical Engineers, Part J: Journal of Engineering Tribology*, vol. 229, pp. 3-29, 2015.